APPENDIX G

Spill Fate and Behaviour Modelling

Trajectory Modelling in Support of the Shelburne Basin Exploration Drilling Program

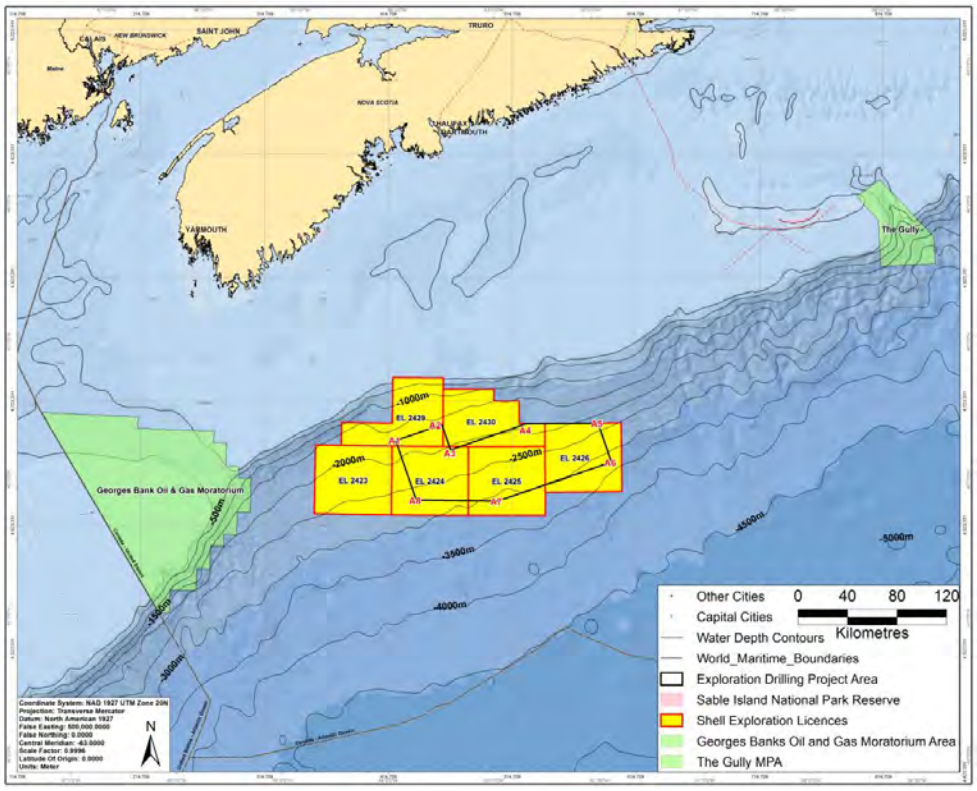

Model Description, Approach, and Summary of Results

By

Matthew Horn, PhD – Project Manager
Email: mhorn@asascience.com

&

Deborah French McCay, PhD – Principal
Email: dfrenchmccay@asascience.com

RPS ASA
55 Village Square Drive
South Kingstown, RI 02879-8248 USA
Tel: +1 401 789 6224
Fax: +1 401 789 1932

RPS ASA 2013-212
27 May 2014

List of Contributors

Matthew Horn, PhD – Project Manager, model input development, lead author
MHorn@asascience.com

Deborah French McCay, PhD – Principal in charge and oil spill model development
DFrenchMcCay@asascience.com

Chris Galagan – Senior advisor and report review
Yong Kim – Hydrodynamics
Tatsu Isaji – Hydrodynamics
Lisa McStay – Model Inputs and report preparation
Deborah Crowley – Release parameter modeler and report preparation
Jenna Turner – GIS figure making
Rachel Shmookler – GIS figure making
Melanie Schroeder – Modelling advisor
Jeremy Fontenault – Model Inputs, GIS figure making
Zachary Singer-Leavitt – Model input and report preparation
Stefanie Zamorski – Hydrodynamics and report preparation
Kathy Jayko – Senior Modeler
Cheryl Morse – Model development and automation
David Stuebe – Model development and automation

List of Appendices

The following appendices provide additional information in support of: Model Description, Stochastic and Deterministic Approach, and Summary of Results

Appendix A: SIMAP Model Description
Appendix B: OILMAP Deep Model Description
Appendix C: Environmental Data

TABLE OF CONTENTS

EXECUTIVE SUMMARY

Oil spill trajectory and fate modelling were performed to support an Environmental Assessment for Shell Canada Limited's Shelburne Basin Venture Exploration Drilling Project. The Project is located approximately 250 km offshore Nova Scotia with exploratory drilling anticipated in water depths ranging from approximately 1500 - 3000 m. Continuous unmitigated subsurface blowout scenarios were developed at two locations (Site 1 and Site 2), which were chosen to consider variations in water depths as well as proximity to sensitive marine features. Additionally, modelled blowout characteristics are representative of the wells that would be drilled for the Project. Model and release duration for all modelled scenarios was 30 days, with a continuous release of Federated Crude Oil, a representative oil type with similar chemical and physical parameters to the expected oil found in the proposed reservoir. Modelled release volumes and rates varied with 747,000 bbl (24,900 bpd) blowouts at Site 1 and 1,474,500 bbl (49,150 bpd) blowouts at Site 2. In addition, two additional surface batch spill releases of 10 bbl and 100 bbl of marine diesel were modelled at a third location (Site 3). All spills were modelled without any countermeasures applied. Table E1 lists the scenarios examined.

Table E1. Modelled Spill Scenarios.

Spill Location	Depth of release	Model Duration	Release Duration	Number of Model Runs	Released Product	Release Type	Release Volume
Site 1 (42.3°N, 64.0°W)	1700 m	30 days	30 days	40 per month x12 months	Federated Crude Oil	Blowout	747,000 bbl (24,900 bpd)
Site 2 (42.15°N, 62.9°W)	2500 m	30 days	30 days	40 per month x12 months	Federated Crude Oil	Blowout	1,474,500 bbl (49,150 bpd)
Site 3 (42.25°N, 63.48°W)	Surface	30 days	Instan-taneous	2 releases	Marine Diesel	Batch Spill	10 bbl & 100bbl

In order to reproduce the dynamic and complex processes associated with deep subsea blowout releases, two models were used. The near-field output data from OILMAP Deep™, which characterizes the subsurface blowout is used as an input to the SIMAP™(Spill Impact Model Application Package), which simulates far-field trajectories and fates in order to estimate potential effects to the marine environment from a release.

Geographical data (habitat mapping and shoreline location) were obtained from the U.S. National Oceanic and Atmospheric Administrations Environmental Sensitivity Index (NOAA ESI), and Maine's Environmental Vulnerability Index (EVI) from the Maine Department of Environmental Protection. For the Canadian shoreline, data from New Brunswick Department of Natural Resources and Nova Scotia Department of Natural Resources was used. Bathymetry

was characterized using databases provided by NOAA National Geophysical Data Center (NGDC) and GEBCO.

Hourly wind speed and direction data were obtained from the U.S. Navy Operational Global Atmospheric Prediction System (NOGAPS). Local wind speed was validated using hourly data from a nearby meteorological station on the Fisheries and Oceans Canada buoy c44137 on the East Scotian Slope.

Hydrodynamics data included both the Global HYbrid Coordinate Ocean Model (HYCOM) general circulation model and the TOPEX/Poseidon Global Inverse Solution TPXO8.0 tidal forcing.

Utilizing these models and inputs, stochastic analyses (multiple runs with varying environmental conditions) were conducted for each of the twelve months per year for each spill site, and 95th percentile (with respect to degree of oil exposure) deterministic (single trajectory) cases were modelled. In association with these modelled scenarios, the following thresholds were identified for each and are reported for stochastic and representative deterministic cases:

- Surface oil average thickness >0.04 µm
- Shore oil average thickness >1.0 µm
- Subsurface (within the water column) dissolved aromatic concentrations >1ppb

Though large footprints of oil contamination are depicted for stochastic analyses, they are not the expected distribution of oil from any *single* release. These maps do not provide any information on the quantity of oil in a given area. They simply denote the probability of oil exceeding the given threshold over the entire ensemble of runs at each point. Note that only probabilities of 1% or greater were included in the map output. Stochastic maps showing water column contamination by dissolved aromatics depict oiling frequency, but do not specify the given depth at which this occurs and do not imply that the entire water column (i.e. from surface to bottom) will experience a concentration above the threshold.

Stochastic results are useful in planning for oil spill response, as they characterize the probability that regions may experience contamination above specified thresholds, taking into account the environmental variability expected from many different release scenarios over time. Stochastic footprints depict an area between 821,000 – 916,000 km^2 for potential surface oiling and water column dissolved aromatic contamination for Sites 1 and 2. This region covers a portion of US waters to the east of the New England area, and in Canadian waters south of Nova Scotia and Newfoundland. However, the majority of this area represents a probability of oiling at less than 10%.

In general, surface oiling and water column dissolved aromatic footprints were similar across months, with transport predominantly to the east and northeast. The majority of oil tends to stay offshore. However a general trend was observed in the results, with what appeared to be winter-

type conditions from October through March, and summer-type conditions from April through September. During winter conditions, oil was more likely to be transported to the east, while under summer conditions transport was uniformly multi-directional.

Higher percentages of the released oil were found within the water column during winter months resulting from increased wind and wave action, which entrains surface oil into the water column. Conversely, the greatest proportion of surface oiling occurred during summer months, with low wind and wave conditions reducing entrainment into the water column.

Shoreline oiling was only observed during May, June, and July. The likelihood that shoreline oiling would occur is less than 10% for both Sites 1 and 2. The reason that shoreline oiling is so unlikely is a combination of the forcing parameters for surface oil (increased probability of winds from the east and northeast) and the location of the release (locations are far offshore and oil would need to travel hundreds of kilometres towards shore). As such, it is expected that the oil that would strand would be highly weathered, as the minimum time to shore would be between 20-30 days. The regions susceptible to potential shoreline oiling within 30 days from a release at Site 1 include the southern tip of Nova Scotia, including the Yarmouth, Barrington, and Shelburne region, as well as Sable Island National Park. The region susceptible to potential shoreline oiling within 30 days from a release at Site 2 includes only the Sable Island National Park.

The amount of evaporation and decay is relatively consistent between model runs. Approximately 50% of the Federated Crude Oil spills evaporated. The majority of variability with the mass balance is found in the amount of oil either on the surface or within the water column. The maximum surface oiling cases resulted in approximately 10-20% of the total mass of released oil on the surface and 30-40% entrained, while the maximum water column dissolved aromatic cases had little surface oiling and closer to 50% entrained.

Accidental batch spills of marine diesel resulted in limited modelled effects. Around 80% of the spill evaporated within 2-3 days, with only about 2 km^2 and 20 km^2 experiencing in water concentrations of dissolved aromatics in excess of 1 ppb at any time for the 10 bbl and 100 bbl spill, respectively. A small portion of weathered diesel may continue to be transported at the surface for some distance; however this mass is quite small. None of the batch spills are predicted to reach the Nova Scotia shoreline.

Document Summary

This report includes an introduction to the region and the modelling, the methodology, and finally the results of the study. The model results are summarized in representative figures and tables in the main body of this document, describing oil contamination within the water column, on the water surface, and along shorelines. This document is broken down into several sections. Section 1 includes an introduction to the Shelburne Basin region and basic modelling approach. Section 2 contains a description of the model inputs and scenarios that were

modelled. Section 3 contains a description of the modelling approach and summary of the OILMAP Deep™ and SIMAP™ models. Section 4 summarizes the stochastic and deterministic oil fates model results. Section 5 summarizes conclusions and Section 6 contains the references cited.

Additional information may be found in supporting appendices. Appendix A provides a detailed description of the SIMAP™ model and the fates processes and algorithms that were used. Appendix B provides a description of the theory and implementation of the OIMAP Deep™ model. Finally, Appendix C provides a summary of environmental data for the Project Area, including hydrodynamics and winds.

LIST OF FIGURES

Main Report: FIgures

LIST OF TABLES

Maine Report: Tables

Appendix A: Tables

Appendix B: Tables

None

Appendix C: Tables

None

List of Acronyms and Abbreviations

3D: Three dimensional, referring to the vertical and horizontal, as in x, y, and z directions

AL: Aliphatic portion of the total hydrocarbon, which is modelled as a volatile fraction within the SIMAP model and can therefore evaporate.

AR: Aromatic portion of the total hydrocarbon, which is modelled as a volatile and soluble fraction within the SIMAP model and can therefore evaporate and dissolve.

ARGO: An oceanographic sensor array composed of 3600 drifting profiling buoys that measure temperature, salinity, and currents

BOP: Blow out preventer, used to seal control, and monitor oil and gas wells

BPD: Barrel per day

BTEX: Benzene, toluene, ethylbenzene, and xylene

C#: The number of carbons contained within an organic molecule (e.g. C3 compounds contain 3 carbon atoms as a chain)

CERC: Coastal Engineering Research Center

CERCLA: The U.S. Superfund or Comprehensive Environmental Response, Compensation, and Liability Act of 1980

CTD: An oceanographic instrument package that measures physical water parameters with depth including Conductivity, Temperature, and Depth.

EEZ: Exclusive Economic Zone

ESI: NOAA Environmental Sensitivity Index

ESMF: Earth System Modeling Framework

ESTC: Environment Canada Environment Science and Technology Center

EVI: The United Nations Environment Programme (UNEP) Environmental Vulnerability Index

GEBCO: The General Bathymetric Chart of the Oceans operated by the International Hydrographic Organization (IHO) and Intergovernmental Oceanographic Commission (IOC) of UNESCO.

GODAE: U.S. Global Ocean Data Assimilation Experiment

GOR: Gas to Oil Ratio

HYCOM: The U.S. Navy HYbrid Coordinate Ocean Model used for currents

MAH: Monocyclic aromatic hydrocarbons (monoaromatic), with only one six carbon ring

MCSST: Multi-Channel Sea Surface Temperature

MEDEM: The U.S. state of Maine (ME) Department of Environmental Management

NBDNR: Canada's New Brunswick Department of Natural Resources

NCODA: U.S. Navy Coupled Ocean Data Assimilation

NGDC: U.S. NOAA's National Geophysical Data Center

NIMA: U.S. National Imagery and Mapping Agency

NOAA: U.S. National Oceanic and Atmospheric Administration

NODC: U.S. National Ocean Data Collection Center of NOAA

NOGAPS: U.S. Navy Operational Global Atmospheric Prediction System for winds

NOMAD: Navy Oceanographic Meteorological Automatic Device

NRC: U.S. National Research Council

NRDA: The U.S. Natural Resource Damage Assessment

NRDAM/CME: Natural Resource Damage Assessment Model for Coastal and Marine Environments

NRDAM/GLE: Natural Resource Damage Assessment Model for Great Lakes Environment

NRL: U.S. Naval Research Laboratory

NSDNR: Canada's Nova Scotia Department of Natural Resources

OPA: U.S. Oil Pollution Act

OTIS: Oregon State University's Tidal Inversion Software

PAH: Polycyclic aromatic hydrocarbons (polyaromatic), with two or more six carbon rings

PPB: Part per billion, as referring to concentration

PPM: Part per million, as referring to concentration

SIMAP™: Spill Impact Model Application Package, a 3D trajectory and fate model

SPM: Suspended particulate matter within the water column

THC: Total hydrocarbons

TPH: Total petroleum hydrocarbons

TPXO: Topex/Poseidon Global Inverse Solution to model ocean tides

UNESCO: United Nations Educational, Scientific, and Cultural Organization

WOA01: World Ocean Atlas, a database from NODC NOAA containing observational data of physical and chemical parameters of seawater from many thousands of cruises.

XBT: Expendable bathythermographs

1 INTRODUCTION

Shell Canada Limited (Shell) contracted RPS Applied Science Associates, Inc. (RPS ASA) to conduct trajectory modelling in support of an Environmental Assessment for the Shelburne Basin Venture Exploration Drilling Project (the Project). The Project Area is located approximately 250 km south of Nova Scotia within a geographical offshore area known as the Southwest Scotian Slope (Figure 1). Water depths in the Project Area range from 500 m to >4000m. Several major currents, including the Labrador Current and the Gulf Stream, influence the circulation in this region.

This modelling was conducted to evaluate possible spill events associated with the Project, including large scale deep-water blowouts at the wellhead and smaller scale batch spills of marine diesel at the surface. Three dimensional oil spill fate and trajectory modelling and analyses were performed to support evaluation of the potential effects from oil spills into the Shelburne Basin using RPS ASA's OILMAP Deep™ blowout model and the Spill Impact Model Application Package (SIMAP™).

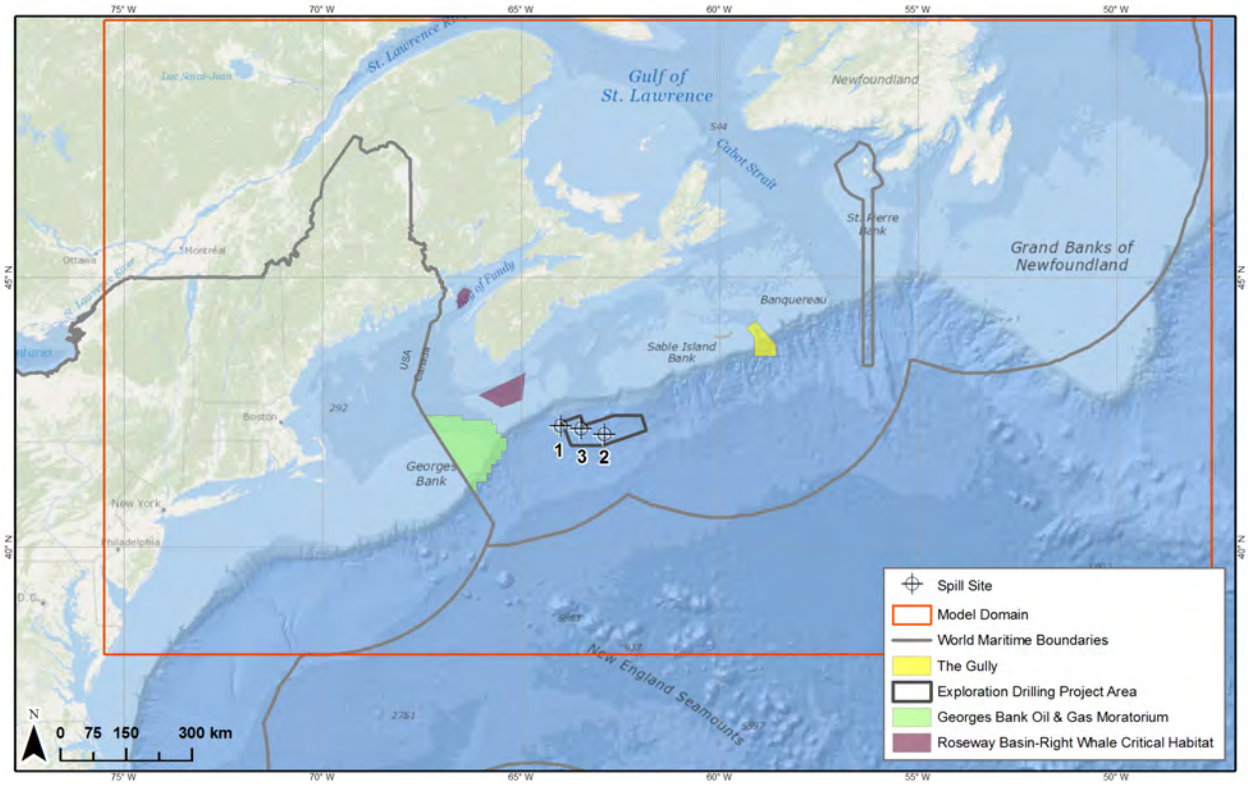

Figure 1. Shelburne Basin Venture Exploration Drilling Project Location

This study involved an analysis of deep-water blowouts of crude oil at depth and the potential in-water, surface, and shoreline oiling that may result. The goal was to assess the transport, fates, and effects of oil and diesel from surface and subsurface releases. The scenario specifications consisted of:

- Spill locations,
- Spill release types,
- Oil types,
- Spill volumes and durations,
- Seasons or time frames (e.g. monthly analysis), and
- Environmental parameters (e.g. hydrodynamics and winds)

This project utilized a stochastic approach to deterministic the potential fate of spills from the two hypothetical drill sites. In a stochastic approach, a spill trajectory model is run repeatedly, with a randomly selected start date that falls within the desired time period covered by the available wind and current data. Using wind and current speed and direction data from modelled hindcasts, each oil spill simulation was run with the appropriate time series starting on a randomly selected date. In this approach, a sufficient number of model runs will adequately sample all of the variability in the wind and current speed and direction in the region of interest and will result in a prediction of the probability of oil pathways for a spill at the prescribed location. Running multiple spill simulations during a given time period will provide a reliable prediction of the oiling probability for a spill occurring during this time period. Additional deterministic analyses were conducted for 95th percentile worst-case scenarios for threshold exceedance of surface oiling, water column contamination, and shoreline oiling. The deterministic trajectory simulations provided an estimate of the oil's fate and transport for a specific release and specific set of environmental conditions, whereas the stochastic output provided overall probability of oiling extent and travel time given a wide range of environmental conditions.

The SIMAP model has been applied to predictions of multiple spill events using the stochastic approach and has been validated against actual spills. Reports describing these applications of the model and validation against actual spills are listed in a special section of Appendix A titled 'References – SIMAP Example Applications and Validations'.

2 MODEL INPUTS AND SCENARIOS

The spill scenarios modelled as part of this analysis were defined in consultation with Shell and were chosen to represent both low probability large scale and more frequent instantaneous small scale spill scenarios that could occur during exploration drilling activities. Possible spills at the offshore sites include crude oil from a well blowout at the seafloor and small volume batch spills of diesel fuel on the sea surface.

Two model systems were used to simulate the spills. The first model, OILMAP Deep™ RPS ASA's blowout model, simulates the near-field dynamics of the plume of a gas/oil mixture discharged from the subsea well blowout, and the second model SIMAP, simulate the far-field transport and weathering of oil released into the water column or at the sea surface. This section describes the spill scenarios considered, and the wind, current, and other data defining the environment.

With the integration of the OILMAP Deep™ blowout plume model into RPS ASA's SIMAP™ oil spill model, stochastic and deterministic simulations may be run to predict impacts on surrounding waters, resources, and shoreline from these hypothetical deep water blowouts. To model these hypothetical scenarios most effectively, a suite of data including geographic and chemical and physical data is included, as well as spatially and temporally variable environmental data.

2.1 SHELBURNE BASIN STUDY AREA

The Project Area is located approximately 250 km south of Nova Scotia within a geographical offshore area known as the Southwest Scotian Slope (Figure 1). Water depths range from 500 m to >4000m. The Project Area is located near the juncture of the cold Labrador Current and the warm Gulf Stream along the Scotian Shelf (Figure 1 and Appendix C: Figure 2). In general, variable currents are common within this region, with lower velocities observed during summer months, and slightly higher velocities during winter months. There is little mixing, due to temperature differentials, between the Labrador Current, which flows to the south and west, and the Gulf Stream, which flows to the east and northeast.

A complete description of local hydrodynamics is provided in Appendix C. Oil at depth is expected to follow local hydrodynamics, steered by the bathymetric contours, which will most likely transport subsurface oil along the shelf, as observed Appendix C: Figure 5. It is likely that these low offshore water velocities will slowly transport oil at depth, however the trajectory of surface oil will more likely be affected by wind conditions at the time of the spill.

2.2 MODEL SCENARIOS

Three locations were modelled to predict the range of expected effects from various spill scenarios for this project (Table 1). The selected spill sites for hypothetical blowouts included two deep-water well locations; Site 1 at 1700 m, and Site 2, at 2500 m. These sites were chosen to consider variations in water depths, as well as proximity to sensitive marine features. The blowouts were modelled as a continuous 30-day release of Federated Crude Oil at the sea floor.

Release volumes and rates varied between Sites 1 and 2. Total volume released over each 30-day release and daily flow rates for the hypothetical drill locations included 747,000 bbl at 24,900 bpd for Site 1 and 1,474,500 bbl at 49,150 bpd for Site 2.

Multiple spill scenarios were modelled to assess the fate of oil spilled at the modelled sites. To reproduce the dynamic and complex processes of a seabed blowout release, a near-field analysis using OILMAP Deep™ was performed prior to simulating the far-field movement of the Federated Crude Oil using the SIMAP™ 3D fates model.

Representative instantaneous surface releases of marine diesel were modelled at a third location (Site 3) between the modelled wellheads at the sea surface using the SIMAP™ 3D fates model. The spill volumes modelled included 10 bbl and 100 bbl. Releases were modelled during calm summer conditions, where low wind and waves would maximize surface effects.

Variable environmental conditions for this region, including wind and currents, were modelled between September 2008 and December 2013. All spill scenarios were simulated as unmitigated spill events (i.e. without the application of any spill counter measures). Ice cover was not considered relevant to the area and thus was not modelled in this study.

Table 1. Complete matrix of spill model scenarios modelled.

Spill Location	Depth of release	Model Duration	Release Duration	Number of Model Runs	Released Product	Release Type	Release Volume
Site 1 (42.3°N, 64.0°W)	1700 m	30 days	30 days	40 per month x12 months	Federated Crude Oil	Blowout	747,000 bbl (24,900 bpd)
Site 2 (42.15°N, 62.9°W)	2500 m	30 days	30 days	40 per month x12 months	Federated Crude Oil	Blowout	1,474,500 bbl (49,150 bpd)
Site 3 (42.25°N, 63.48°W)	Surface	30 days	Instan-taneous	2 releases	Marine Diesel	Batch Spill	10 bbl & 100bbl

Stochastic analyses for Sites 1 & 2 included 480 individual model runs per site, for a total of 960 individual model runs. Additional deterministic analyses were conducted for 95th percentile

worst-case scenarios for threshold exceedance of surface oiling, water column contamination, and shoreline oiling. Deterministic analyses for instantaneous surface releases of marine diesel were also modelled at Site 3.

2.3 OIL CHARACTERIZATION

The oil types modelled in this study included Federated Crude Oil and Marine Diesel. Federated Crude Oil (2002) is a relatively "light" crude with low viscosity and a high aromatic content. The marine diesel is a standard diesel that is also low viscosity with a high aromatic content.

Federated Crude Oil was selected for this study as reported properties, including API and viscosity, were similar to anticipated chemical and physical values within the reservoir (ESTC, 2013). Additionally, the low viscosity and higher aromatic content of the Federated Crude Oil also provides a more conservative approximation of anticipated effects within the water column.

The physical and chemical data on these oils were measured by Environment Canada (ESTC, 2013).The physical and chemical data on the oils were taken from ESTC datasheets for Federated Crude Oil (ESTC, 2013). The MAH, PAH, and volatile aliphatic concentrations were calculated from data in this report. The three aromatic pseudo-components and three aliphatic pseudo-components were then modelled in SIMAP^{TM}, along with the total hydrocarbons. The volatile aliphatics are evaporated and volatilize from the surface water and so their mass is accounted for in the overall mass balance. However, as they do not dissolve in significant amounts, they have little influence on the biological effects on water column and benthic organisms. Minimum oil slick thicknesses were determined based on McAuliffe (1987), NRC (1985) and the Bonn Agreement (Daling et al. 1999). Summaries of the physical parameters for each oil are provided in Table 2. The aromatic and aliphatic concentrations, as well as the fraction of whole oil are provided for each spilled oil are included in Table 3 and Table 4. The degradation rates used in modelling are included in Table **5**.

Table 2. Oil parameters for the spilled oils.

Physical Parameters	Federated Crude Oil (2002)	Marine Diesel
Oil Type	Light Oil, may form Emulsion	Diesel
Minimum Slick Thickness (µm)	0.1	0.01
Surface tension (dyne/cm)	28.0	27.5
Pour Point (C)	-24	-24
API Gravity	38.9	38.8
Density at 25^{o}C (g/cm^{3})	0.8250	0.8310
Viscosity (cP) @ 25^{o}C	4.0	2.76

Table 3. Aromatic (AR), aliphatic (AL), and total hydrocarbon (THC) fractional composition of whole oil for Federated Crude Oil (2002). THC is the sum of AR and AL. (Numbers of carbons in the included compounds are listed, e.g., >C8-C10 indicates greater than 8 carbons and including 9 and 10-carbon hydrocarbons.)

Fraction of Whole Oil

Federated Crude Oil	AR	AL	THC
1 (AR = BTEX & MAHs >C8-C10) (AL = >C6-C10)	0.02890	0.25110	0.28000
2 (AR = MAHs and PAHs >C10-C12) (AL= >C10-C12)	0.00440	0.17010	0.17450
3 (AR = PAHs >C12-C16) (AL = >C12-C16)	0.06600	0.17450	0.23150

Table 4. Aromatic (AR), aliphatic (AL), and total hydrocarbon (THC) fractional composition of whole oil for marine diesel. THC is the sum of AR and AL. (Numbers of carbons in the included compounds are listed, e.g., >C8-C10 indicates greater than 8 carbons and including 9 and 10-carbon hydrocarbons.)

Fraction of Whole Oil

Marine Diesel	AR	AL	THC
1 (AR = BTEX & MAHs >C8-C10) (AL = >C6-C10)	0.019333	0.144667	0.164000
2 (AR = MAHs and PAHs >C10-C12) (AL= >C10-C12)	0.011410	0.478690	0.490100
3 (AR = PAHs >C12-C16) (AL = >C12-C16)	0.015605	0.303295	0.318900

Table 5. Degradation rates of oil within various partitions of the model (French et al. 1996).

Partition	Degradation Rate day^{-1}
Surface (0-1m) & Shore	0.01
Hydrocarbons in Water (1-200 m)	0.01
Hydrocarbons in Water (>200 m)	0.01
Oil in Sediment	0.001

2.4 WIND DATA

The model uses time-varying wind speeds and directions for the specific time and space of the spill and simulation. Wind data was gathered from the U.S. Navy Operational Global Atmospheric Prediction System (NOGAPS), a state-of-the-art meteorological model developed over the past twenty years at the Naval Research Laboratory (NRL) in Monterey, CA (NRL, 2013). The specific NOGAPs 10 metre wind dataset used for this study was sourced from a version of the dataset compiled by the HYCOM Consortium, which takes the original NOGAPS output hosted by the U.S. Global Ocean Data Assimilation Experiment (GODAE) and applies a QuickSCAT correction (at 0.5 degree horizontal resolution with a 3-hour time step) to them providing a more accurate representation of regional wind patterns. Additional wind information was obtained from a nearby Canadian NOMAD buoy, Station 44137 – East Scotia Slope (42.234°N, 62.018°W) for validation of modelled wind speeds (NOAA NDBC, 2013). This buoy is owned and maintained by Environment Canada and provided verification that the modelled wind data was appropriate. The NOGAPS gridding, hypothetical drill sites, and location of the buoy is provided in Figure 2.

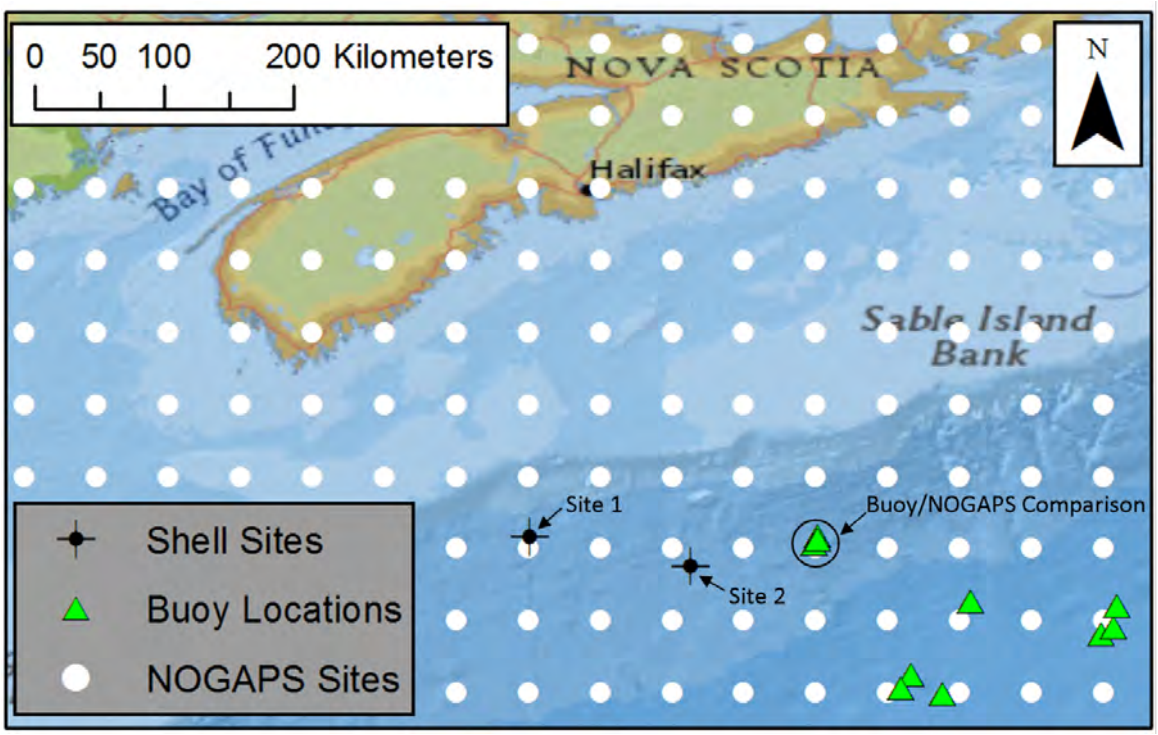

Figure 2. NOGAPS wind gridding, spill sites, and buoy data for empirical comparisons.

Time varying wind speed and directions from 2008 through 2013 were used to force surface oil for this modelling. Winds may physically transport oil on the water surface and wind speed and direction at the water surface may make a difference between limited or extensive transport.

The wind drift was calculated at each point in the model in space and time adding both surface transport and vertical mixing of the surface water (Youssef and Spaulding, 1994).

The general wind driven transport of surface oil throughout the year is mainly offshore and to the east. Strong (>20 kt) winds from the northwest are most common during winter months, while moderately strong (10-20 kt) winds from the south west are most likely during summer months.

An overview of the NOGAPS dataset, a seasonal wind analysis by site, and a comparison of modelled winds to the Canadian NOMAD buoy, Station 44137 is provided in Appendix C.

2.5 HYDRODYNAMIC DATA

Currents are one of the most significant environmental forcing parameters for the trajectory and fate of hydrocarbon discharges. To simulate oceanic circulation in the project area, vertically and time varied currents from the HYbrid Coordinate Ocean Model (HYCOM) were combined with TPXO8.0 tidal forcing to generate a complete hydrodynamics dataset at the required spatial and temporal resolution (Bleck, 2002; Egbert and Erofeeva, 2014).

Global HYCOM with 1/12° horizontal resolution at the equator (~7 km at mid-latitudes) is the ocean model component of an eddy-resolving operational nowcast/forecast system. There are 26-27 vertical layers within the selected modelled region. Data is available at daily resolution for the five-year run between 2008-2013 (Figure 3).

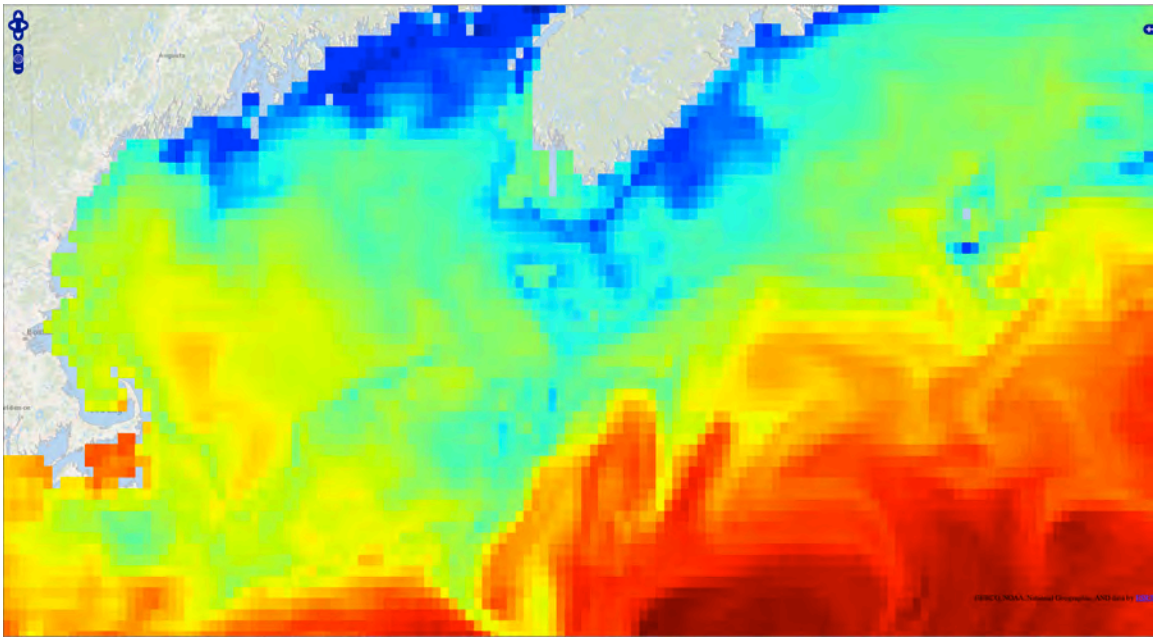

Figure 3. An example HYCOM current field for a given daily snapshot where colour indicates water velocity from low (blue) to high (red).

Depth averaged tidal currents for the dispersion simulations were derived using the Oregon State University TOPEX/Poseidon Global Inverse Solution TPXO, a global model of ocean tides (Egbert and Erofeeva, 2014). The TPXO solution is provided on a 1440x721, ¼ degree by ¼ degree resolution full global grid. Tidal forcing is stored as a harmonic constant.

Currents at a given location in both space and time were calculated by combining HYCOM and TPXO8.0 hydrodynamics data sets. Daily HYCOM files were augmented by adding the tidal forcing at the resolution of the modelled time step, which was 30 minutes. This was done for each grid point (location and depth) throughout the domain for the entire five-year period, between 2008-2013, providing a complete hydrodynamic forcing supplied at 30-minute time intervals.

The highly variable currents at the surface, and interannual fluctuations in flow intensity emphasize complex spatial and temporal circulation patterns in the region. The seasonal variability in currents are regular and repeatable features for all years in the time series and the dataset maintains these oscillations for depths above 150 m. At both locations, current directions become more consistent with depth and net westerly/south-westerly flow in the model becomes apparent at depths below 500 m. Bottom currents at all sites are characterized by generally weak, westerly oriented currents that persists year-round.

Oil at depth is expected to follow local hydrodynamics, steered by the bathymetric contours, which will most likely transport subsurface oil along the shelf, as observed in (Appendix C: Figure 5). It is likely that low offshore water velocities will slowly transport oil at depth, however the trajectory of surface oil will more likely be affected by wind conditions at the time of the spill.

A general description of local hydrodynamics, an overview of each dataset, and a complete summary of the site-specific currents is provided in Appendix C.

2.6 WATER TEMPERATURE AND SALINITY

For this study, temperature and salinity values were obtained from the World Ocean Atlas 2001 (WOA01) high-resolution dataset, version 2. The WOA01 dataset is compiled and maintained by the United States National Oceanographic Data Center (www.nodc.noaa.gov). The World Ocean Atlas originated from the Climatological Atlas of the World Ocean (Levitus, 1982) and was updated with new records in 1994, 1998, and 2001 (Conkright et. al., 2002). These records consist of observations that have been obtained from various global data management projects. After a comprehensive quality control process, the remaining data were averaged yearly, seasonally, and monthly and interpolated to fit a grid with ¼ degree horizontal resolution. The yearly dataset, used in this study, includes 33 depth bins and covers depths from the ocean surface down to 5,500 m depth.

Water temperature and salinity varies throughout the year and with depth. An average water temperature profile (varies with depth) was extracted for each site. The air immediately above the water is assumed to have the same temperature as the water surface, this being the best estimate of air temperature in contact with floating oil. Local temperature (i.e. different at each depth) is used to parameterize oil properties (e.g. viscosity) in time and space throughout the model. An average salinity profile was also extracted for each site. In general, salinity has little influence on the fate of the oil. This parameter is mainly used to determine local water density (along with temperature), which is used to calculate the buoyancy of submerged droplets. The crude oil modelled here is significantly less dense than the surrounding seawater and results in positively buoyant oil in the model.

2.7 HABITAT AND GEOGRAPHIC DATA

Spatial geographic location data for the area of interest including shoreline and habitat types (e.g., wetland, submerged aquatic vegetation, rocky shore) were assembled, processed, and gridded for use in RPS ASA's spill models. This data is required to accurately quantify contamination to varying shore and habitat types.

For geographical reference, SIMAP^{TM} uses a rectilinear grid to designate the location of the shoreline, the water depth (bathymetry), slope, bottom roughness, and the shore or habitat type. The grid is generated from a digital shoreline or other geographical information using the ESRI Arc/Info compatible Spatial Analyst program. Throughout the modelled domain, the grid scale resolution varies slightly from 2.0 x 3.1 km up to 2.4 x 3.1 km, due to the curvature of the earth, with an average cell area of 6.8 km^2. All cells are coded for depth and habitat type. Note that the model identifies the shoreline using this grid. Thus, in model outputs, the land-water map is only used for visual reference; it is the habitat grid that defines the actual location of the shoreline in the model.

Multiple data sources characterizing geographical data including habitat mapping and digital shoreline were used to characterize the regions along the U.S. and Canadian coast. For the U.S. Shoreline (Delaware to Maine), data from NOAA's Environmental Sensitivity Index (ESI) and Maine's Environmental Vulnerability Index (EVI). For the Canadian shoreline, data from New Brunswick Department of Natural Resources and Nova Scotia Department of Natural Resources was used (NOAA ESI, 2013; MEDEP 2013; NBDNR 2013; NSDNR 2013). Bathymetry in this region was characterized using databases provided by NOAA National Geophysical Data Center (NGDC) and GEBCO (NOAA NGDC, 2013; GEBCO, 2013).

A description and overview of habitat type gridding used in the SIMAP^{TM} model is provided in Appendix A.

2.8 SHORELINE OIL RETENTION

Retention of oil on a shoreline depends on the shoreline type, width and angle of the shoreline, viscosity of the oil, the tidal amplitude (in estuarine areas), and the wave energy. In the NRDAM/CME (French et al., 1996), shore holding capacity was based on observations from the *Amoco Cadiz* spill in France and the *Exxon Valdez* spill in Alaska (based on Gundlach, 1987) and later work summarized in French et al., 1996a). These data are used here (Table 6). The shore width (zone width where oiling would occur) was set to 1 m, as a realistic shore width for oiling given the spill volumes and shore types involved.

Table 6. Maximum oil thickness (mm) for various shore types as a function of oil viscosity (from French et al., 1996a, Based on Gundlach, 1987).

	Maximum Oil Thickness (mm) by Oil Type		
Shore Type	**Light (<30 cSt)**	**Medium (30-2000 cSt)**	**Heavy (>2000 cSt)**
Rocky shore	1	5	10
Gravel shore	2	9	15
Sand beach	4	17	25
Mud flat	6	30	40
Wetland	6	30	40
Artificial	1	2	2

3 Model Description

3.1 Overall Modelling Approach

This modelling study utilized a stochastic and deterministic approach to determine the potential fate of spills from the Shelburne Basin Venture Exploration Drilling Project. A paired stochastic and deterministic modelling approach is used to provide a probabilistic view that a given region may experience effects from a spill over many possible environmental conditions, as well as a representative view of a given individual spill, based upon specific parameters for a single given release. Together, they provide a more complete view of both likelihood and severity of any potential effects.

The oil spill scenarios listed in Table 1 were simulated using a paired approach with OILMAP Deep™ defining the blowout plume in the near-field. This described the oil and gas within the blowout plume, including the range of oil droplet sizes generated during the release. The outputs from the OILMAP Deep™ are an intermediate step in the ultimate modelling of oil trajectory and fate. SIMAP™ was initialized using the OILMAP Deep™ subsea blowout information and used to characterize the fate and trajectory of the modelled oil spill in 3D for the far field. Each simulation used the environmental conditions for each randomly selected start date from sets of environmental data spanning 2008-2013. Each simulation was modelled as a continuous unmitigated release of oil for 30 days with total model duration of 30 days. A total of 40 releases were modelled at each Spill Site for each month of the year, providing a range of trajectories using environmental conditions applicable to the Project Area.

3.2 Stochastic Approach

In the first phase of this study, SIMAP's stochastic model was used to determine risk to various resources being exposed to oil based upon the variability of meteorological and oceanographic conditions. A stochastic scenario is comprised of many individual trajectories (i.e., tens to hundreds of individual trajectories) of the same spill scenario. The stochastic analysis is a

statistical analysis of results generated from many different individual trajectories of the same spill event (characteristics), with each trajectory having a different spill start time selected at random from a relatively long-term window. The random start time allows for the same type of spill to be analyzed under varying environmental conditions. The results provide the probable behaviour of the potential spills.

In order to reproduce the natural variability of winds and currents, the model requires both spatially (multiple points) and temporally (changing with time) varying data sets. Historical observations and models of multiple-year wind and current records were used to perform the simulations within the coinciding time period. These data sets allow for reproduction of the natural variability of the wind and current direction and speed. Optimally, the minimum time window for stochastic analysis is at least five years. Modelled here is the period between 2008 and 2013. Using wind and current data for each specific time period, a sufficient number of model runs will adequately sample the variability in the wind and current speed and direction in the region of interest, and will result in a prediction of the probability of oil pathways for a spill at the prescribed location.

Stochastic analyses provide two types of information: 1) areas associated with probability of oiling and 2) the shortest time required for oil to reach any point within the areas predicted to be oiled. The following figures illustrate the stochastic modelling process for a generic example spill scenario (Figure 4). The left panel of Figure 4 depicts four individual trajectories predicted by SIMAP^{TM} for the example scenario. Because these trajectories started on different dates/times, they were exposed to varying environmental conditions, and thus traveled in different directions. To compute the stochastic results, tens to hundreds of individual trajectories (like the four shown) were overlain and the number of times that a given location is reached by different trajectories was used to calculate the probability of oiling for that location. This is shown as the stacked runs in the right panel of Figure 4. The predicted cumulative footprint or area and probabilities of oiling were generated by a statistical analysis of all the individual trajectories.

The number of individual trajectories and timeframe of a given stochastic analysis play role in the spatial extent of stochastic footprints. Higher numbers of individual runs encorporate a larger percentage of environmental variability, which may result in larger footprints. As the number of trajectories modelled increases, the confidence and resolution of reported probabilities also increases. Annual footprints result in the largest footprint, encompassing all environmental variability throughout the years. Monthly footprints will be significantly smaller, encompassing only the environmental variability expected within a given monthly climatology. It is important to note that a single trajectory encounters only a small portion of an overall probability footprint. An individual trajectory, the path that oil from a single release would travel, may be less than 10% of an annual stochastic footprint. Stochastic information was presented for surface oil, shoreline oil, and subsurface oil for the full year, and by month. Individual representative deterministic trajectories that characterize a single spill scenario are also presented.

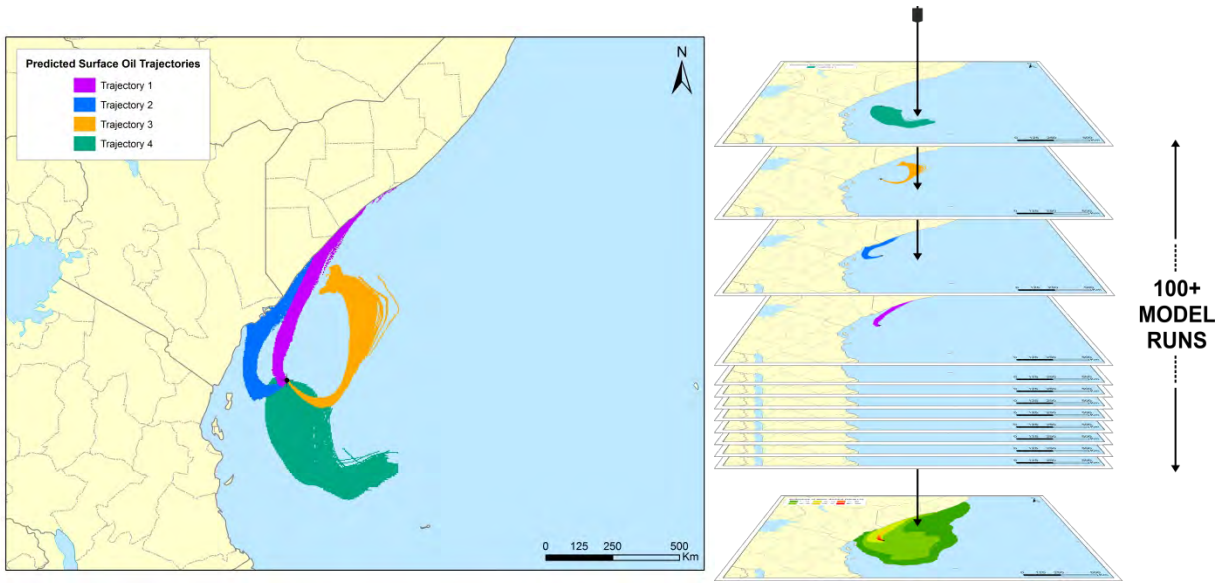

Figure 4. Examples of four individual spill trajectories predicted by SIMAP^{TM} for a generic spill scenario. Tens to hundreds of individual trajectories are overlain upon one another (shown as the stacked runs on the right), and the frequency of contact with given locations is used to calculate the probability of impacts during a spill.

Stochastic analyses of deep-water blowouts were modelled at Sites 1 and 2 using five years of variable environmental data found in Section 2 and the physical-chemical properties of Federated Crude Oil (2002) (Table 2 and Table 3). At each location, a total of 40 individual deterministic oil spill trajectories were modelled for each of the 12 months a year. This totaled 480 individual deterministic trajectories per year per site, for a total of 960 unique runs between the two sites. The duration of each model run was 30 days with a continuous unmitigated 30-day blowout.

The stochastic model is capable of evaluating areas affected and concentrations over a prescribed minimum threshold or cut-off value. Often these thresholds are based on response requirements or environmental impact assumptions.

3.3 THRESHOLDS OF INTEREST

Stochastic modelling includes many tens or hundreds of individual deterministic runs over a range of environmental conditions for a given scenario. When combined with one another, the many individual deterministic footprints generate an area of probability that describes the possible area of oil contamination from the entire suite of modelled conditions. Stochastic footprints are therefore much larger than the expected effects from any single incident.

Floating oil mass loading is expressed as g/m^2, where 1 g/m^2 corresponds to an oil layer that is approximately 1 micron (µm) thick. Table 7 gives approximate thickness and mass loading ranges for surface oil of varying appearance. Dull brown sheens are about 1 µm thick. Rainbow

sheen is about 0.2-0.8 g/m^2 (0.2-0.8 µm thick) and silver sheens are 0.05-0.8 mg/m^2 (0.05-0.8 µm thick; NRC, 1985). Crude and heavy fuel oil that is greater than 1mm thick appears as black oil. Light fuels and diesel that are greater than 1mm thick are not black in appearance, but appear brown or reddish. Floating oil will not always have these appearances, however, as weathered oil would be in the form of scattered floating tar balls and tar mats where currents converge.

Table 7. Oil thickness (µm) and equivalent mass loading (g/m^2) and appearance on water (NRC, 1985).

Minimum	Maximum	Appearance
0.05	0.2	Colourless and silver sheen
0.2	0.8	Rainbow sheen
1	4	Dull brown sheen
10	100	Dark brown sheen
1,000	10,000	Black oil

To analyze the probability or likelihood of potential effects, specific thresholds for surface oil thickness, in water concentration, and shoreline oiling are used. Cutoff thresholds defining the minimum value for expected potential effects were defined, along with higher thresholds for comparative purposes (Table 8). Variability in the observation and measurement of oil thickness and visible appearance do exist. The visible threshold for a colourless and silver sheen may potentially be observed at a lower threshold and a value of 0.04 µm was chosen as a conservative approximation (French-McCay et al. 2011).

Table 8. Stochastic thresholds used to define regions with potential effects.

Stochastic Threshold	Cutoff Threshold	Rationale
Surface Oil Thickness	*0.04 µm	Visible threshold used to determine impacts on socioeconomic resources (e.g. possibility of fisheries closure). This minimum thickness would relate to a slick being barely visible as a colourless or silver sheen (French-McCay et al. 2011).
	10 µm	Biological threshold for ecological impacts to the water surface (i.e. birds) (French-McCay 1996 & 2009 oil spill fate and effects model). Oil would appear as a dark brown.
Shoreline Oil Mass	*1.0 g/m^2	This thickness is the threshold for potential effects on socio-economic resource uses, as this amount of oil would conservatively trigger the need for shoreline cleanup on amenity beaches. Oil would appear as a dull brown sheen (French-McCay et al. 2011).
	10.0 g/m^2	This thickness provides a more conservative screening threshold for potential ecological effects to shoreline habitats, which has typically been 100 g/m^2, based upon a synthesis of the literature showing that shoreline life has been affected by this degree of oiling (French et al., 1996; French McCay 2009). The oil would appear as dark brown coat or opaque/black oil.
In Water Concentration	*1.0 ppb of dissolved aromatics, roughly equivalent to 1.0 ppm TPH	Exposure concentration below which no significant biological effects are expected for sensitive marine resources (Trudel, 1989 and French-McCay, 2004) in S.L. Ross 2011 modelling for Old Harry in Gulf of St. Lawrence). This value is a conservative threshold for early contact on herring larvae.

*Thresholds used in supporting figures.

3.4 DETERMINISTIC APPROACH

Individual or “deterministic” trajectories of interest were identified and selected from the stochastic ensemble of results. The deterministic trajectory simulations provided an estimate of the oil’s fate and transport for a specific set of environmental conditions. While the stochastic analysis provides insight into the probable behaviour of oil spills given historic wind and current data for the region, it does not provide an individual trajectory, oil weathering information, expected concentrations and thickness of oil contamination, mass balance, and other information related to a single spill at a given location and time.

For the second phase of the study, individual 3D or “deterministic” trajectories were identified from stochastic outputs. Each modelled run (single run) within a stochastic analysis (tens or hundreds of runs) represents a specific wind and current condition for the modelled time period. When analyzed together, they provide a range of expected effects. The effects between each case may differ greatly, as the trajectory of each modelled spill is unique. Therefore, the area of surface oiling, mass of oil along the shoreline, and mass of oil within the water column, will be different for each modelled run. As a conservative approximation, erring on the side of larger effects, representative “worst” cases for each site, during both summer and winter seasons, were identified by characterizing the 95th percentile degree of effects for 1) surface area oiled, 2) mass of oil along the shoreline, and 3) mass of oil within the water column.

A 3D deterministic trajectory and fate simulation was performed for each 95th percentile run as identified in the stochastic analysis. Identified representative cases were rerun deterministically for each site to produce fates and weathering information for each particular run, representative of specific conditions, selected from the stochastic parent scenario. As an example, the Site 1, summer, 95th percentile surface oiling case would represent the specific individual trajectory that resulted in one of the largest areas (95th percentile) of surface oiling predicted over all of the 240 summer trajectories for Site 1. This case would have it’s own trajectory, mass balance, surface oiling, in water concentration of dissolved aromatics, etc. The Site 1, summer, 95th percentile water column oiling case would be a different deterministic trajectory, with a different start date, and its own mass balance, surface oiling, in water concentration of dissolved aromatics, etc. A complete list of representative deterministic cases is included in Table 11.

The results of the deterministic simulations provide a time history of oil weathering over the duration of the spill (mass balance), expressed as the percentage of spilled oil on the water surface, on the shoreline, evaporated, entrained in the water column, and decayed. In addition, times series snapshots of the individual trajectories showing concentration of floating surface oil, shoreline oil, and the concentration of dissolved aromatics in the water column (surface and profile view) are provided.

3.5 Blowout Releases of Crude Oil

Blowout scenarios were simulated at Sites 1 and 2 in the Project Area. Both discharges originated at the sea floor, as deep subsea releases of crude oil at a depth of 1700 m for Site 1 and 2500 m for Site 2. When blowouts occur in deep water, it is necessary to use a model that considers the effects of the complex mixture of oil and gas, as well as the release parameters that control the size of oil droplets discharged from the source. These calculations will determine the movement of oil throughout the water column and inform the rates of chemical and physical processes that occur along the way to the sea surface based upon ambient conditions and the specific oil type.

OILMAP Deep™ contains two sub-models, a plume model and a droplet size model. The plume model predicts the evolution of plume position, geometry, centerline velocity, and oil and gas concentrations until the plume either surfaces or reaches a terminal height at which point the plume is trapped. The droplet model predicts the size and volume (mass) distribution of the oil droplets. Provided below is an overview of blowout plume dynamics, modelling implementation, and modelling results.

3.5.1 Plume Dynamics

In shallow water (< 200 m) oil and gas released from the seabed are driven into the water column as a jet due to the momentum of the discharge (Figure 5). The jet region is confined to the vicinity of the seabed and is relatively short in length (< 1 m). As the discharge moves upward the density difference between the expanding gas bubbles in the plume and the receiving water result in a buoyant force, which drives the plume. The resulting plume is analogous to a thermal plume, with the important exception that for blowouts the plume is bubble starved, because the bubbles are few in number and large. The presence of the bubbles leads to a two-layer structure with an inner core bubble plume and an outer ring of mostly entrained water.

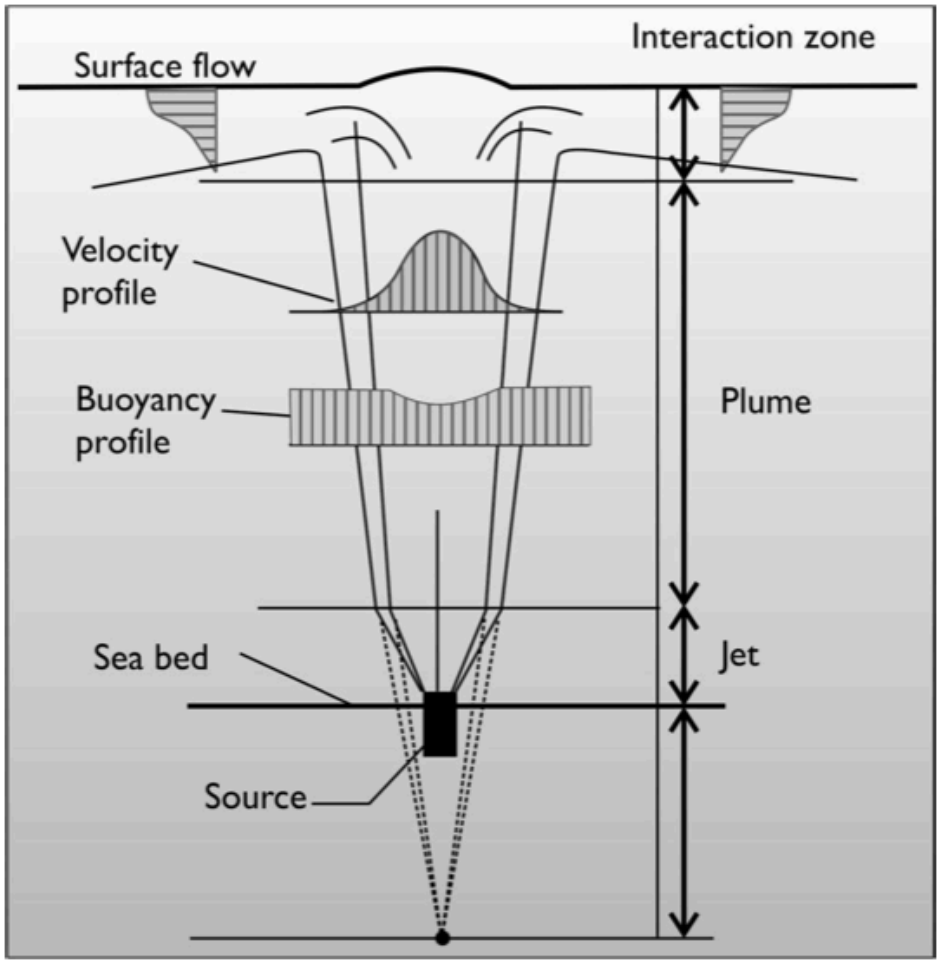

Figure 5. Schematic of a surfacing blowout plume in shallow water

As the plume rises, it continues to entrain ambient seawater due to the velocity difference between the rising plume and the receiving water. This entrainment reduces the plume's velocity and buoyancy and increases its radius. The oil in the release is rapidly mixed by the turbulence in the rising plume causing it to break up into small droplets. These droplets (typically a few micrometres to millimetres in diameter) are rapidly transported upward by the rising plume; their individual rise velocities contributing little to their upward motion in this region. If the plume reaches the sea surface it is deflected in a radial, surface flow zone without appreciable loss of momentum as can be seen in Figure 5. This radial jet, with its origin at the surface directly above the blowout, carries the oil particles rapidly away from the centre of the plume. The velocity and oil concentrations in this surface flow zone decrease while the depth of the zone increases. Finally in the far field, where the plume buoyancy has been dissipated, ambient currents and wind-generated waves determine the subsequent transport and dispersion of the oil.

There are several important modifications that may alter this basic description of jet/plume behaviour. If the buoyant driving force for the plume is dissipated by entrainment before it

reaches the surface, the oil droplets in the plume will be carried to the surface solely by their own rise velocities and the surface interaction zone will effectively disappear. The plume behaviour can also be altered by variations in the ambient density field, which can cause trapping of the plume, or a portion of it, in the water column as seen in Figure 6. Furthermore the plume gas bubbles may potentially dissolve in part or in total, which can also cause the plume to trap. Finally in the presence of ambient currents the plume path can be substantially altered as the current forces the jet to bend from its preferred vertical direction (as can also be seen in Figure 6). If the current velocity profile with depth varies with time the path of the plume can become very complicated.

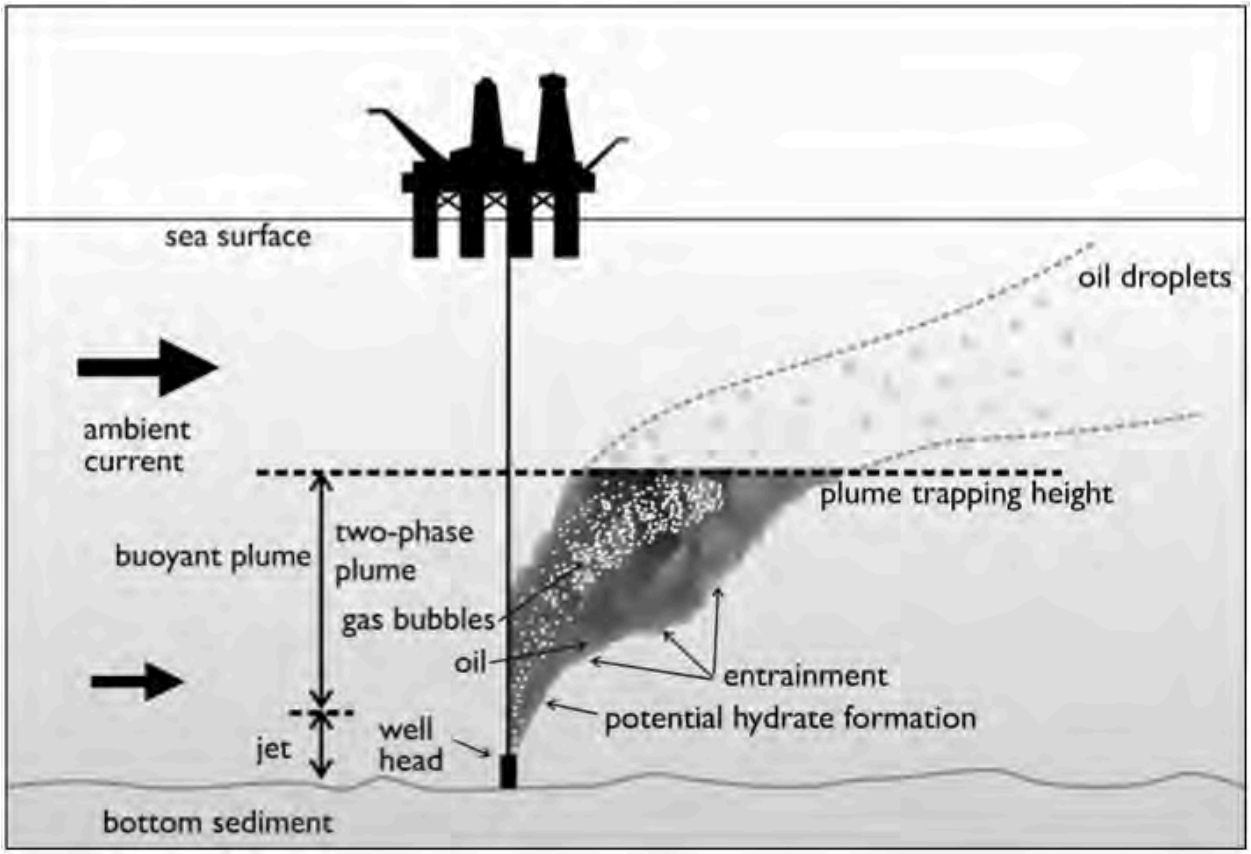

Figure 6. Blowout plume example showing the various stages of the plume in the water column for a scenario where the blowout plume traps below the water surface.

As water depths become deeper (> 200 m) the basic dynamics of the oil/gas jet/plume become more complicated, principally due to the increase in hydrostatic pressure at the seabed which leads to the possibility of the formation of gas hydrate solids. Gas hydrates constitute a class of solids in which small molecules occupy almost spherical holes in ice-like lattices made up of hydrogen-bonded water molecules. This class of solids is known as clathrates. Clathrate compounds are characterized by the structural combinations of two substances which remain associated not through strong attractive forces, but because strong mutual binding of the

molecules of one sort makes possible the firm enclosure of the other. Hydrate formation was not modelled for this study.

A review of the literature shows that our understanding and ability to model the dynamics of rising oil and gas plumes in shallow water is extensively developed. Early work by Fannelop and Sjoen (1980a,b), Spaulding (1982), and Milgram (1983), using integral plume theory, has been extended by Rye (1994) and Kolluru (1993) into operational models to predict plume dynamics and oil concentrations. Zheng and Yapa (1997;1998;1999) have further developed and refined this basic approach for buoyant oil jets and smoke plumes. Their model has been extensively tested against analytic and theoretical results and laboratory and field experiments. Rye et al. (1996) describe a 1995 experiment in the North Sea. In all cases the models performed well against theory and field observations. They also correctly predicted the height of the transition zone from when oil transport was dominated by plume dynamics to when oil droplet rise velocities dominated its movement.

3.5.2 Modelling a Deepwater Blowout

The OILMAP Deep™ model incorporates basic dynamics of the oil/gas jet/plume and the complications from increased hydrostatic pressure at depths deeper than 200 m. The blowout plume models the jet created due to the momentum of the oil discharge, the density difference between the expanding gas bubbles in the plume and the receiving water, the entrainment of seawater into the plume, the mixing by turbulence in the plume, hydrate formation, and the transport by local ambient currents.

For oil discharged during a deep water blowout, the oil droplet size distribution has a profound effect on how oil is transported after the initial release as a buoyant plume, as the size of the individual droplets dictates how long the oil will remain suspended in the water column. Large droplets will reach the surface faster than small ones, potentially generating a floating oil slick that is transported by winds and surface currents. Small droplets will remain in the water column longer than the large droplets and be subjected to the subsurface advection-diffusion transport. As the oil is transported by subsurface currents away from the well site, natural dispersion of the oil droplets quickly reduces aromatic and hydrocarbon component concentrations in the water column, with decreasing concentration at increasing distance away from the well site. However, lower rise velocities of the oil droplets correspond to longer residence times of oil suspended in the water column and thus a larger volume of affected water.

The droplet size distribution was calculated using the specific release parameters at each spill location. The droplet size distribution predicted by OILMAP Deep™ was calculated based on an estimate of a characteristic diameter (d95) and the Rosin-Rammler distribution. The predicted d95 is most heavily influenced by the exit velocity of the discharge, which is an indicator of the energy associated with the release, and the volume of oil released. The interfacial tension (IFT) of the oil is relatively low for a crude and results in smaller droplets.

The results obtained from OILMAP Deep™ are an intermediate step in the ultimate trajectory modelling. These outputs were used as the initial conditions of the far-field modelling conducted in SIMAP and include the:

- Location and size of the plume at the termination height, and
- Characterization of the oil droplets size distribution.

A more detailed review of the theory and implementation of blowout modelling may be found in Appendix B.

3.5.3 Blowout Model Scenarios

The blowout model was used to simulate the plume trap height and droplet size distributions for two different sites, each with one flow rate and oil as well as an annually averaged water column profile. The pertinent modelling inputs for each scenario are summarized in Table 9. The blowout modelling requires specification of the water column profile of temperature and density. The profiles for Sites 1 & 2 are shown in respectively (Figure 7).

Table 9. Blowout scenario parameters.

Spill Site	Water Depth (m)	Oil Release Rate (bpd)	Oil Density @ 15 ° C (g/cm^3)	Oil- Water Interfacial Tension (dyne/cm)	Gas to Oil Ratio (GOR) (scf/stb)	Pipe Diameter (inches)	Discharge Temperature (° C)
Site 1	1,770	24,900	0.83	28	1,000	12.13	85
Site 2	2,500	49,150	0.83	28	1,000	12.13	85

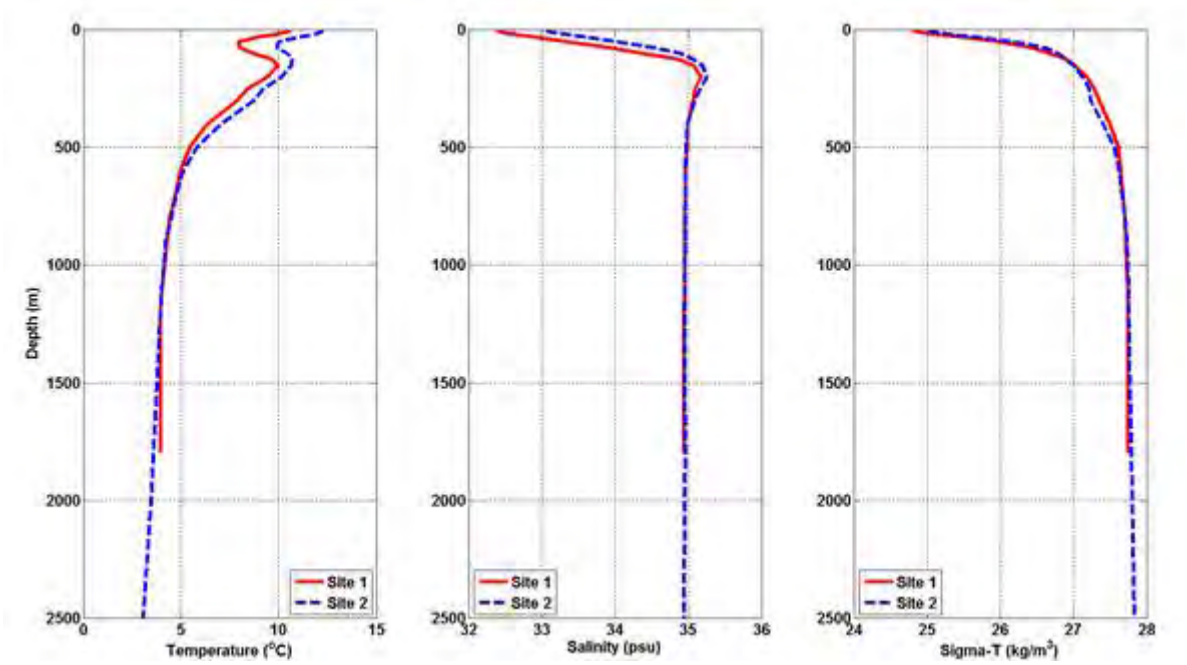

Figure 7. Water column profiles of temperature (left), salinity (middle) and corresponding density (right), represented as sigma-t. The density profile was generated based on the temperature and salinity profile using equations of state as published by UNESCO, 1981 (EOS-80).

3.5.4 Blowout Model Results

The droplet size distribution and volume of oil within each droplet size bin was characterized individually for each release location and is summarized in Table 10. The individual and cumulative droplet size distributions for both sites are depicted in Figure 8 and Figure 9, respectively. The model predicted trap height (or depth at which trapping is expected to occur) for Site 1 is 1319 m below the surface and for Site 2 is 2113 m below the surface. The free rise velocity in metres per hour is presented in Figure 10. This figure illustrates both the approximate

free rise for droplets of the oil over an extended range of sizes as well as the model predictions for rise velocity for the release conditions. Note that the free rise velocity changes slightly as the density differential between oil and water changes, and therefore changes as the oil decays and as it enters different regimes of density within the water column. The far field model continually updates the actual rise velocity throughout the simulation.

Table 10. Droplet size distribution and bins for hypothetical spill Site 1 and 2.

Site 1 Depth of Plume Trapping = 1319 m				*Site 2 Depth of Plume Trapping = 2113 m*		
Diameter (µm)	**Percent**	**Cumulative Percent**		**Diameter (µm)**	**Percent**	**Cumulative Percent**
1,181	13.12	13.12		1,429	8.31	8.31
2,363	21.84	34.96		2,857	15.27	23.58
3,544	21.67	56.64		4,286	17.73	41.31
4,726	17.67	74.30		5,714	17.69	59.00
5,907	12.65	86.95		7,143	16.12	75.12
7,088	8.19	95.13		8,571	13.75	88.87
8,270	4.87	100.00		10,000	11.13	100.00

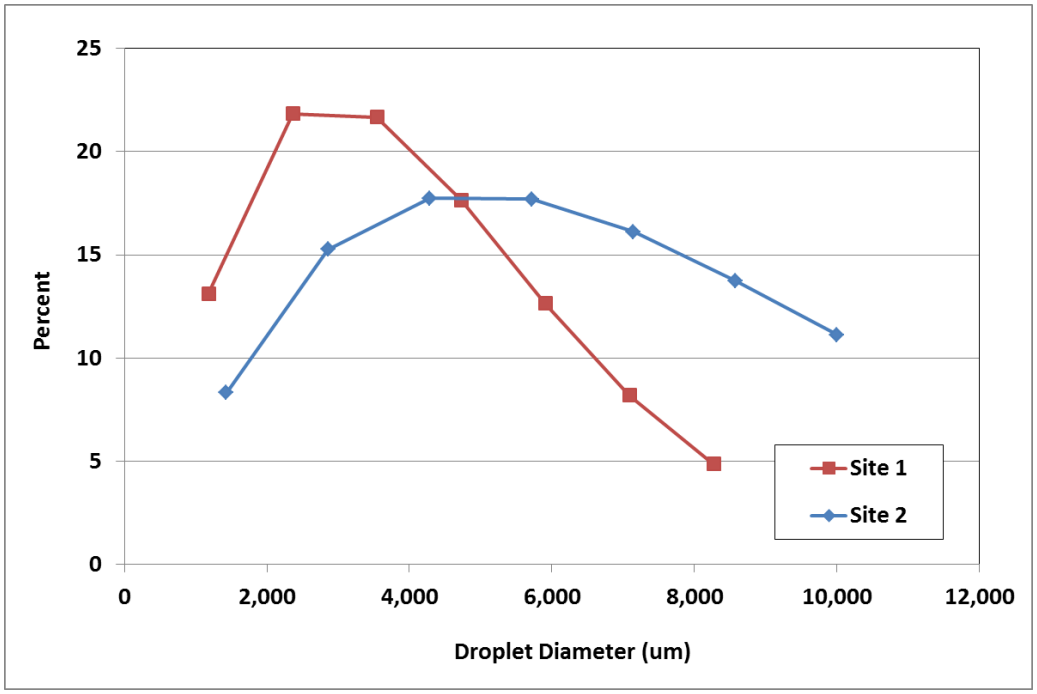

Figure 8. Individual droplet size distributions for Site 1 (red) and Site 2 (blue), representing distribution of mass used in far-field modelling.

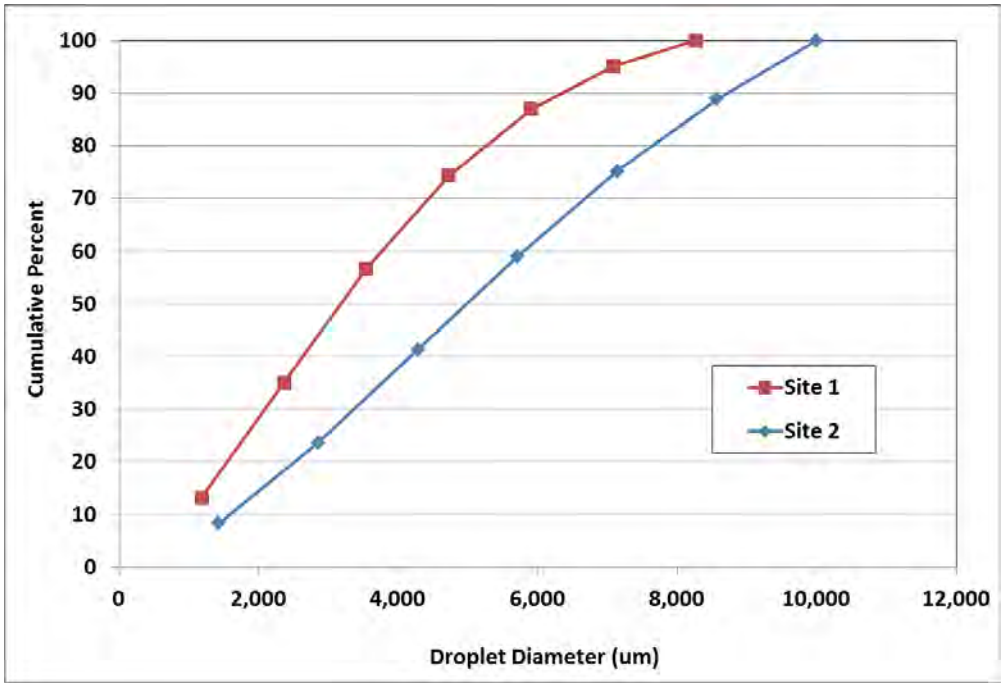

Figure 9. Cumulative droplet size distributions for Site 1 (red) and Site 2 (blue) of the distribution of mass used in far-field modelling.

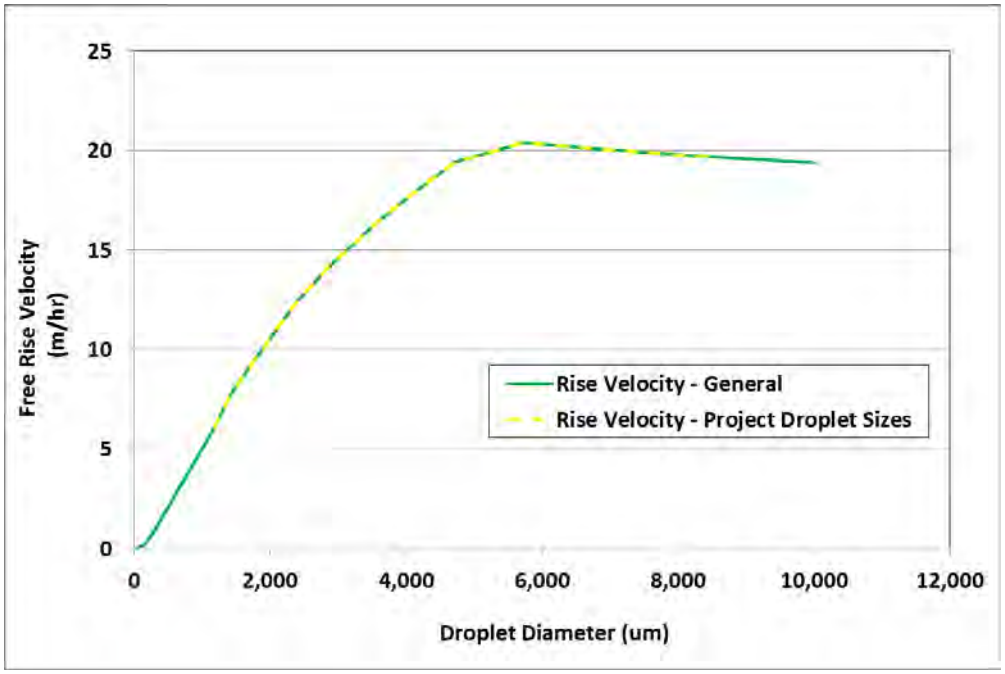

Figure 10. Free rise velocity as a function of droplet size for the project oil for both the predicted size range of the two sites as well as an extended range for general reference.

3.6 TRAJECTORY AND FATE MODELLING WITH SIMAP™

3.6.1 GENERAL SIMAP™ DESCRIPTION

The SIMAP™ modification of the Natural Resource Damage Assessment Model for Coastal and Marine Environments (NRDAM/CME) model (developed by Applied Science Associates (ASA) for use by the U.S. Department of the Interior in CERCLA NRDA type A regulations and for oil spill assessments under the U.S. Oil Pollution Act (OPA)) was used for this study. This model comprises three-dimensional oil fate and biological effects models that assess acute effects and provide data to estimate ecological and socioeconomic effects of spills in marine and freshwater environments.

In order to determine the range of effects to resources, multiple subsea release scenarios and environmental conditions were evaluated.

Model input data was prepared for the area and surrounding region where the spills were simulated. RPS ASA's data input requirements for this oil spill modelling study included:

- Description of the spill scenarios (e.g., volume and duration of the oil releases);
- Description of the deep subsea blowout release parameters;
- Quantification of the physical and chemical properties of the oil;
- Geo-referenced shoreline (definition of the land and water boundaries), classified shore types/habitats, and bathymetric (water depth) mapping;
- Characterization of the winds for the area of interest (long-term wind time series);
- Characterization of the major circulation features of the water body (long-term hydrodynamic time series); and
- Characterization of the vertical structure of the water column (temperature and salinity).

Depending on the environmental conditions near the spill location, there may also be significant degradation (decay) of the oil before surfacing occurs. The oil decay rate is variable in different environments where biological productivity may be high and microbial organisms may play an active role in the breakdown of oil. Thus, if the oil remains in the water column longer, there may be significantly less oil by mass that eventually surfaces.

The SIMAP™ model breaks down whole oil into three categories of aromatic (AR) and aliphatic (AL) constituents, based upon boiling point and solubility. This number of components provides sufficient accuracy for the evaporation and dissolution calculations, particularly given the time frame (minutes) over which dissolution occurs from small droplets and the rapid resurfacing of large droplets. The AR fraction is allowed to evaporate into the atmosphere and dissolve into the water column, while the AL fraction may only evaporate. The alternative of treating oil as a single compound with empirically-derived rates (e.g., Mackay et al., 1980; Stiver and Mackay, 1984) does not provide sufficient accuracy for environmental effects analyses because the effects to water column organisms are caused by monoaromatics (MAHs) and polycyclic

aromatic hydrocarbons (PAH), which have specific properties that differ from the other volatile and soluble compounds.

In turbulent waters (e.g., during storms or riverine environments) and at higher wind speeds than about 12 knots, oil will entrain into the water column, unless it has become too viscous to do so after weathering and the formation of mousse. Once oil is entrained in the water in the form of small droplets, MAHs and PAHs dissolve into the water column over time. The MAHs and PAHs are the most toxic portion of the oil by virtue of their relative solubility in water, making them available to aquatic biota for uptake. The dissolution rate of MAHs and PAHs from entrained oil is very sensitive to the droplet size (because it involves mass transfer across the surface area of the droplet), and the amount of hydrocarbon mass dissolved is a function of the mass entrained and droplet size distribution. These are in turn a function of soluble hydrocarbon content of the oil, the amount of evaporation of these components before entrainment from the water surface, oil viscosity (which increases as the oil weathers and emulsifies), oil surface tension (which may be reduced by surfactant dispersants), and the energy in the system (the higher the energy the smaller the droplets). Large droplets (greater than a few hundred microns in diameter) resurface rapidly, and so dissolution from those is also inconsequential. Dispersant application facilitates the entrainment of oil into the water in a smaller size distribution than would occur naturally with the median droplet size about 20 µm (Lunel, 1993a,b).

Thus, the fate of MAHs and lighter or more volatile PAHs in surface oil is primarily volatilization to the atmosphere, rather than to the water unless entrainment of the surface oil into the water is significant. If oil is entrained before it has weathered and lost the lower molecular weight aromatics to the atmosphere, dissolved MAHs and PAHs in the water can reach concentrations where they can affect water column organisms or bottom communities (French McCay and Payne, 2001).

A more complete description of the physical fates, modelled processes and algorithms, and example applications and validations of SIMAP^{TM} may be found in Appendix A. Additional descriptions of the algorithms and assumptions in the model are detailed in published papers (French McCay, 2002; 2003; 2004; 2009). The model has been validated with more than 20 case histories, including the *Exxon Valdez* and other large spills (French and Rines, 1997; French McCay, 2003; 2004; French McCay and Rowe, 2004) as well as test spills designed to verify the model (French et al., 1997).

3.6.2 SIMAP^{TM} Model Output

The SIMAP^{TM} physical fates model creates output files recording the distribution of a spilled substance in three dimensional space and time. The quantities recorded are:

- cumulative area covered by oil and thickness on the water surface ("swept area");
- volumes in the water column at various concentrations of dissolved aromatics;
- volumes in the water column at various concentrations of total hydrocarbons in suspended droplets;

- total hydrocarbon and aromatic mass in surface sediment;
- lengths and locations of shoreline affected by oil and volume of oil ashore in each segment.

The dissolved aromatic hydrocarbon concentration in the water column is calculated from the mass in the Lagrangian elements, as follows. Concentration is contoured on a three dimensional Lagrangian grid system. This grid is scaled each time step to just cover the volume occupied by aromatic particles, including the dispersion around each particle centre. This maximizes the resolution of the contour map at each time step and reduces error caused by averaging mass over large cell volumes. Distribution of mass around the particle centre is described as Gaussian in three dimensions, with one standard deviation equal to twice the diffusive distance ($2D_xt$ in the horizontal, $2D_zt$ in the vertical, where D_x is the horizontal and D_z is the vertical diffusion coefficient, and t is particle age). The plume grid edges are set at one standard deviation out from the outer-most particle. These data may be used by the biological effects model to evaluate exposure, toxicity and acute effects.

3.7 SIMAP™ Model Uncertainty

The SIMAP™ model has been developed over many years to include as much information as possible to simulate the fates and effects of oil spills. However, as in all science, there are limits to the complexity of processes that can be modelled, as well as gaps in knowledge regarding the environment that is affected, and some behaviours in ecosystems. In addition, in the unlikely event of an actual oil spill, fate and effects will be strongly determined by the specific environmental conditions, the precise locations, and a myriad of details related to any one specific event. Thus, the results contained within are a function of the scenarios simulated and the accuracy of the input data used. As described in the preceding sections, assumptions based on available scientific information and professional judgment were made in the development of the model, which represent our best assessment of the processes and potential mechanisms for effects that would result from oil spills.

The major sources of uncertainty in the oil fates and biological effects model are:

- Oil contains tens of thousands of chemicals, each with differing physical and chemical properties that determine their fate in the environment. The model must, out of necessity, treat the oil as a mixture of a limited number of components, grouping chemicals by physical and chemical properties.
- The fates model contains a series of algorithms that are simplifications of complex physical-chemical processes. These processes are understood to varying degrees.
- The model treats each spill as an isolated singular event and does not account for any potential cumulative effects.
- Various physical parameters including but not limited to the full suite of environmental parameters (e.g. hydrodynamics, winds, total suspended solids concentration, etc.) were not sampled directly for this study. The data that currently exists were applied to each

location, and other sources of information, including professional judgment as appropriate, were used to determine the parameter values implemented in the model.

The goal of this study was not to forecast every detail that could potentially occur for a given spill, but to describe a range of possible consequences that may be expected throughout any given month of the year such that an informed analysis could be made as to the likely environmental effects of oil spills under various scenarios.. Thus, the modelling is used to provide quantitative guidance in the analysis of the environmental effects.

4 MODEL RESULTS

Stochastic analyses of deep-water blowouts were modelled at Sites 1 and 2 using five years of variable environmental data and the physical-chemical properties of Federated Crude Oil (2002) found in Section 2. At each location, a total of 40 individual deterministic oil spill trajectories were modelled for each of the 12 months a year. This totaled 480 individual deterministic trajectories per year per site, for a total of 960 unique runs between the two sites. The duration of each model run was 30 days with a continuous 30-day blowout.

4.1 EXPLANATION OF MODEL RESULTS

Stochastic Analysis Results

The figures presented in the stochastic modelling results section illustrates the spatial extent of surface oiling, water column concentrations of dissolved aromatics, and shoreline oiling probabilities and associated minimum travel times for the spills. Certain scenarios did not impact every environmental compartment (e.g. shoreline oiling). Only output for an affected compartment is presented herein. These maps present model output in gridded format. For each scenario:

Probability of oiling: The map defines the area and the associated probability in which sea surface oiling, shoreline oiling, or water column contamination by dissolved aromatics, is expected to exceed the specified thresholds (Table 8) if the oil transport (direction and pathway) under specific environmental conditions included in the historical record were to occur. The coloured lines in the stochastic maps signify the boundary for given percentiles that may receive oil pollution in the event of that particular spill scenario. The darker the colour, the more likely an area would be affected. The lighter colours denote that an area is less likely to be affected. In the lower probability areas, the exact location of a particular spill event would be more difficult to predict. The probability of oiling was based on a statistical analysis of the resulting ensemble of individual trajectories for each spill scenario (40 for monthly figures and 480 for annual figures). These figures do not imply that the entire contoured area, or even a large portion, would be covered with oil in the event of a spill. These maps do not provide any information on the

quantity of oil in a given area. They simply denote the probability of oil exceeding the given threshold over the entire ensemble of runs at each point. Note that only probabilities of 1% or greater were included in the map output. Stochastic maps showing water column contamination by dissolved aromatics depict oiling frequency, but do not specify the given depth at which this occurs and does not imply that the entire water column (i.e. from surface to bottom) will experience a concentration above the threshold.

Minimum Travel Times: The footprint on this map corresponds to the associated probability of oiling map. Each figure illustrates the shortest time required for oil to exceed the defined thickness or concentration thresholds (Table 8) at each point within the footprint, from the ensemble of all individual trajectories.

As a note, the Exclusive Economic Zone (EEZ) for Canada and the United states, as well as the international border are depicted on each map to provide context in regards to the spatial extent and potentially effected territorial waters from any potential release (VLIZ, 2014). Additional sets of higher thresholds were also analysed to provide area of expected threshold exceedance for comparison with conservatively low values.

Representative Individual Trajectory Results

Representative deterministic trajectories for 95th percentile for degree of surface, shoreline, and water column effects were identified from each parent stochastic analyses conducted with the starred thresholds summarized above (Table 8). The figures presented in the individual trajectory modelling results sections include modelled trajectories, mass balance charts, time series maps of gridded floating surface oil, floating surface oil thickness, water column dissolved aromatic concentrations and profiles, shoreline oil thickness, and tables summarizing various areas associated with a range of thresholds exceeded (Table 8). Corresponding mapped results are only presented here for each type of representative deterministic trajectory (i.e., maps of surface oiling only for 95th percentile run for surface oiling; maps of shoreline impact only for 95th percentile run for shoreline oiling). Mass balance charts are presented for all representative deterministic trajectories.

Trajectories: The hydrocarbon trajectory provides a history of modelled oil throughout the modelled domain in both time and space. Components of the oil are tracked as entrained droplets of oil, dissolved aromatic constituents, floating surface oil, and stranded shoreline oil. Components are only displayed when the modelled value exceeded the starred thresholds summarized above (Table 8). Darker colours indicate the presence of a portion of the oil after the 30 day modelled period, at the last time step. The lighter shade of each (surface oil as grey, entrained oil as light blue, and dissolved aromatics as light green) indicates that oil exceeding the given threshold had previously passed through the region over the 30 day modelled period, as a swept area or time history.

1. Mass Balance: The mass balance charts provide an estimate of the oil's weathering and fate for a specific run for the entire model duration as a fraction of the oil spilled up to that point. Components of the oil tracked over time include the amount of oil on the sea surface, the total entrained hydrocarbons in the water column, amount of oil ashore, oil evaporated into the atmosphere, and that which has decayed (accounts for both photo-oxidation and biodegradation).
2. Surface Oil Time Series Maps: Maps showing the footprint of maximum floating surface oil and the associated thicknesses (µm) at all time steps during the individual 30-day spill simulation. Surface oil contamination figures show only thicknesses greater than 0.04 µm.
3. Water Column Time Series Maps: Maps showing the footprint of maximum water column concentration of dissolved aromatics (ppb) at all time steps during the individual 30-day spill simulation. Dissolved aromatics are the portion of the oil having the greatest potential to affect water column biota, and the footprints were typically smaller than the extent of total oil contamination in the water column. Water column contamination figures show only concentrations ≥1 ppb. Concentrations below 1 ppb are considered low and result in little water column impact.
4. Shoreline Impact: Figure showing mass of oil deposited onto shoreline. Only shoreline oiling exceeding 1 µm, which is equivalent to 1 g/m^2, is depicted.

4.2 Annual Oil Fates Results

A total of 480 individual model runs were conducted for both Site 1 and Site 2, representing a 30-day continuous unmitigated deep-water blowout, modelled for 30 days. Site 1 was a smaller and shallower release, at 1700 m depth and 24,900 bpd of Federated Crude oil, while Site 2 was larger and deeper, at 2500m and 49,150 bpd of Federated Crude oil. Annual summaries of stochastic analyses of potential surface oiling (Figure 11 & Figure 12) and water column contamination by dissolved aromatics (Figure 13 & Figure 14) depict an area of potential oil contamination in US waters to the east of the New England area, and in Canadian waters south of Nova Scotia and Newfoundland, for Sites 1 and 2, respectively. As a note, the sharp cut off in the southern portion of the outermost contour is an artifact of the spatial extent of the modelled domain (Figure 1).

As noted above, these large footprints are not the expected oiling from any single release of oil. In fact, the majority of the area represents a probability of oiling at less than 10%. The area with greater than 10% probability of surface oiling exceeding the threshold is much smaller (approximately 300 km x 300 km), while only an area of 50 km x 50km has a probability greater than 75% (Figure 11 & Figure 12). Water column dissolved aromatic threshold exceedance follows this general trend as well, although the area of probability >10% is slightly larger (Figure 13 & Figure 14). The Site 2 stochastic figures are shifted slightly to the east, with respect to the Site 1 figures, as the hypothetical release location is further offshore and to the east.

The shortest time for a threshold exceedance in either the surface oil or water column dissolved aromatic concentration to reach an area near shore (Nova Scotia) is in excess of 20 days for Site 1 and in excess of 30 days for Site 2.

The likelihood that shoreline oiling would occur is less than 10% for both Sites 1 and 2 (Figure 15 & Figure 16). It is expected that the oil that would strand would be highly weathered, as the minimum time to shore would be between 20-30 days. The regions susceptible to potential shoreline oiling within 30 days from a release at Site 1 include the southern tip of Nova Scotia, including the Yarmouth, Barrington, and Shelburne region, as well as Sable Island National Park. The region susceptible to potential shoreline oiling within 30 days from a release at Site 2 includes only the Sable Island National Park.

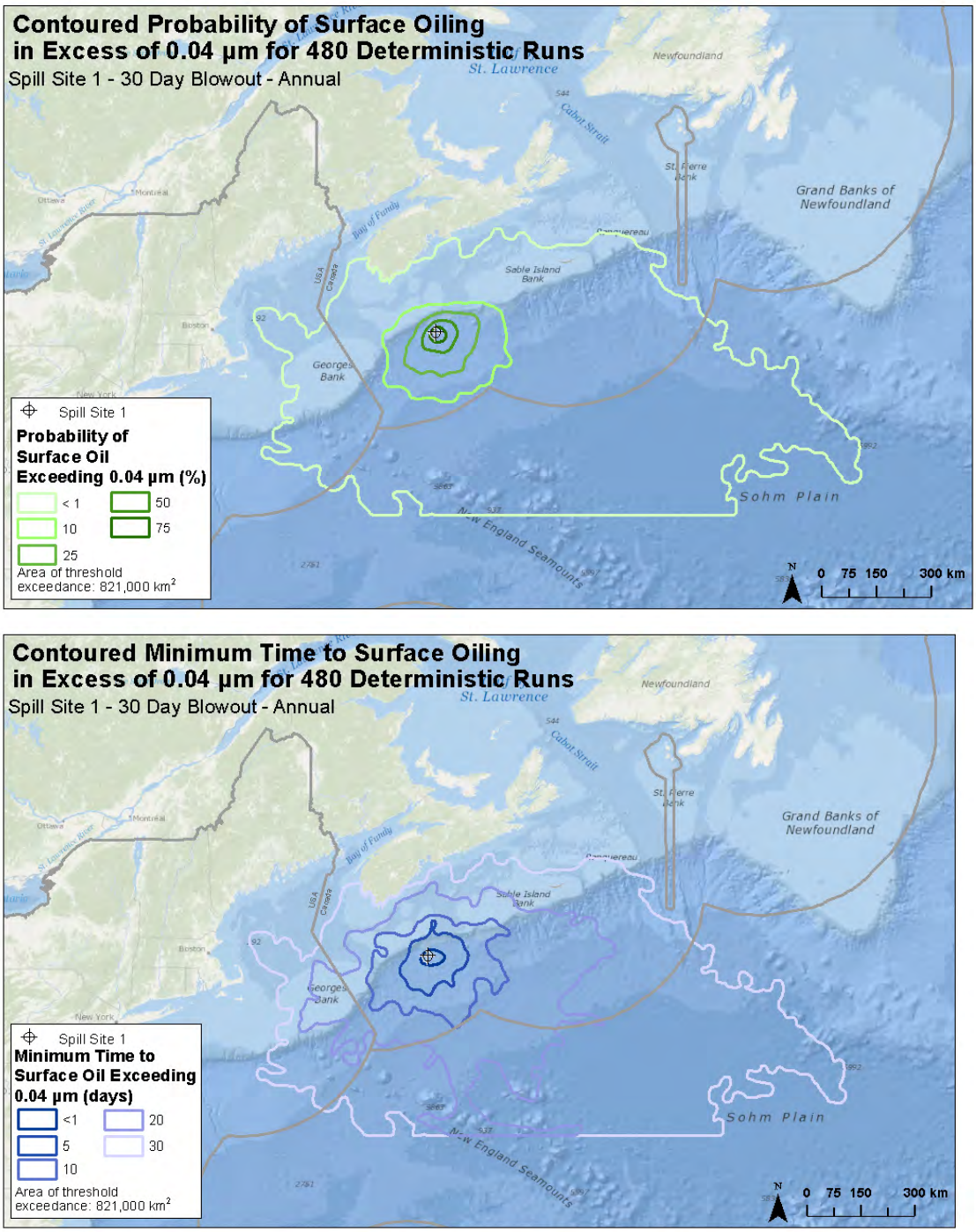

Figure 11. Annual stochastic model output (480 individual model runs) showing maps of the predicted probability of sea surface oiling exceeding the 0.04 µm thickness threshold (top panel) and the associated minimum travel times (bottom panel) for a 24,900 bpd, 30-day continuous blowout of Federated crude at Site 1.

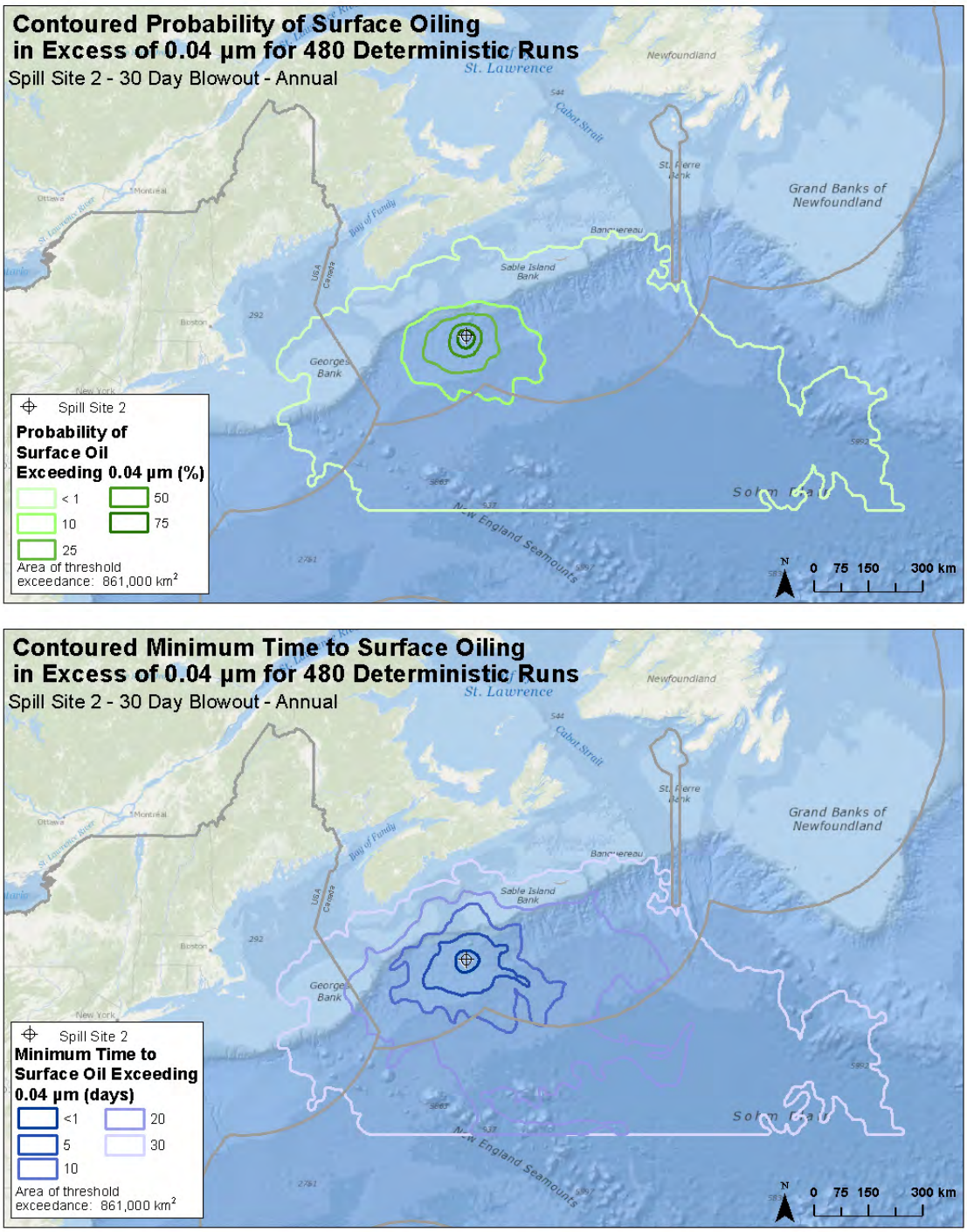

Figure 12. Annual stochastic model output (480 individual model runs) showing maps of the predicted probability of sea surface oiling exceeding the 0.04 µm thickness threshold (top panel) and the associated minimum travel times (bottom panel) for a 49,150 bpd, 30-day continuous blowout of Federated crude at Site 2.

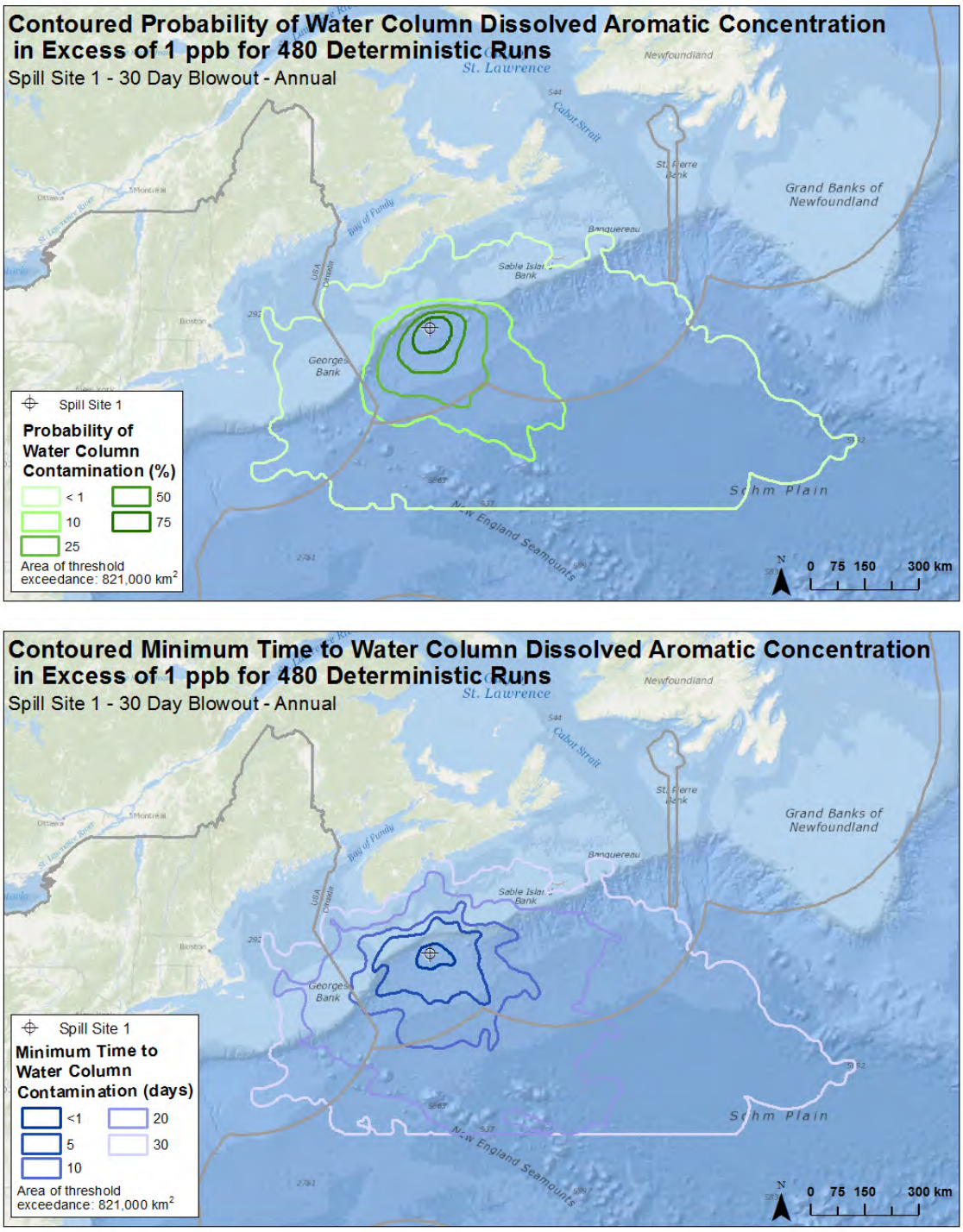

Figure 13. Annual stochastic model output (480 individual model runs) showing maps of the predicted probability of water column dissolved aromatic concentrations exceeding the 1 ppb threshold (top panel) and the associated minimum travel times (bottom panel) for a 24,900 bpd, 30-day continuous blowout of Federated crude at Site 1.

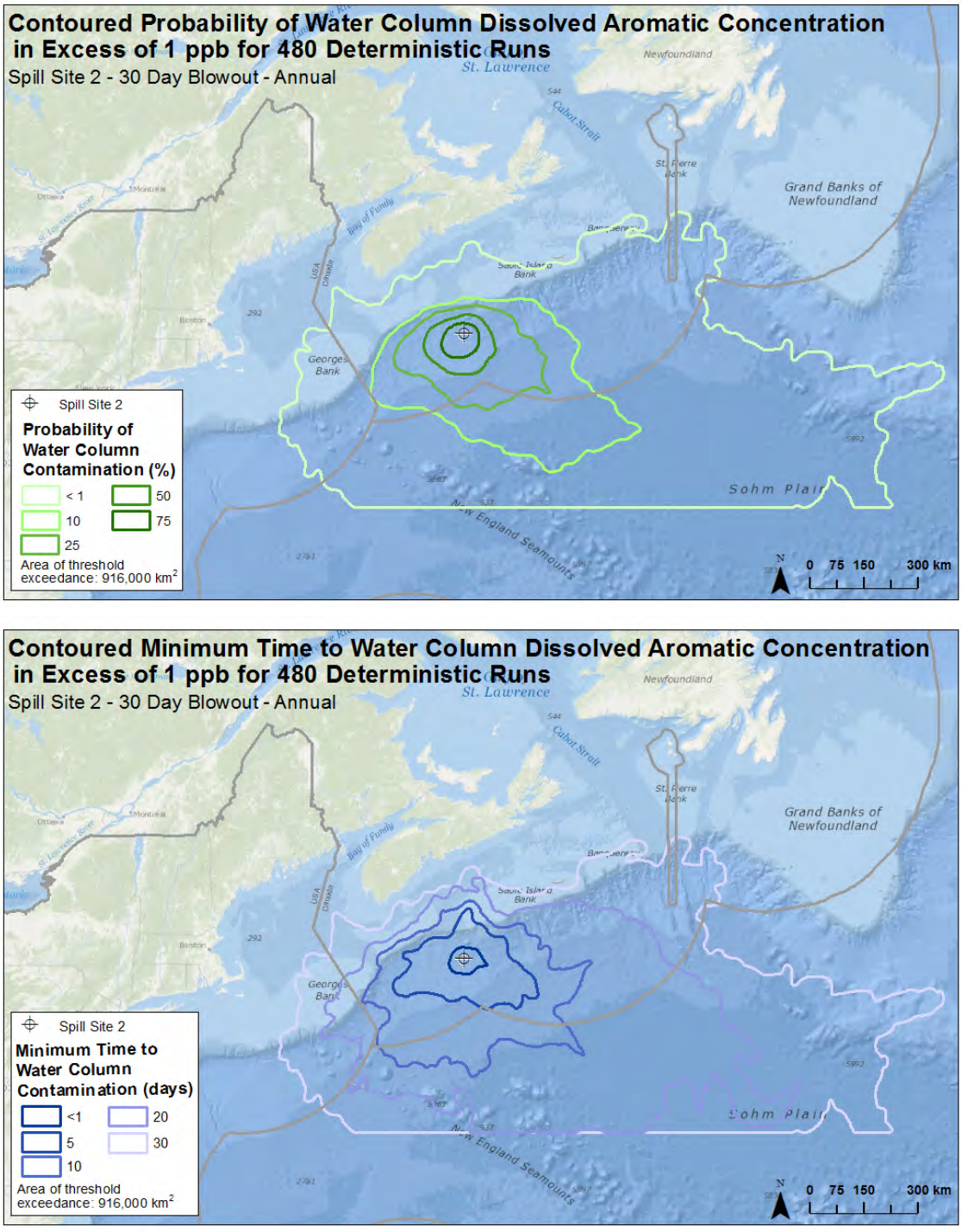

Figure 14. Annual stochastic model output (480 individual model runs) showing maps of the predicted probability of water column dissolved aromatic concentrations exceeding the 1 ppb threshold (top panel) and the associated minimum travel times (bottom panel) for a 49,150 bpd, 30-day continuous blowout of Federated crude at Site 2.

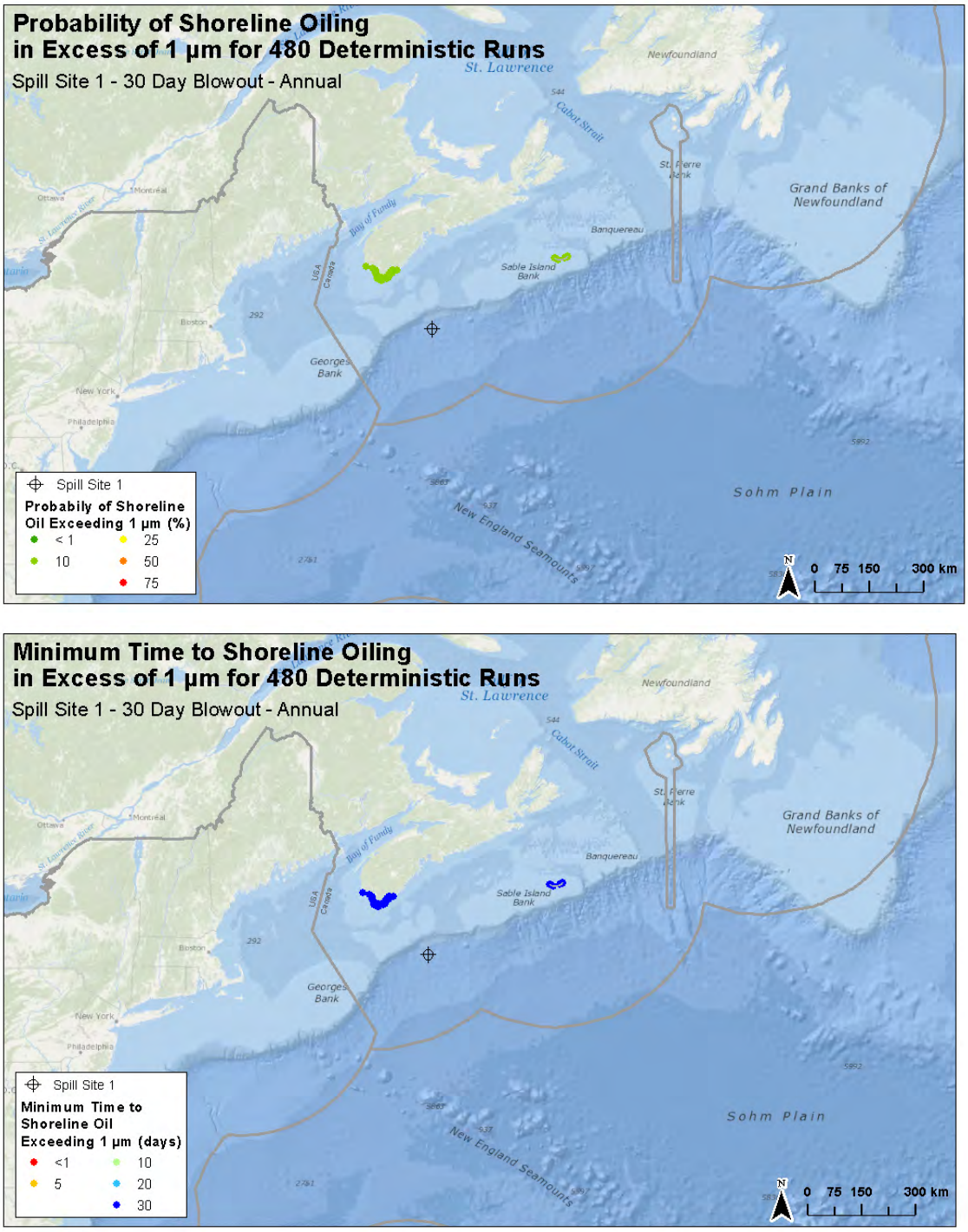

Figure 15. Annual stochastic model output (480 individual model runs) showing maps of the predicted probability of shoreline oiling exceeding the 1µm threshold (top panel) and the associated minimum travel times (bottom panel) for a 24,900 bpd, 30-day continuous blowout of Federated crude at Site 1.

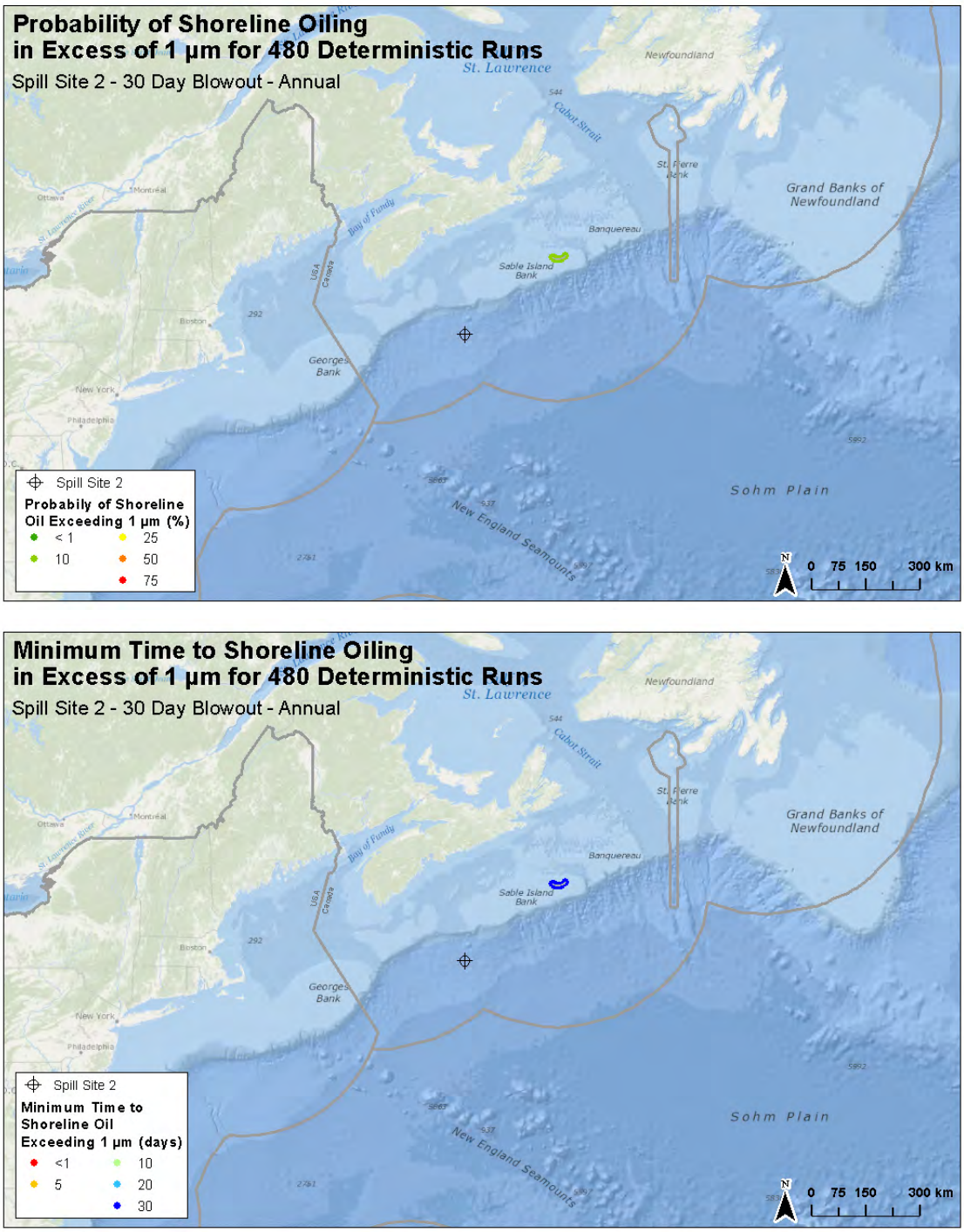

Figure 16. Annual stochastic model output (480 individual model runs) showing maps of the predicted probability of shoreline oiling exceeding the 1µm threshold (top panel) and the associated minimum travel times (bottom panel) for a 49,150 bpd, 30-day continuous blowout of Federated crude at Site 2.

4.3 MONTHLY DESCRIPTION FOR STOCHASTIC OUTPUTS

A total of 40 individual model runs were conducted for each of the 12 months of the year for each site's stochastic analyses. In general, surface oiling and water column dissolved aromatic footprints showed similarities across months, with transport predominantly to the east and northeast. However a general trend was observed in the data, with what appeared to be winter-type conditions from October through March, and summer-type conditions from April through September (Figure 17 & Figure 18). During winter conditions, oil appeared more likely to be transported to the east, while summer conditions were more variable, with a higher frequency of transport to the north and west. Site 1 seemed to have a more pronounced seasonal pattern, while the more offshore Site 2 had similar trends, but slightly damped.

The apparent seasonality in stochastic model outputs is consistent with observed hydrodynamics and wind data at hypothetical spill Sites 1 and 2, as well as the buoy data used to validate the NOGAPS wind dataset (Appendix C Figure 21 and Figure 22). During the winter, strong prevailing winds from the north and west are observed, which would transport surface oil to the east, out to sea. During the summer months, wind speeds are lower and are predominantly from the south and west, resulting in a more variable spill trajectory pattern. Additionally, there is a higher probability of winds from the east-northeast during the summer months, which would transport surface oil towards shore. Local hydrodynamics in this region are more directionally variable at the surface (Appendix C: Figure 6 and Figure 7). The resulting combination of both wind and currents yields slightly more circular (increased variability in trajectory) patterns during the summer, with a higher likelihood of shore oiling, and slightly more skewed (higher probability of transport offshore and to the east) patterns during the winter.

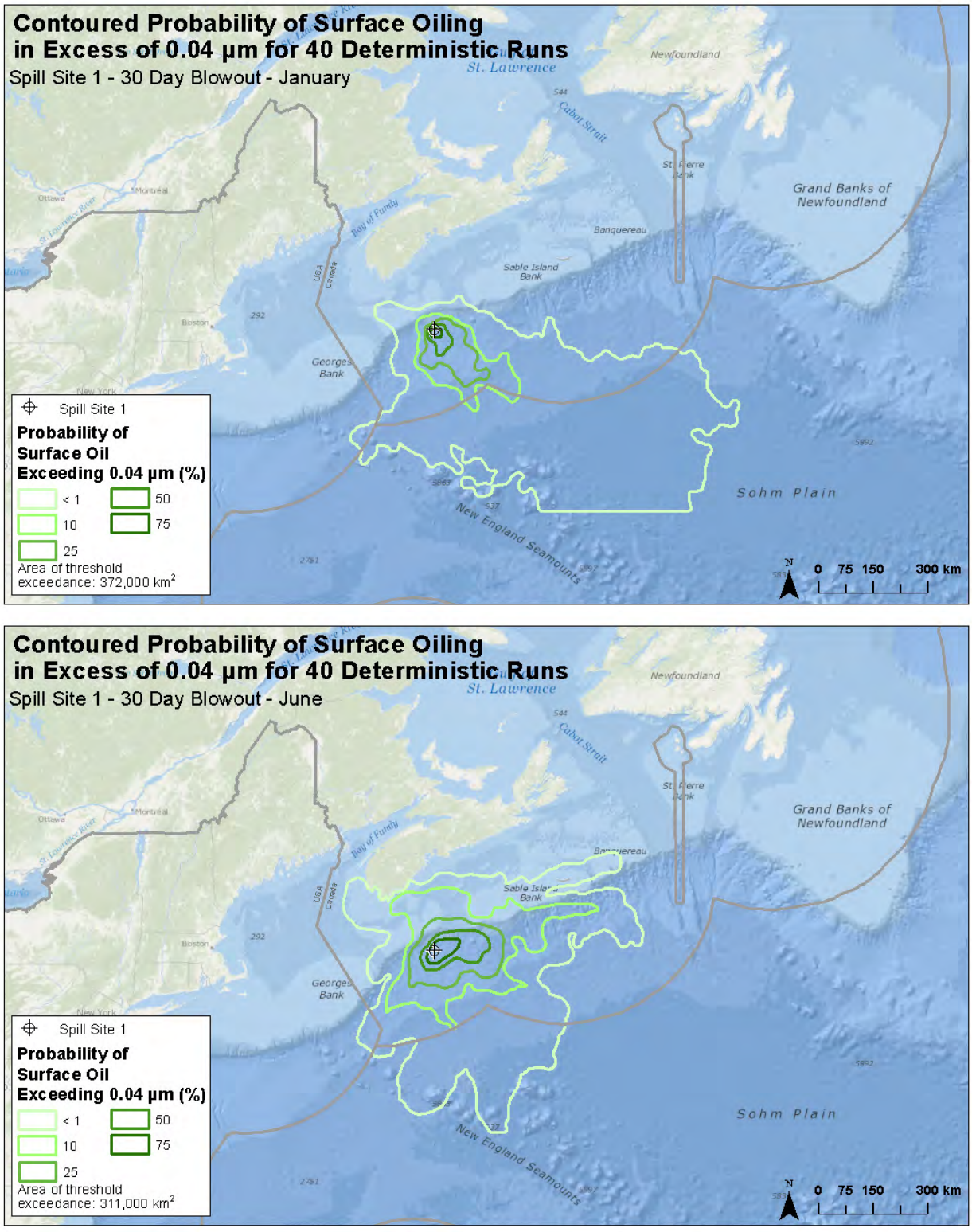

Figure 17. Stochastic contoured probability of surface oiling in excess of 0.04 µm for Site 1. January (top) depicts a more eastward transport of surface oil, while June (bottom) depicts more variable transport and a higher likelihood of shoreline oiling.

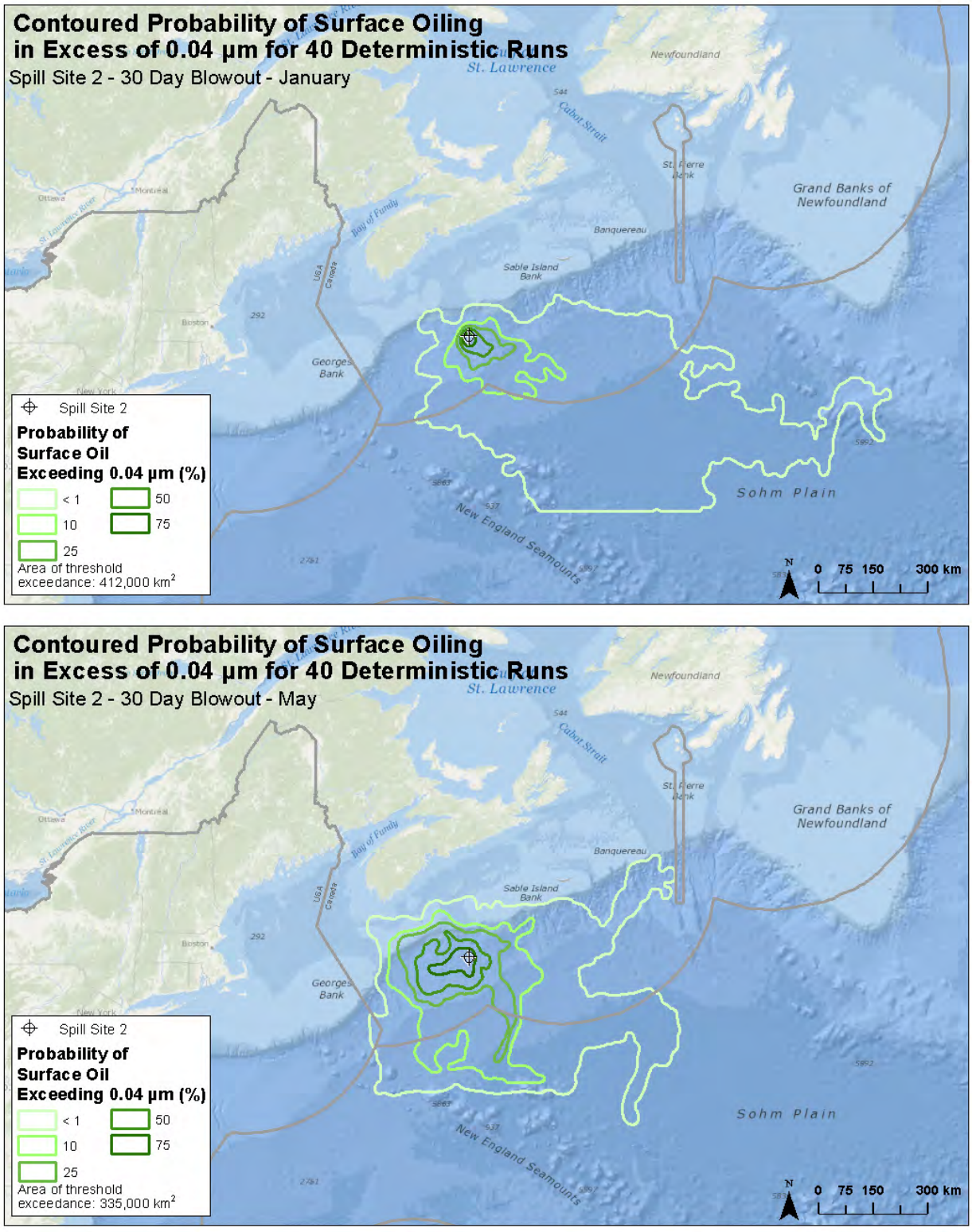

Figure 18. Stochastic contoured probability of surface oiling in excess of 0.04 µm for Site 2. January (top) depicts a more eastward transport of surface oil, while May (bottom) depicts more variable transport.

4.4 REPRESENTATIVE DETERMINISTIC CASES

The 95th percentile results for oil exposure for surface oiling, water column dissolved aromatic concentrations, and shoreline oiling were identified for each of the 12 monthly stochastic model scenarios. These identified cases were separated into winter and summer bins, and the scenario with the maximum effects within each seasonal bin was identified and run as an individual deterministic trajectory. Therefore, the month and individual run for maximum surface oiling effects for summer differed from the month and individual run for maximum water column dissolved aromatics effects for summer. This report contains figures corresponding to each identified representative case (e.g. shoreline oiling figure for the 95th percentile shoreline oiling scenario).

The representative deterministic cases identified for surface oiling, water column dissolved aromatic contamination, and shoreline oiling, comprising the individual trajectory that resulted in the 95th percentile effects from each stochastic analysis for Sites 1 and 2 are provided for both winter and summer seasons. Included in these tables are the areas exceeding specific thresholds (Table 11).

Table 11. Representative deterministic cases and associated areas exceeding specified thresholds for Sites 1 and 2.

SITE 1	Season	Modelled Start Date	Area Exceeding Thresholds
Surface Oiling Effects (95th Percentile)	Winter	2010 Mar. 18 02:02	0.04 µm = 40,800 km^2 10µm = 2,500 km^2
	Summer	2009 July 14 19:08	0.04 µm = 75,300 km^2 10µm =2,300 km^2
Water Column Dissolved Aromatic Effects (95th Percentile)	Winter	2008 Dec. 8 04:52	1 ppb dissolved aromatics = 57,400 km^2 (approximately equivalent to 1ppm TPH)
	Summer	2010 Sep. 27 17:04	1 ppb dissolved aromatics = 58,600 km^2 (approximately equivalent to 1ppm TPH)
Shoreline Oiling Effects (95th Percentile)	Summer	2009 June 10 06:22	1 µm = 110 km 10µm = 110 km
SITE 2	**Season**	**Modelled Start Date**	**Area Exceeding Thresholds**
Surface Oiling Effects (95th Percentile)	Winter	2010 Mar. 16 19:17	0.04 µm = 33,100 km^2 10µm = 2,300 km^2
	Summer	2009 Aug. 7 06:59	0.04 µm = 83,500 km^2 10µm = 7,300 km^2
Water Column Dissolved Aromatic Effects (95th Percentile)	Winter	2009 Dec. 8 21:33	1 ppb dissolved aromatics = 204,000 km^2 (equivalent to 1ppm TPH)
	Summer	2010 Apr. 30 00:19	1 ppb dissolved aromatics = 74,400 km^2 (equivalent to 1ppm TPH)
Shoreline Oiling Effects (95th Percentile)	Summer	N/A	N/A

The hydrocarbon trajectory provides a history of each individual particle of oil throughout the modelled domain in both time and space. Components of the oil were tracked as entrained droplets of oil, dissolved aromatic constituents, floating surface oil, and stranded shoreline oil. Darker colours indicate the presence of a portion of the oil after the 30 day modelled period, at the last time step. The lighter shade of each (surface oil as grey, entrained oil as light blue, and dissolved aromatics as light green) indicates that oil exceeding the given threshold had previously passed through the region over the 30 day modelled period, as a swept area or time history. The hydrocarbon trajectory for the 95th percentile surface scenario for Site 2 during the summer is provided as an example trajectory (Figure 21), along with the spatial extent of surface oil in excess of 0.04 µm at given time steps into the spill (Figure 22).

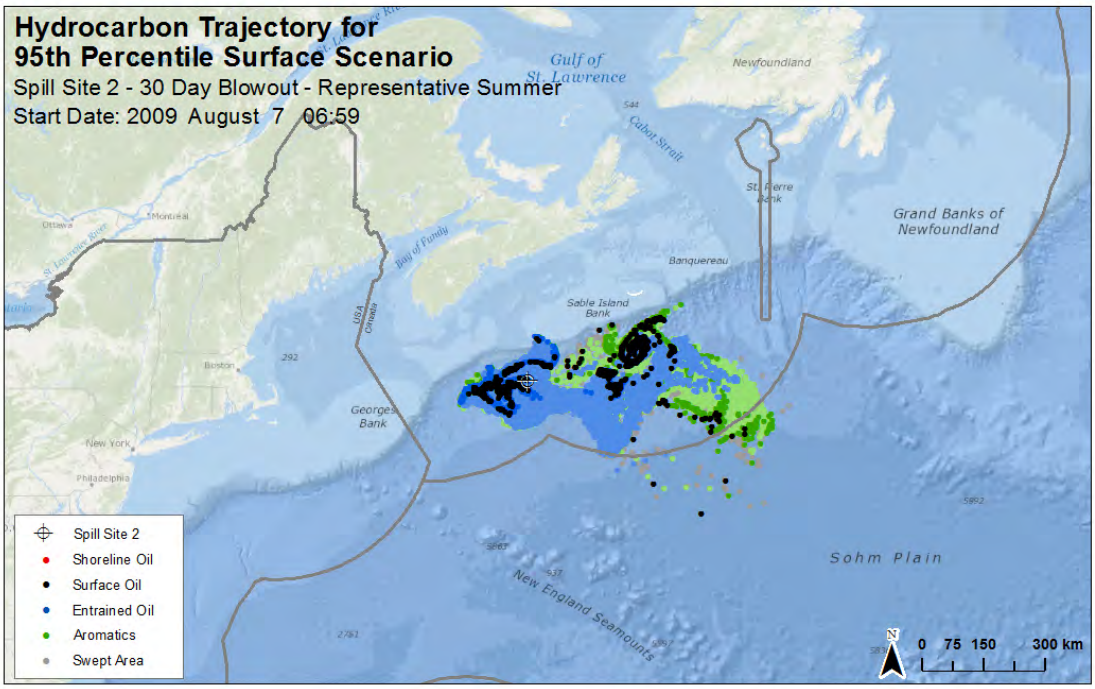

Figure 19. Particle trajectory map for the representative deterministic Site 2 summer scenario for 95th percentile surface oil exposure**.**

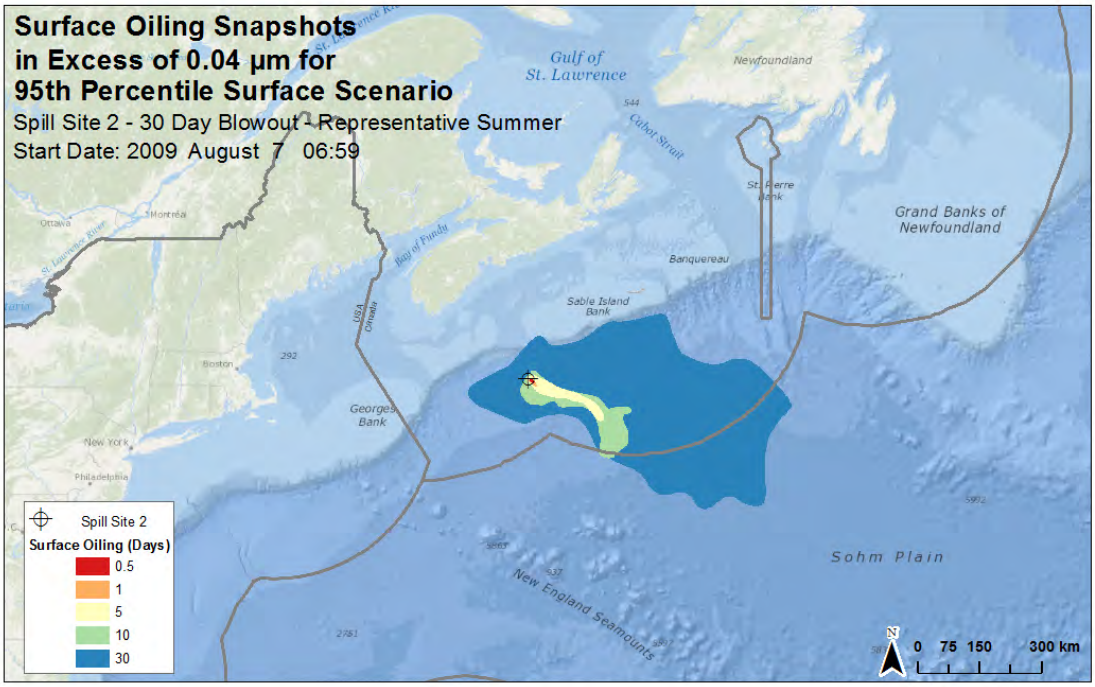

Figure 20. Extent of surface oiling in excess of 0.04 µm at given time steps (days after spill start) for the representative deterministic Site 2 summer scenario for 95th percentile surface oil exposure.

4.4.1 Surface Oiling Cases

Identified 95th percentile surface oiling scenarios had a maximum of approximately 10-20% of the total mass of the released oil on the surface at any one time (Figure 21, Figure 22, Figure 23, and Figure 24). In general, winter type conditions and their associated strong wind and waves only had approximately 5-10% of the total mass of oil on the surface, while the more quiescent summer conditions resulted in closer to 10-20% of the total mass of oil on the surface

Federated crude oil is relatively light, with a high propensity to volatilize. For the winter cases, a little less than 50% of the total oil spilled evaporates into the atmosphere, while for the summer cases, a little more than 50% of the total oil spilled evaporates to the atmosphere.

During winter conditions, lower temperatures (as opposed to summer) reduce weathering and evaporation rates, thus maintaining fresher and therefore lower viscosity oil. The higher wind speeds and associated waves result in significantly more entrainment during the winter months, forcing a larger percentage of surface oil into the water column, when compared to the summer (Appendix C: Figure 19 and Figure 20)

The slightly thicker, more viscous oil found during the warmer and more quiescent summer conditions is the result of higher weathering and evaporation rates, which increases the surface oil viscosity and thickness, thus reducing the likelihood that oil will be entrained into the water column. A greater areal extent of surface oiling is observed during the summer, the result of reduced entrainment (from higher viscosity and more quiescent conditions) and resulting surface transport (Table 11). In general, only a small area of the surface water affected by oil exceeds the 1 µm threshold, as only 3-6 % of the total areal coverage is in excess of 0.04 µm for Site 1 and 7-9 % for Site 2. The higher value for Site 2 scenarios is the result of the larger volume of oil released, nearly double that of Site 1.

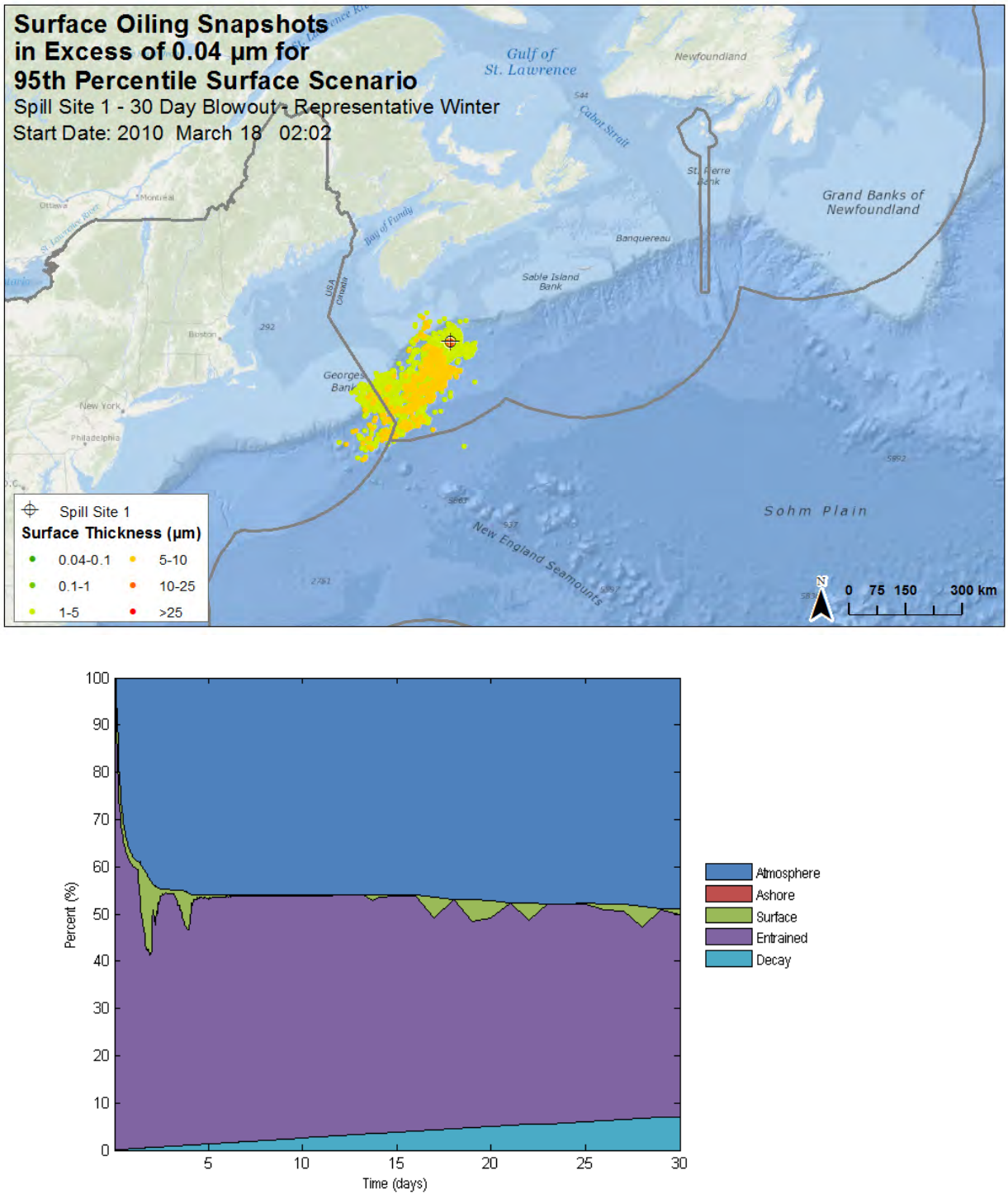

Figure 21. Representative Site 1 winter deterministic scenario for 95th percentile surface oil thickness (top). The maximum thickness of surface oil in excess of 0.04 µm is displayed at all modelled time steps. The associated mass balance graph is included (bottom).

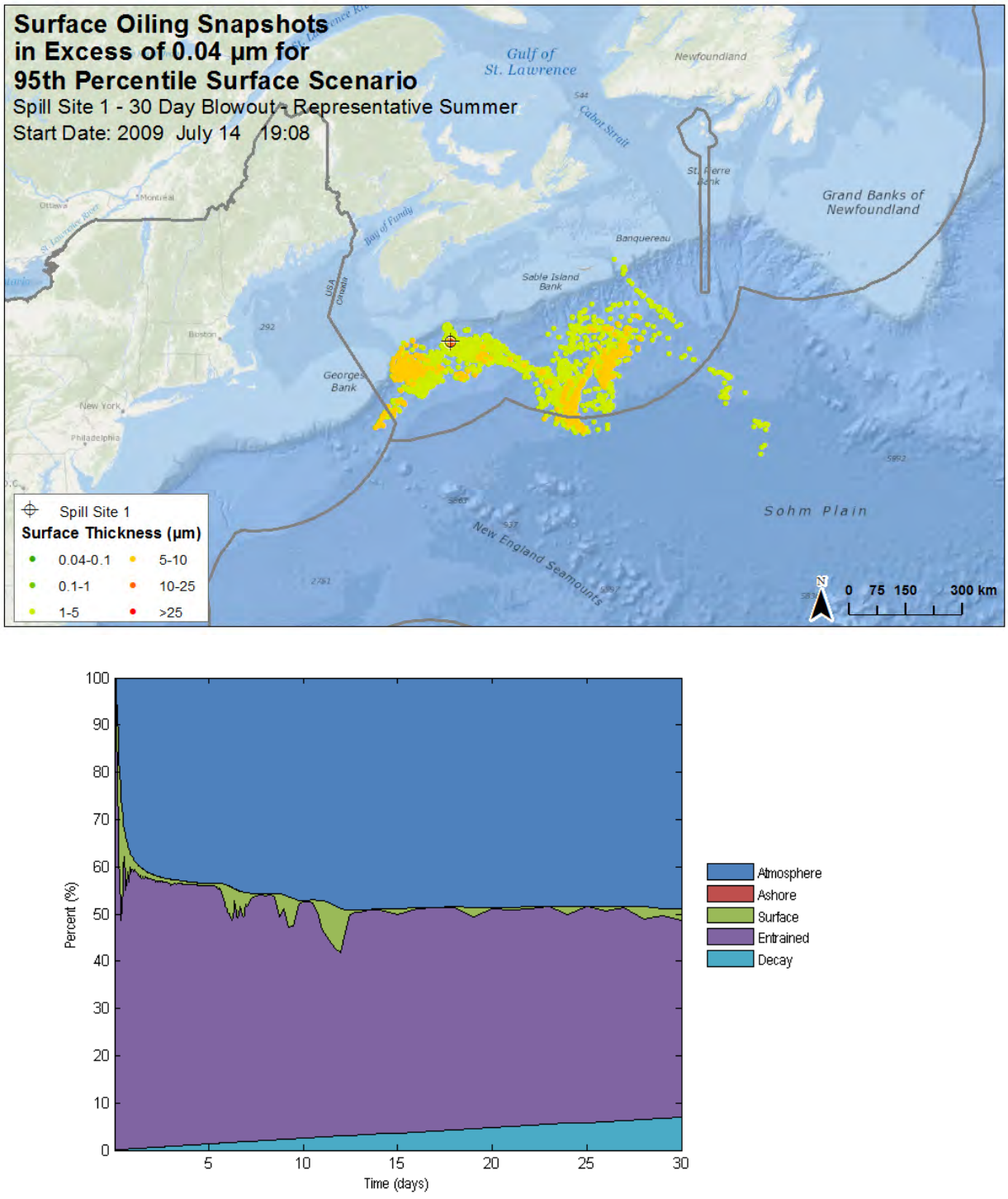

Figure 22. Representative Site 1 summer deterministic scenario for 95th percentile surface oil thickness (top). The maximum thickness of surface oil in excess of 0.04 µm is displayed at all modelled time steps. The associated mass balance graph is included (bottom).

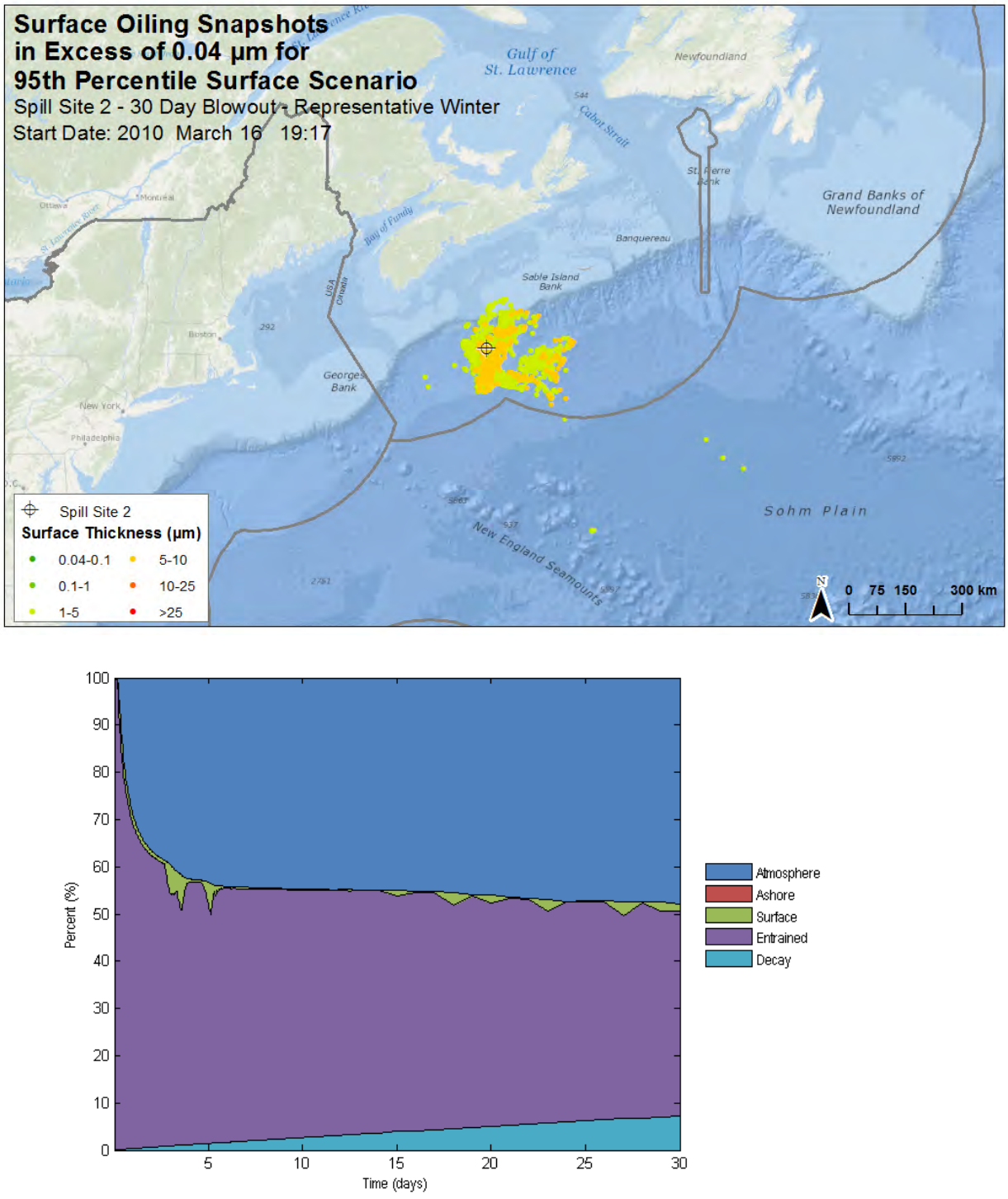

Figure 23. Representative Site 2 winter deterministic scenario for 95th percentile surface oil thickness (top). The maximum thickness of surface oil in excess of 0.04 µm is displayed at all modelled time steps. The associated mass balance graph is included (bottom).

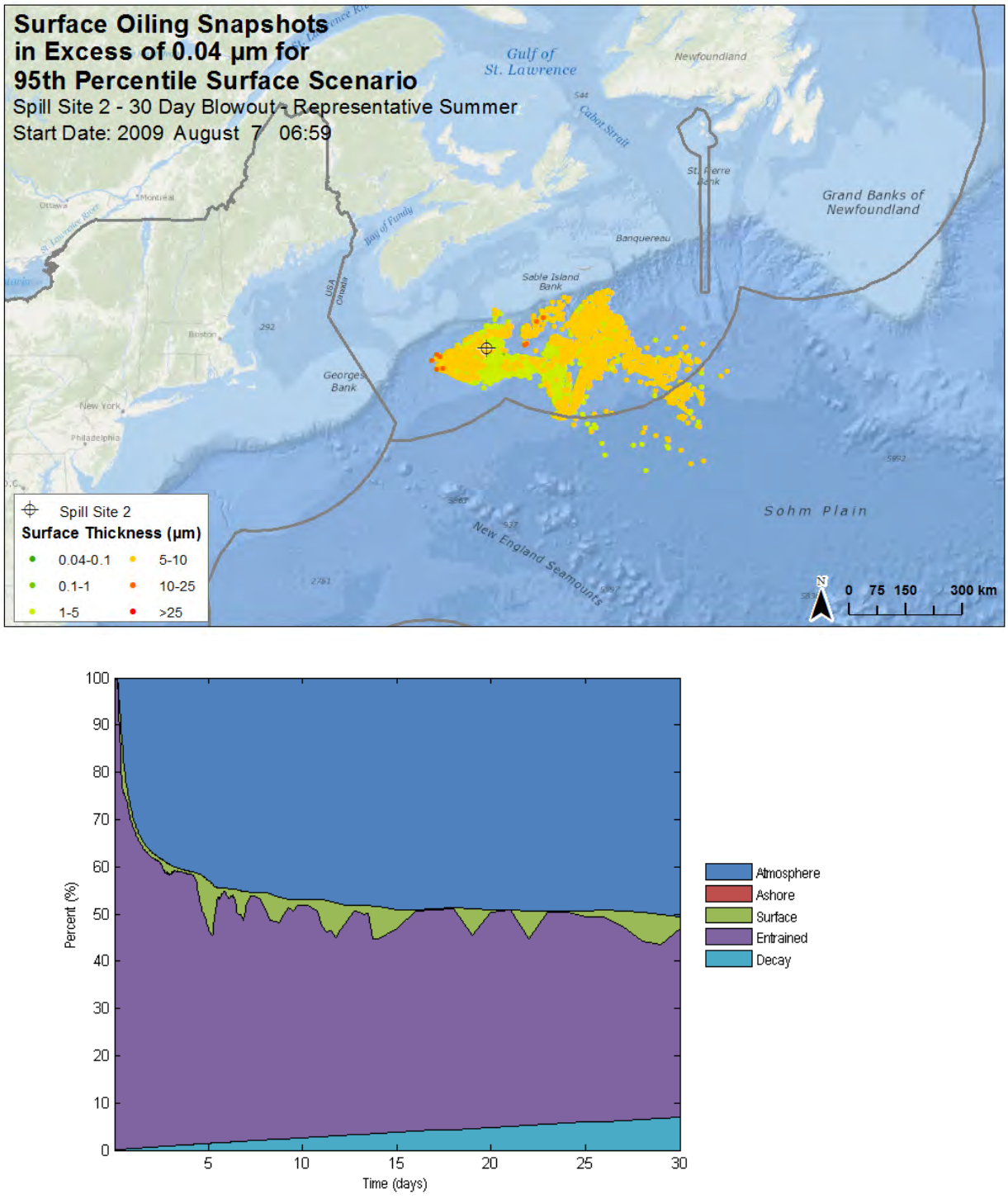

Figure 24. Representative Site 2 summer deterministic scenario for 95th percentile surface oil thickness (top). The maximum thickness of surface oil in excess of 0.04 µm is displayed at all modelled time steps. The associated mass balance graph is included (bottom).

4.4.2 Water Column Dissolved Aromatic Exposure Cases

Identified 95th percentile water column dissolved aromatic exposure scenarios have regions of high dissolved aromatic concentrations localized around the wellhead, with highest observed concentrations near the surface (Figure 25). Dissolved aromatic concentration in the water column dissipates as distance from the wellhead increases (Figure 26, Figure 27, Figure 28, and Figure 29). However, the majority of dissolved aromatics are in the surface mixed layer, a layer that is roughly 50-100 m deep throughout the year. The large oil droplet sizes defined by the release scenario (Table 10 and Figure 9) result in rapid rise velocities (Figure 10) that carry oil quickly to the surface. Some high solubility fractions may dissolve at depth, however the majority of the soluble portion of the oil is found at and near the surface, where soluble aromatics in surface oil and entrained oil droplets (that may be re-entrained from wave action) dissolve into the water column. Greater than 50% of the total mass of released oil (total hydrocarbons, of which the dissolved aromatics are a small portion) is expected within the water column.

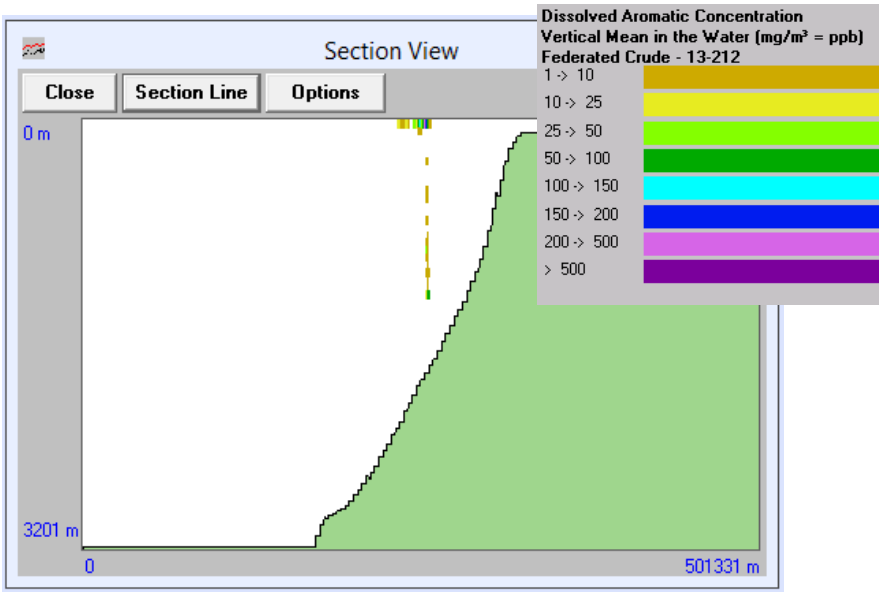

Figure 25. Subsurface plume predicted for a deep-water blowout during the winter season (March) at Site 1. This figure is a single snapshot in time that shows the predicted dissolved aromatic concentration throughout the water column.

During winter conditions, a little less than 50% of the total spilled oil is observed to evaporate into the atmosphere. A portion of this volatile fraction dissolves, and results in slightly more dissolved aromatic mass in the water column. However, the increased wind and waves in winter dissipates this mass over a larger volume, resulting in concentrations >1ppb over a large area (Figure 26 and Figure 28).

Conversely, during quiescent summer conditions, enhanced evaporation results in a little more than 50% of the total spilled oil in the atmosphere. Decreased wind and wave action during the summer result in slightly less mass of dissolved aromatics in the water column. However, reduced transport localizes this mass, resulting in slightly higher concentrations of dissolved aromatics in the water column over a smaller area during the summer (Figure 27 and Figure 29).

Large areas of the surface mixed-layer experience a concentration of dissolved aromatics in excess of 1 ppb at some point during each 30 day scenario (Table 11). However, <2% of this area is in excess of 15 ppm total petroleum hydrocarbons (TPH), and an even smaller portion is in excess of 30 ppm TPH. The areal extent of water column concentration threshold exceedance is greater for Site 2, as the modelled volume of oil released into the environment was double that for Site 1.

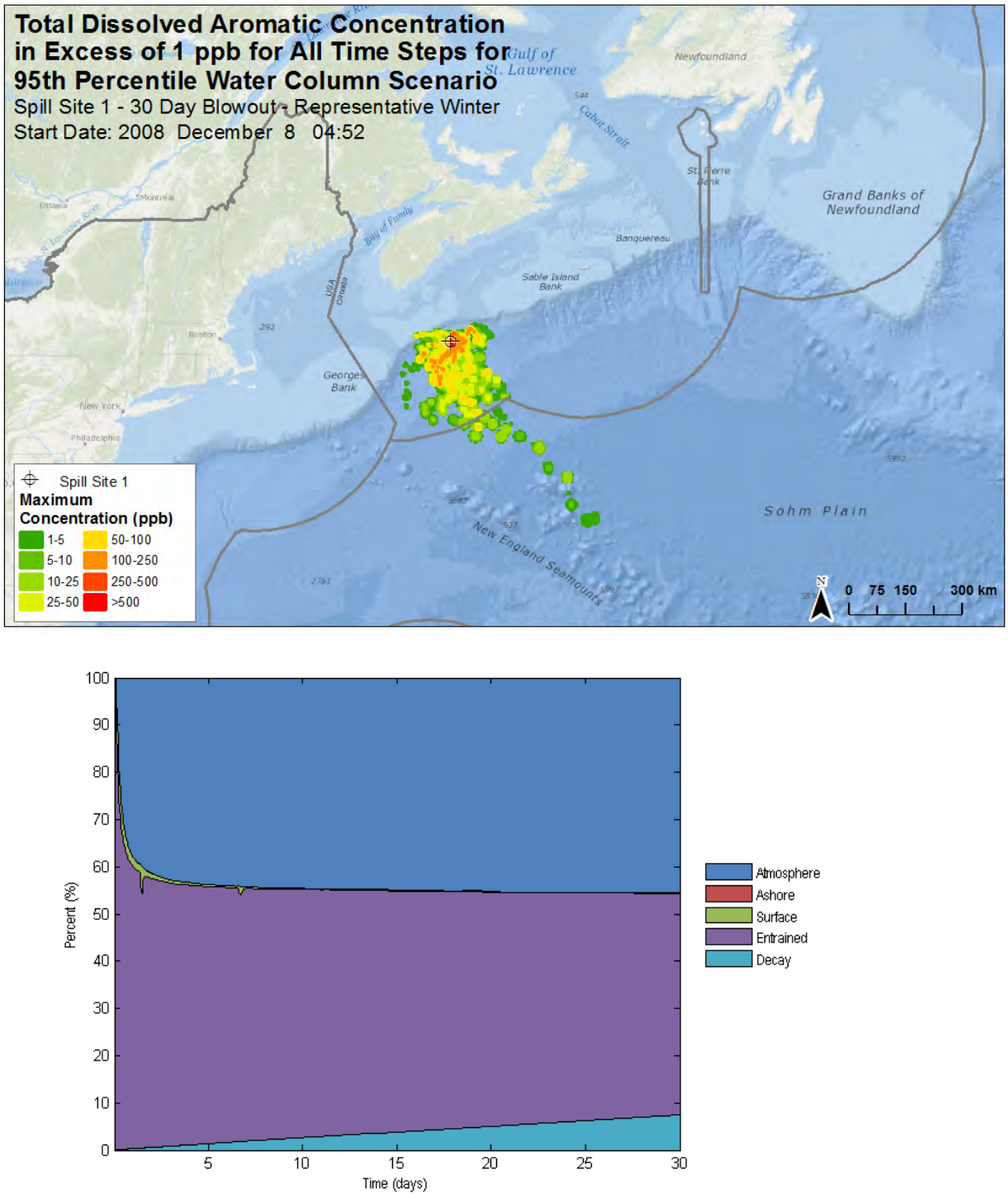

Figure 26. Representative Site 1 winter deterministic scenario for 95th percentile water column dissolved aromatic concentration (top). The maximum concentration of dissolved aromatics in excess of 1ppb is displayed at all modelled time steps. The associated mass balance graph is included (bottom).

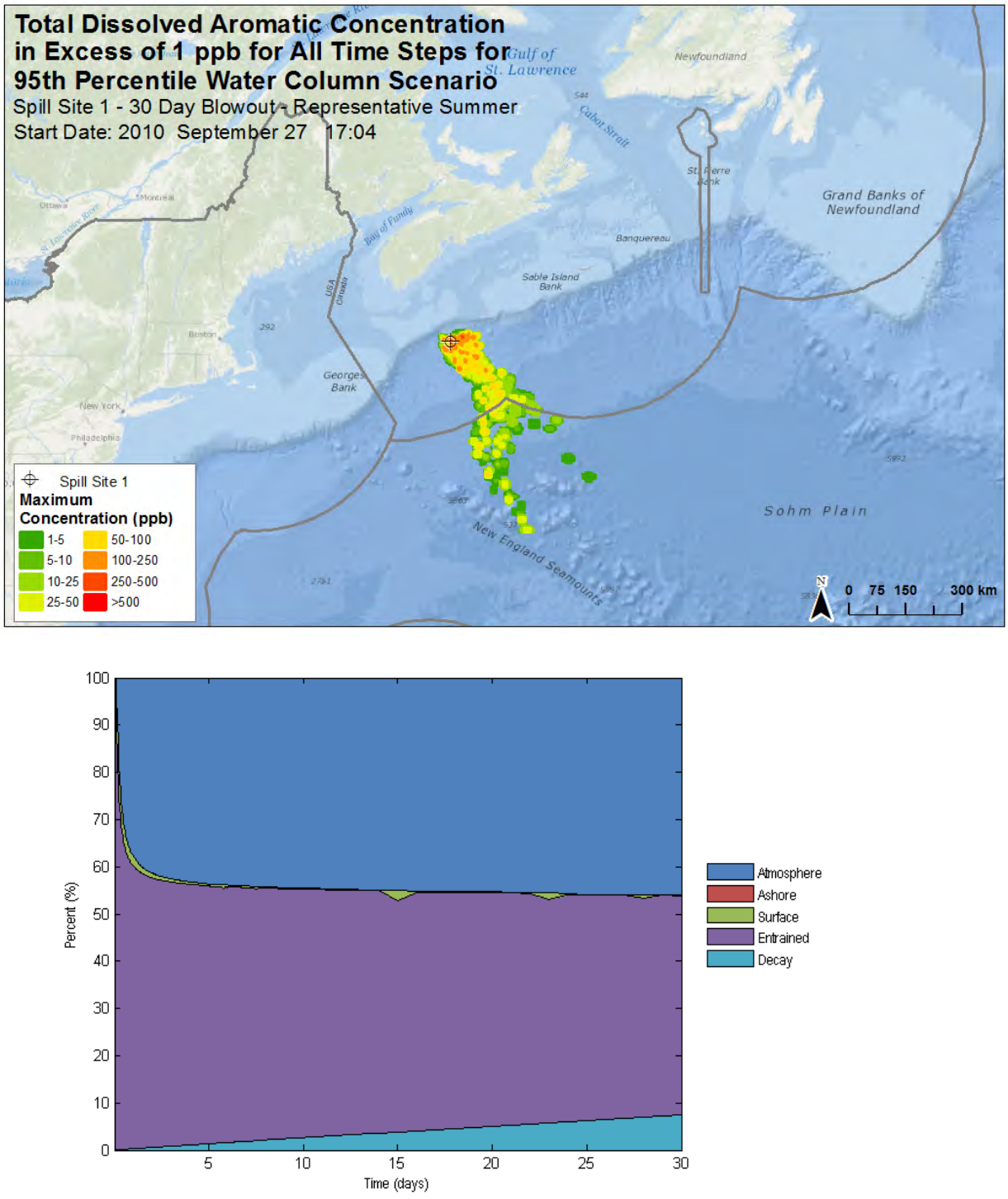

Figure 27. Representative Site 1 summer deterministic scenario for 95th percentile water column dissolved aromatic concentration (top). The maximum concentration of dissolved aromatics in excess of 1ppb is displayed at all modelled time steps. The associated mass balance graph is included (bottom).

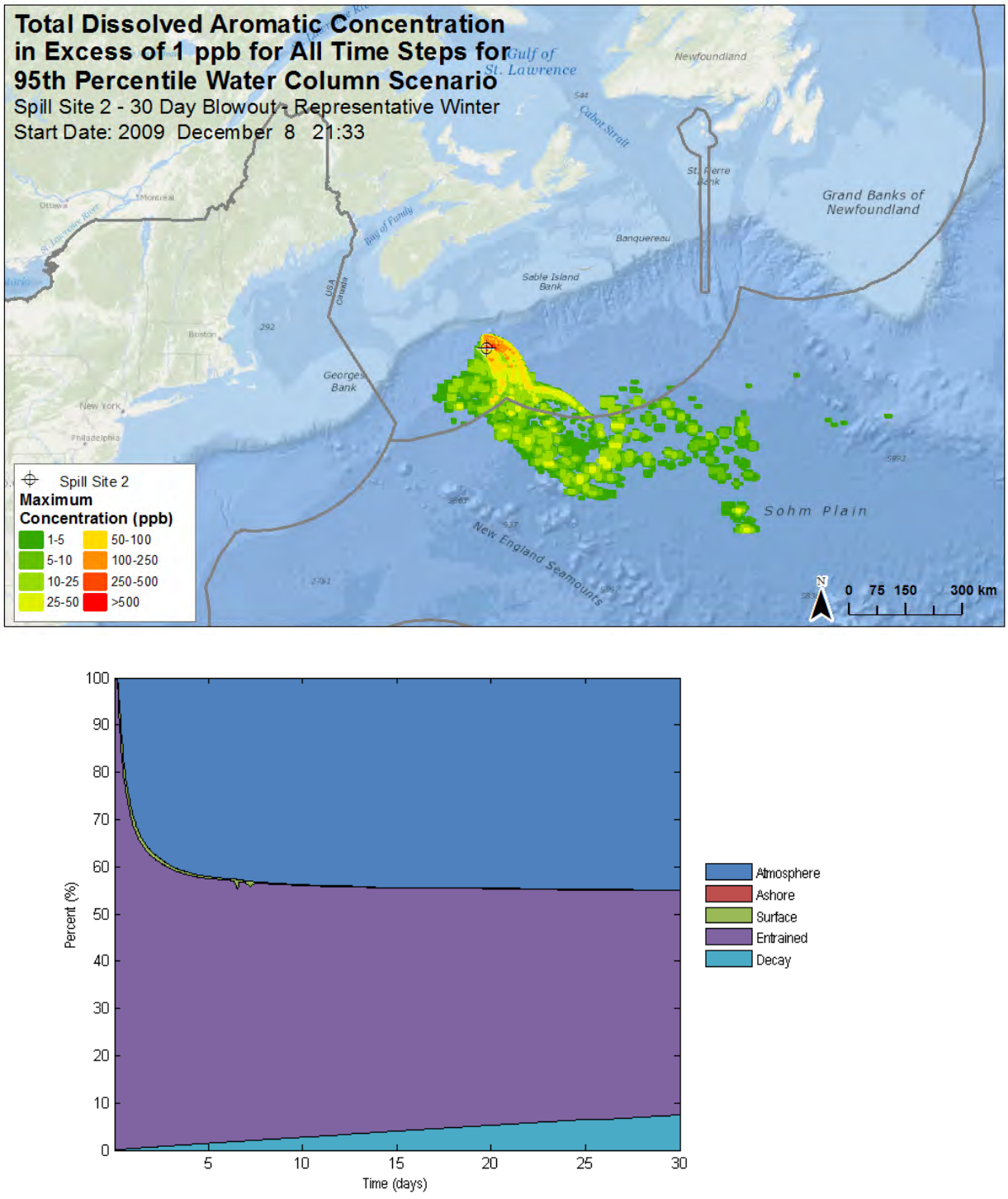

Figure 28. Representative Site 2 winter deterministic scenario for 95th percentile water column dissolved aromatic concentration (top). The maximum concentration of dissolved aromatics in excess of 1ppb is displayed at all modelled time steps. The associated mass balance graph is included (bottom).

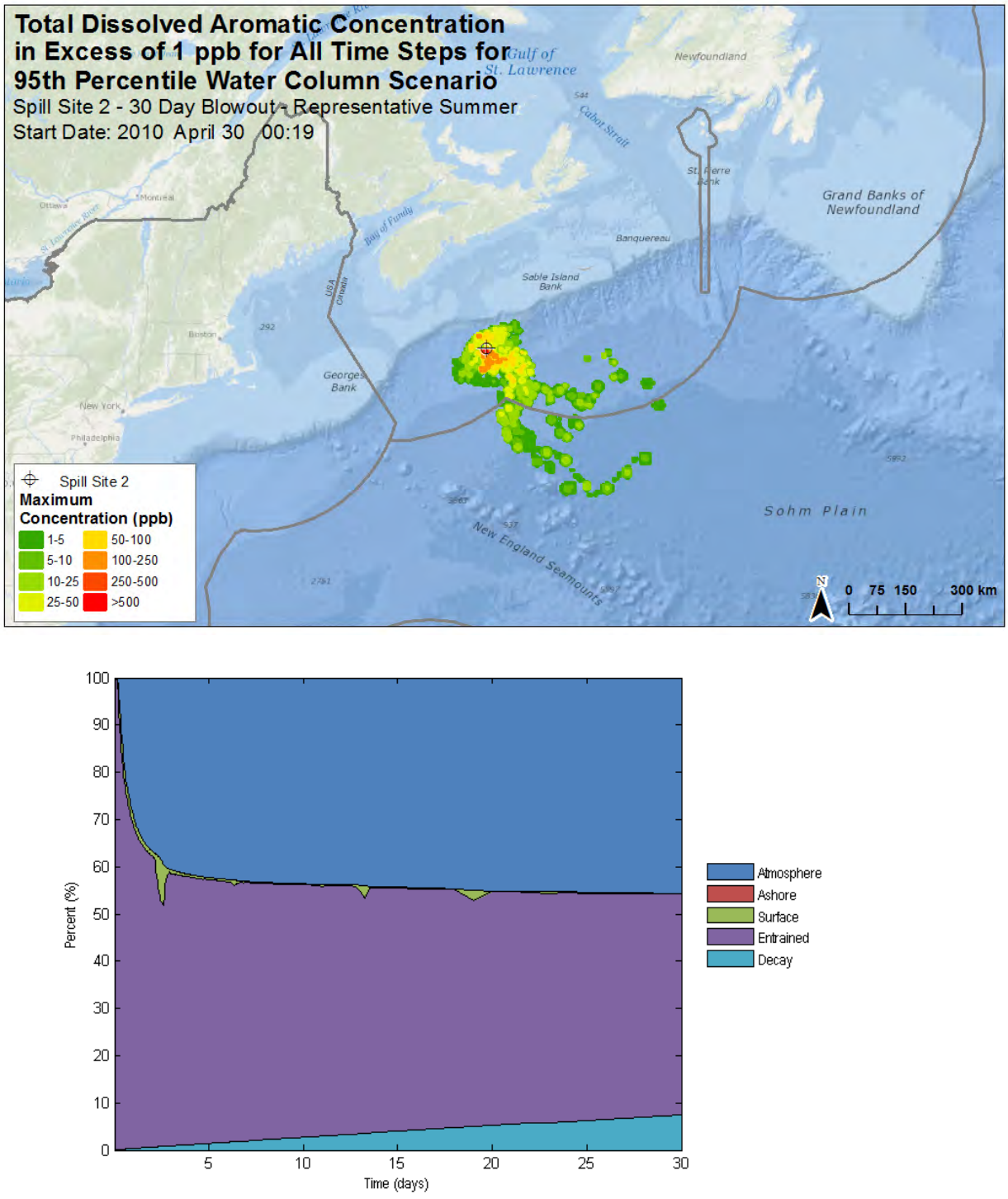

Figure 29. Representative Site 2 summer deterministic scenario for 95th percentile water column dissolved aromatic concentration (top). The maximum concentration of dissolved aromatics in excess of 1ppb is displayed at all modelled time steps. The associated mass balance graph is included (bottom).

4.4.3 SHORELINE OILING

The probability of shoreline oiling was very low for the modelled scenarios, between 0.83-1.88%. Only 9 scenarios out of 480 for the modelled Site 1 release and only 4 scenarios out of 480 for the modelled Site 2 release resulted in any shoreline oiling. All shoreline oiling cases occurred during the summer season, limited to the months of May, June, and July, with shoreline contamination occurring 20-30 days after the initiation of the release (Figure 30 to Figure 34). As such, it is expected that the oil that would strand would be highly weathered.

The reason that shoreline oiling is so unlikely is a combination of the forcing parameters for surface oil and the location of the release. The modelled wellheads are far offshore and oil would need to remain on the surface for order of one month or more to be transported the hundreds of kilometres towards shore. Furthermore, the predominantly westerly winds would transport surface oil away from the coast (Appendix C: Figure 20 and Figure 21) and variable surface currents (Appendix C: Figure 6 and Figure 7) do not continuously transport surface oil in any one specific direction for significant periods of time. During more quiescent summer conditions, where a higher percentage of oil remains on the surface, there is a slightly increased probability (although still unlikely) that winds may come from the east and northeast, thus transporting surface oil towards land.

The identified 95th percentile shoreline oiling scenario for the Site 1 release predicted that 10-20% of the oil would be on the surface for nearly 15 days (Figure 35). This, in combination with reduced wind speeds and favorable direction, resulted in measurable oiling of the southern tip of Nova Scotia, including the Barrington and Shelburne region. The result was an expected thickness of shoreline oiling of between 100-250 µm, which would be observed as a dark brown colour, totalling approximately 16.5 MT, that would trigger then need for a shoreline response and clean up. The expected thickness is well in excess of the highly conservative 1 and 10 µm thresholds investigated for shoreline oiling (Table 11), resulting in equal areas of contamination above the low thresholds.

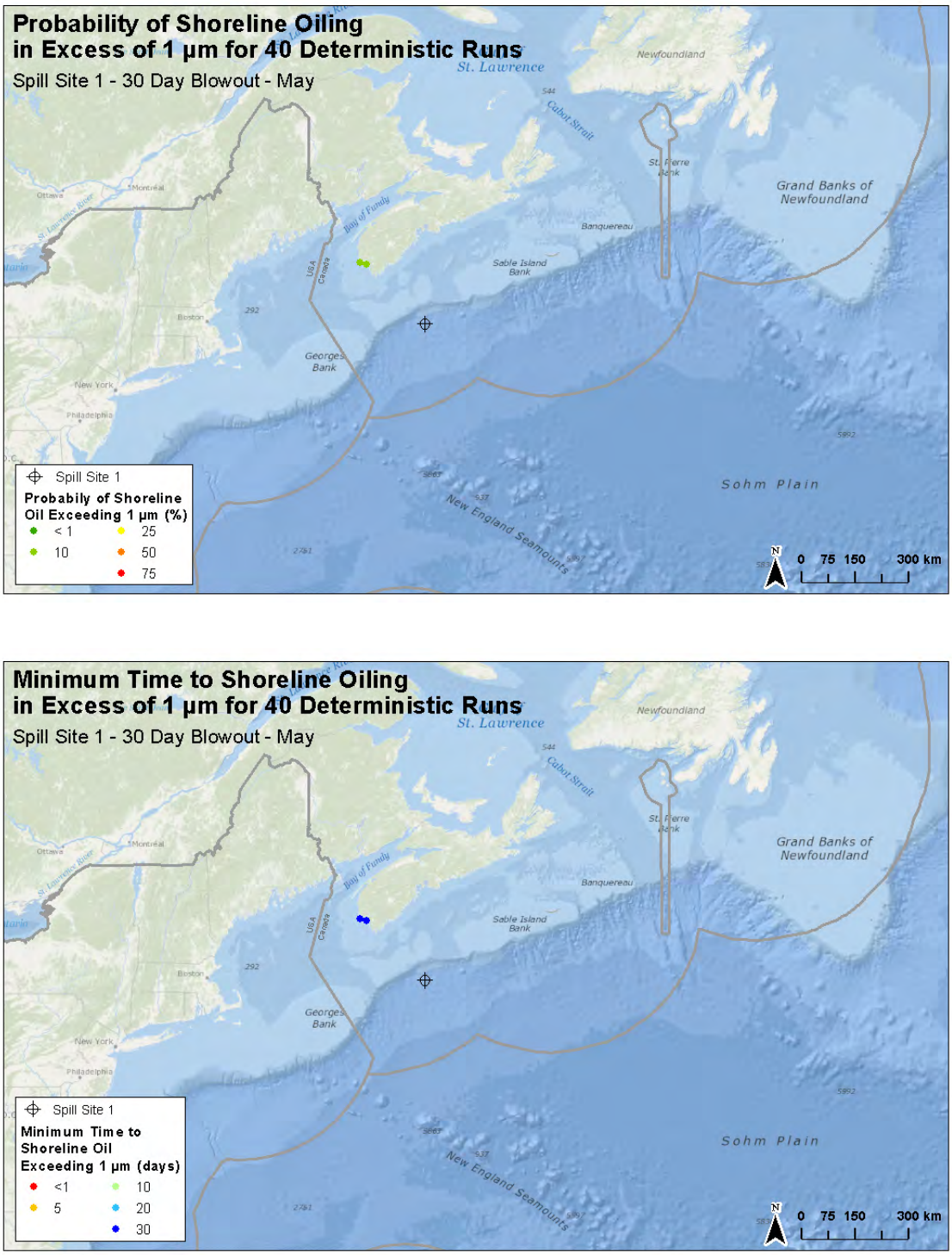

Figure 30. Stochastic model output maps depicting the predicted probability of shoreline oiling (top panel) and the associated minimum times (bottom panel) for a 24,900 bpd, 30-day blowout of Federated crude in May from Site 1.

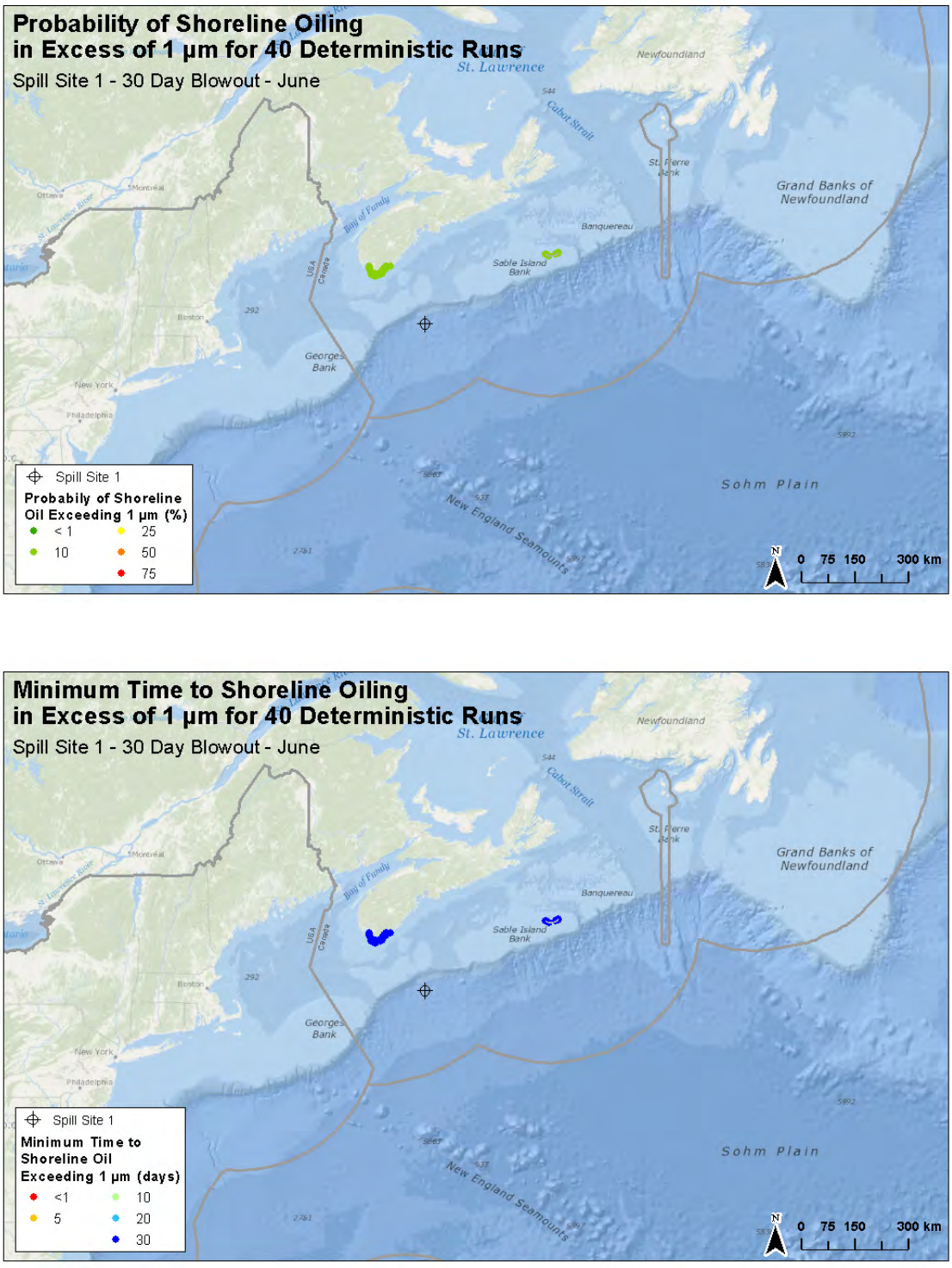

Figure 31. Stochastic model output maps depicting the predicted probability of shoreline oiling (top panel) and the associated minimum times (bottom panel) for a 24,900 bpd, 30-day blowout of Federated crude in June from Site 1.

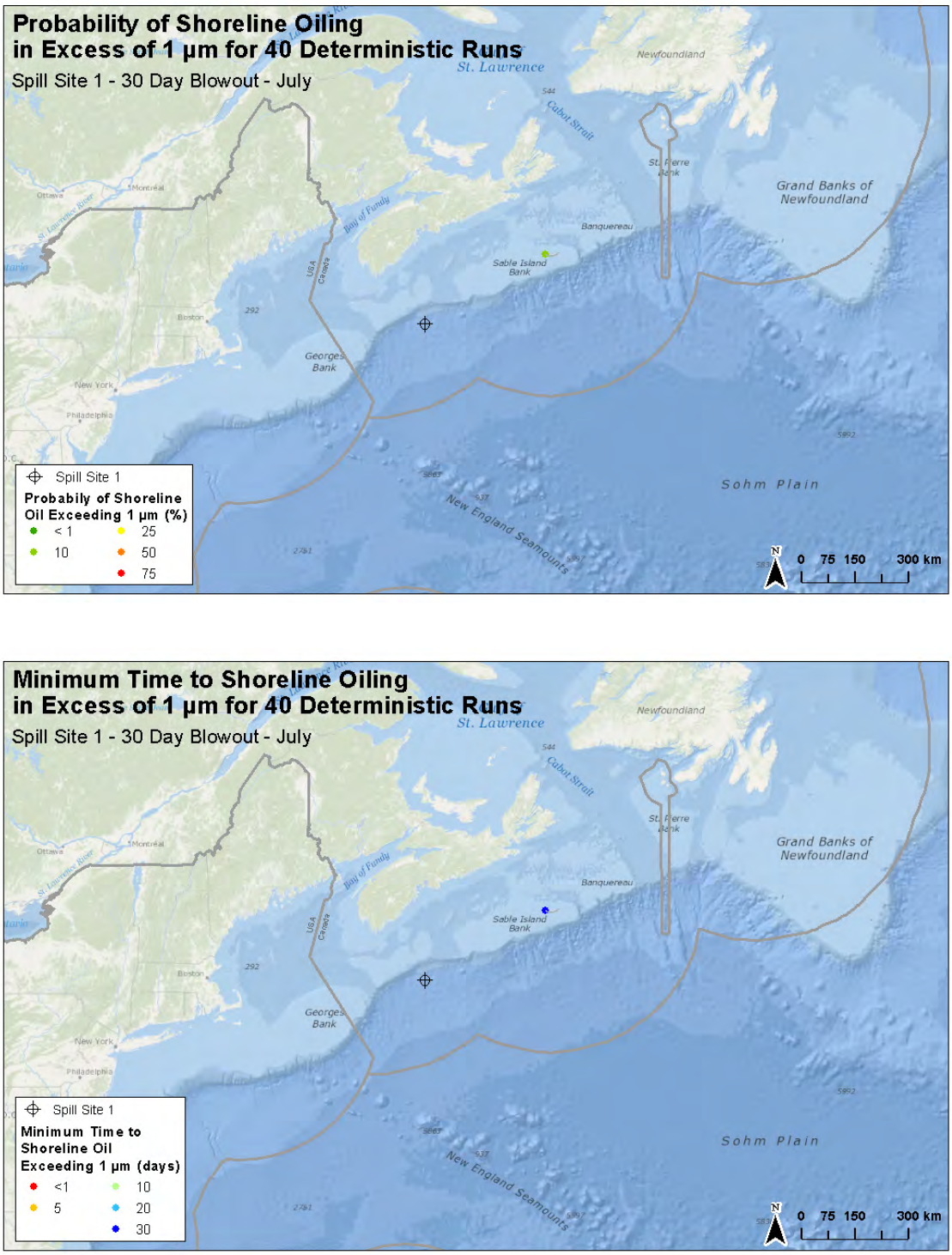

Figure 32. Stochastic model output maps depicting predicted probability of shoreline oiling (top panel) and the associated minimum times (bottom panel) for a 24,900 bpd, 30-day blowout of Federated crude in July from Site 1.

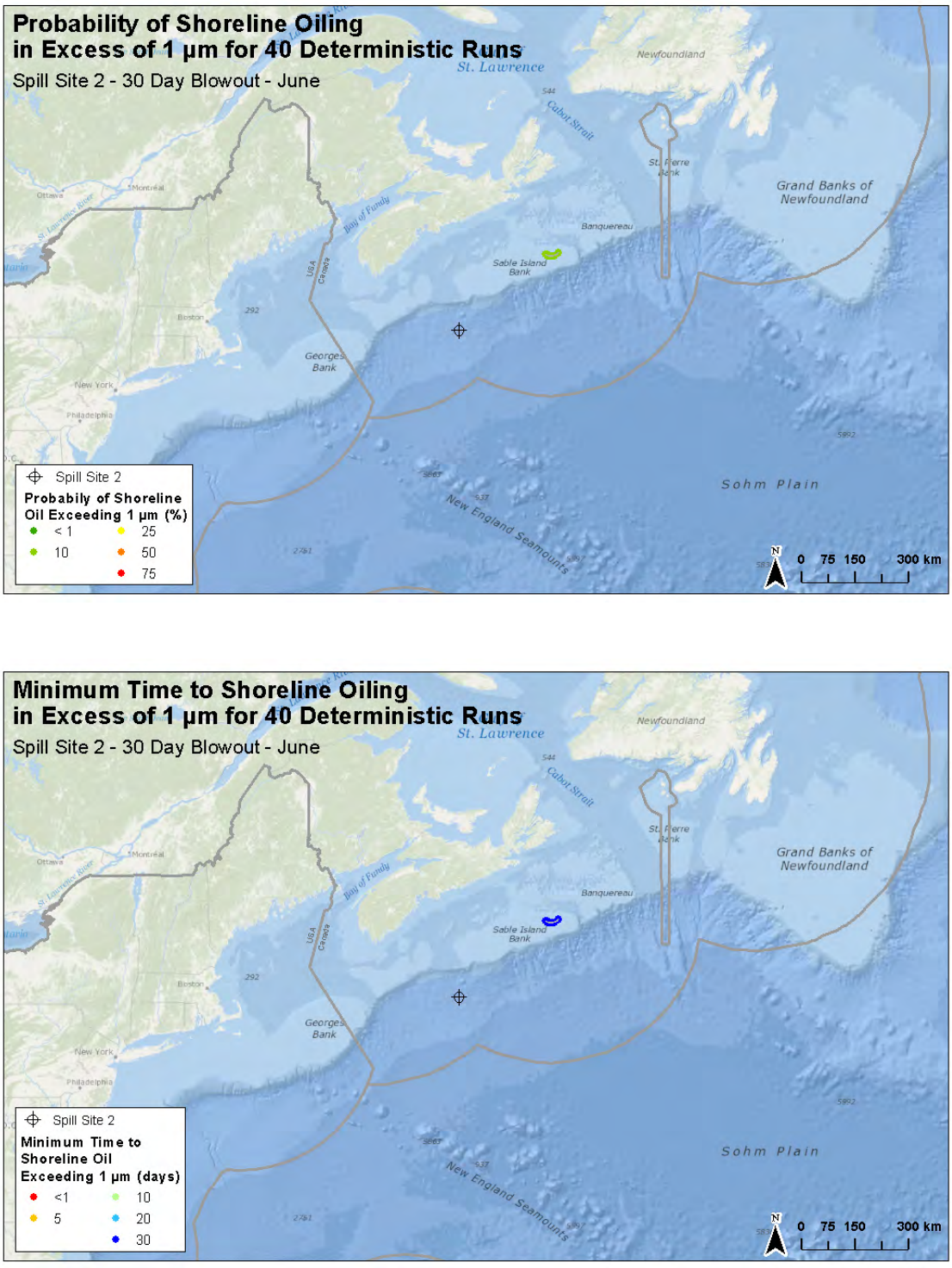

Figure 33. Stochastic model output maps depicting the predicted probability of shoreline oiling (top panel) and the associated minimum times (bottom panel) for a 24,900 bpd, 30-day blowout of Federated crude in June from Site 2.

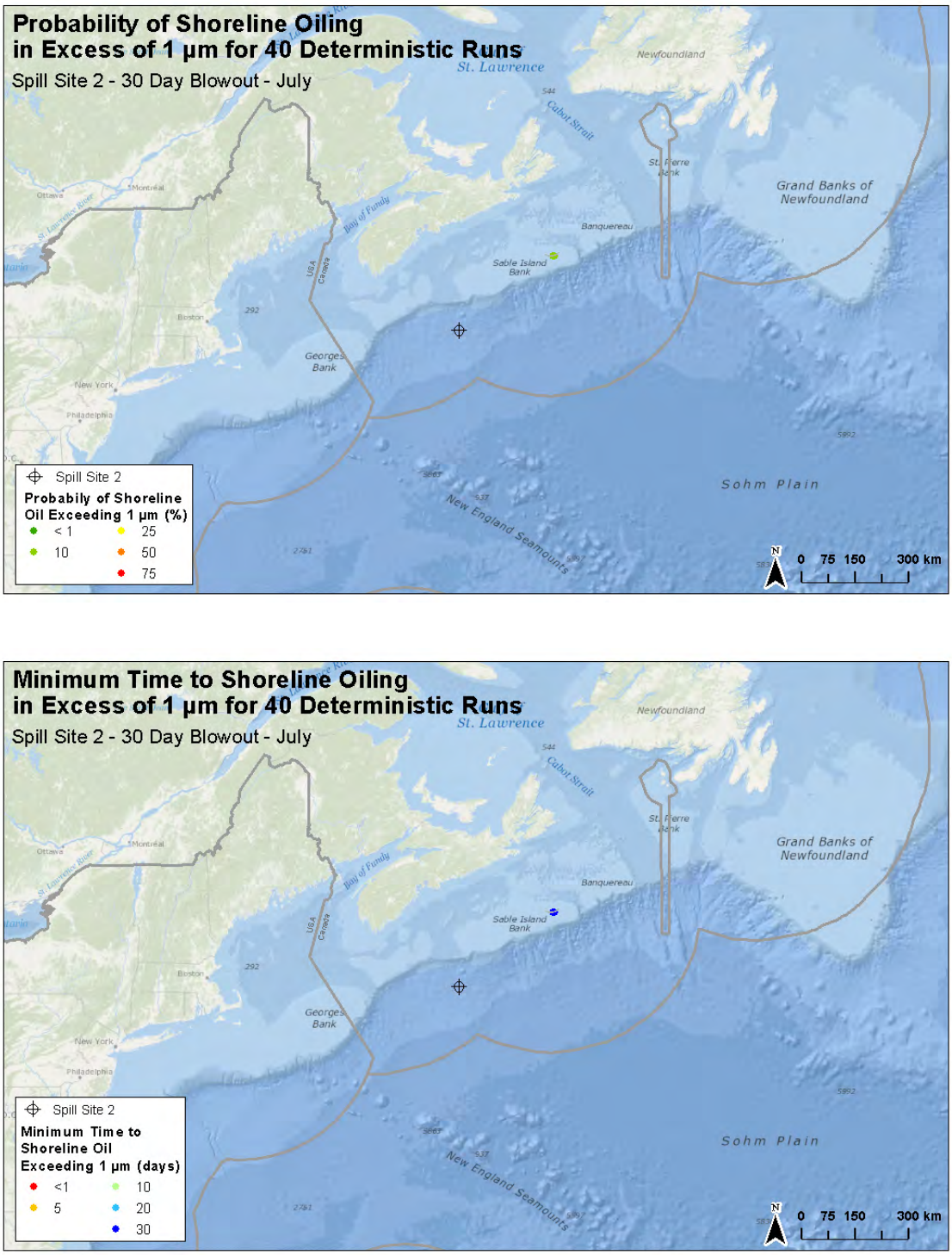

Figure 34. Stochastic model output maps depicting the predicted probability of shoreline oiling (top panel) and the associated minimum times (bottom panel) for a 24,900 bpd, 30-day blowout of Federated crude in July from Site 2.

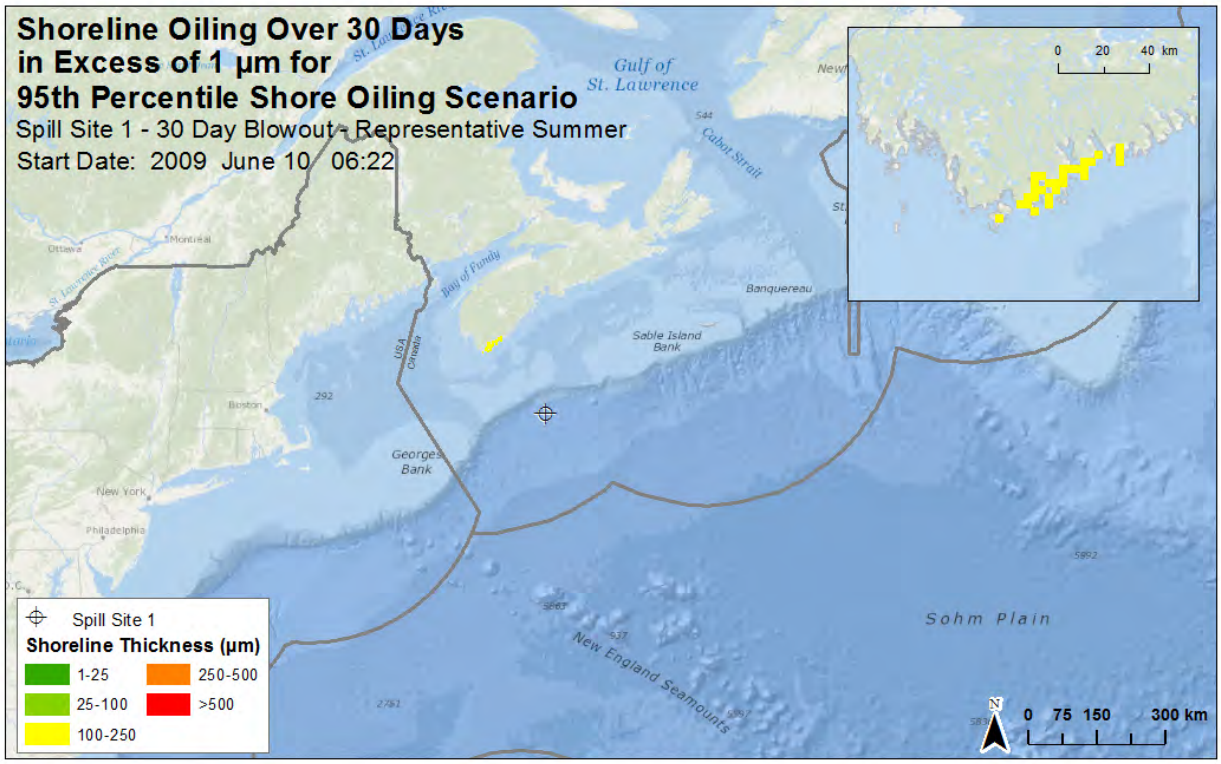

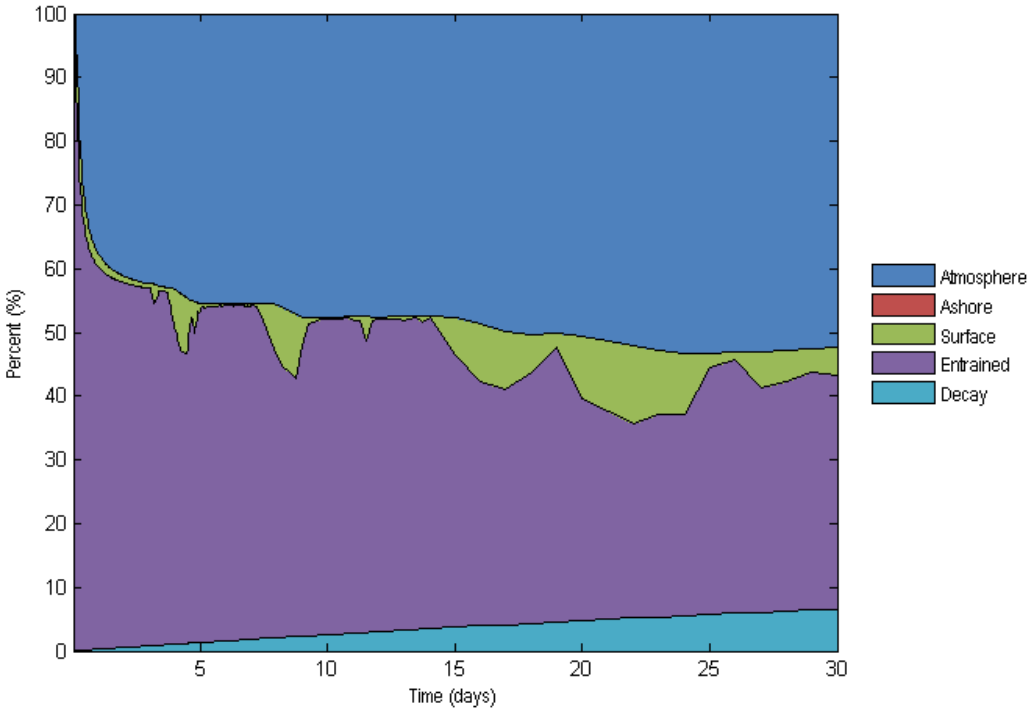

Figure 35. Representative Site 1 summer deterministic scenario for 95th percentile shoreline oiling (top). The associated mass balance graph is included (bottom).

4.5 Oil Fates Results for Batch Spills at Site 3

To simulate accidental discharges from operational vessels, two batch spills of marine diesel were modelled as surface releases. Two releases of 10 bbl and 100 bbl were modelled for thirty days (Figure 36 and Figure 37). The marine diesel is a standard diesel that has a low viscosity and a high aromatic content. Releases expected to maximize water surface exposure were modelled with a release date of June 1, 2009 at 15:13. The following 30 day period that was modelled contained low but representative wind speeds and no major storms, so entrainment and dispersion would be relatively low. During these model runs, 80% of the spilled mass evaporated rapidly, within 2-3 days.

The thickness of the slick at the instant of release is greater than 25 µm. As the fresh diesel spreads, it thins to a sheen, between 0.04-0.1 µm, where high rates of evaporation occur. After the lighter aromatic and aliphatic fractions evaporate, the residual oil at a more weathered state increases in viscosity and therefore thickness.

A total of approximately 80% of the diesel oil is expected to evaporate from this surface release. The area of surface water exposure in excess of 1 ppb of total dissolved aromatics is approximately 2 km^2 for the 10 bbl release and approximately 20 km^2 for the 100 bbl release. A maximum of 1-5 ppb is expected for the 10 bbl release, with localized concentrations as high as 25 ppb (or potentially slightly higher) in the region directly around the spill for the 100 bbl release.

A small swath of surface oiling in excess of 0.04 µm is observed in both releases (middle of Figure 36 and Figure 37) extending roughly 100 km to the west and 100 km to the north. However, this is the result of a small proportion of the release, the residual oil with a thickness of approximately 1 µm, being transported by surface currents during this quiescent period. This weathered diesel continues to be transported at the surface for this distance. However, the total mass is quite small, at <1% of the total spill. Because the surface snapshot includes all time steps, the relatively few particles are swept to the west and north, appearing as a continuous swath. In reality, this swept area would be exposed to patchy sheen and weathered oil over a small portion of this swath at any single time. This surface feature is an artifact of the quiescent environment modelled, and under more turbulent periods this diesel slick would dissipate more rapidly with a smaller surface footprint. None of the batch spills are predicted to reach the Nova Scotia shoreline.

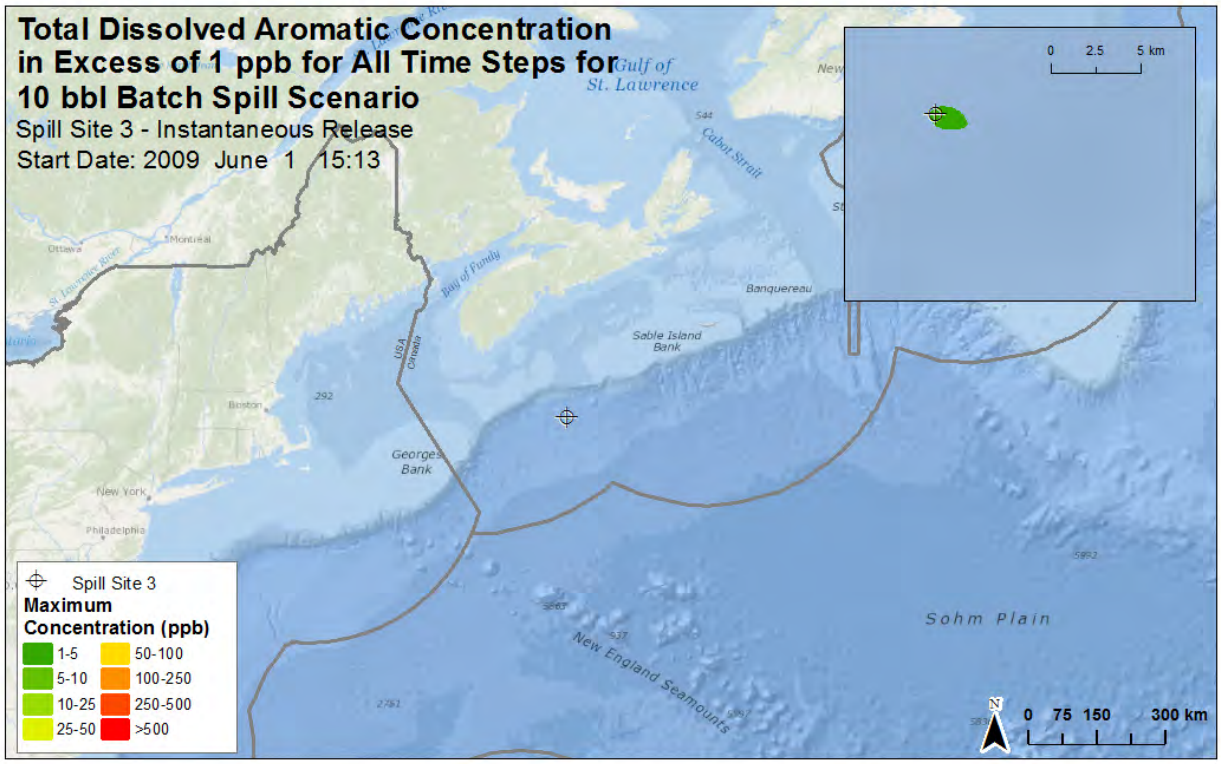
Total Dissolved Aromatic Concentration
in Excess of 1 ppb for All Time Steps for
10 bbl Batch Spill Scenario
Spill Site 3 - Instantaneous Release
Start Date: 2009 June 1 15:13
Gulf of St. Lawrence
Cabot Strait
Bay of Fundy
Sable Island Bank
Banquereau
Georges Bank
New England Seamounts
Sohm Plain
Montreal
Ottawa
Boston
New York
Philadelphia
USA
Canada
0 2.5 5 km
Spill Site 3
Maximum Concentration (ppb)
1-5
5-10
10-25
25-50
50-100
100-250
250-500
>500
0 75 150 300 km

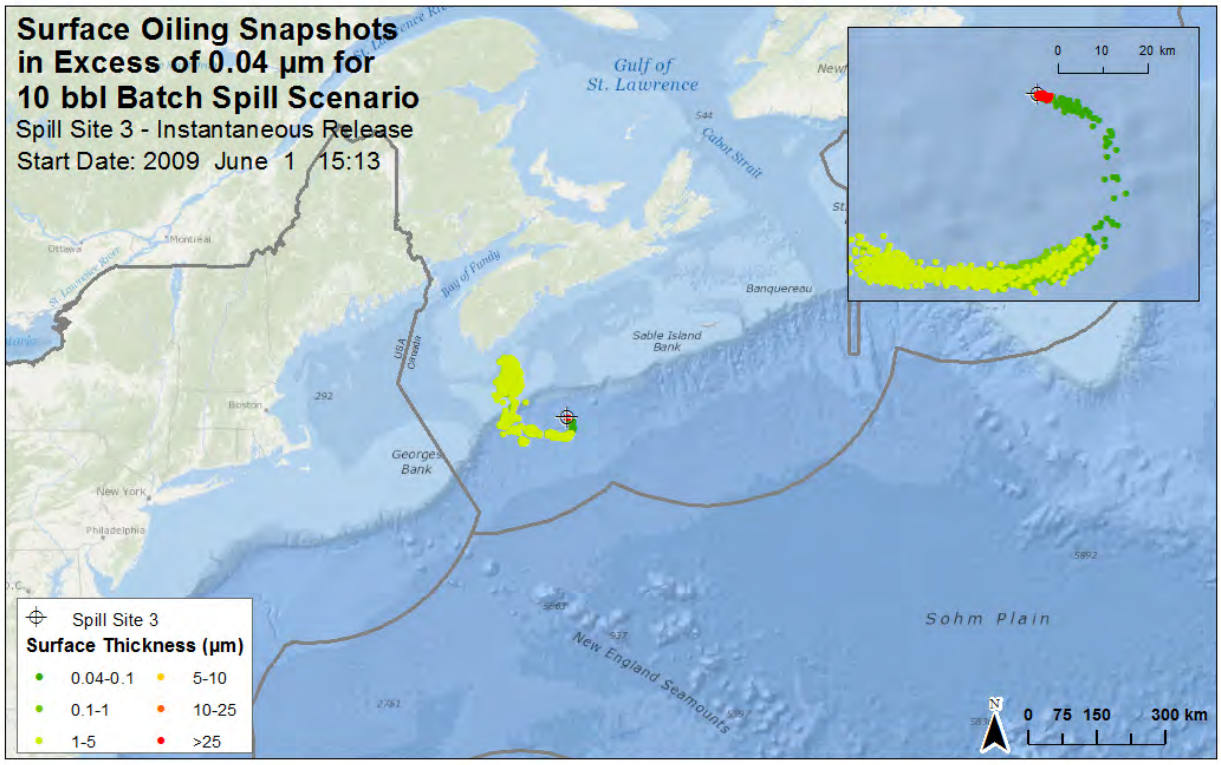
Surface Oiling Snapshots
in Excess of 0.04 µm for
10 bbl Batch Spill Scenario
Spill Site 3 - Instantaneous Release
Start Date: 2009 June 1 15:13
Gulf of St. Lawrence
Cabot Strait
Bay of Fundy
Sable Island Bank
Banquereau
Georges Bank
New England Seamounts
Sohm Plain
Montreal
Ottawa
Boston
New York
Philadelphia
USA
Canada
0 10 20 km
Spill Site 3
Surface Thickness (µm)
0.04-0.1
0.1-1
1-5
5-10
10-25
>25
0 75 150 300 km

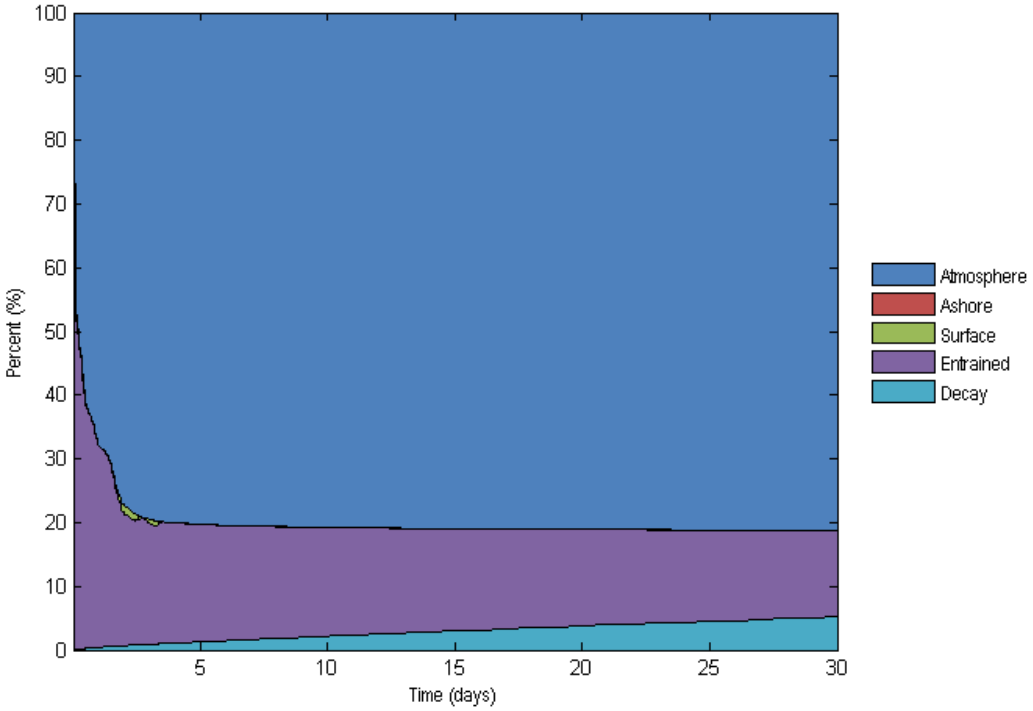

Figure 36. The total dissolved aromatic concentration in excess of 1ppb is depicted for the 10 bbl batch diesel spill at Site 3 (top of previous page), along with the associated surface thickness that is expected over the modelled 30 day period (bottom of previous page). The associated mass balance graph is included (above).

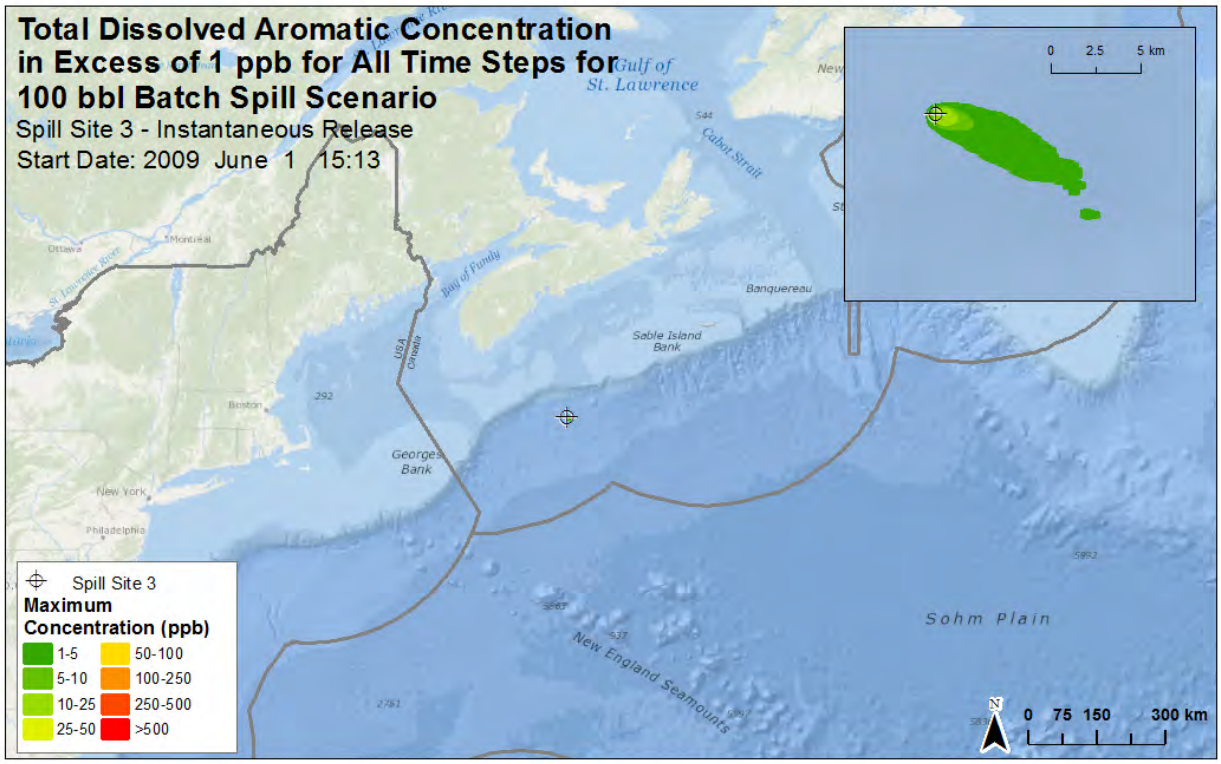
Total Dissolved Aromatic Concentration
in Excess of 1 ppb for All Time Steps for
100 bbl Batch Spill Scenario
Spill Site 3 - Instantaneous Release
Start Date: 2009 June 1 15:13
Gulf of St. Lawrence
Cabot Strait
Bay of Fundy
Banquereau
Sable Island Bank
Georges Bank
Sohm Plain
New England Seamounts
Montreal
Ottawa
Boston
New York
Philadelphia
USA
Canada
0 2.5 5 km
Spill Site 3
Maximum Concentration (ppb)
1-5
5-10
10-25
25-50
50-100
100-250
250-500
>500
0 75 150 300 km

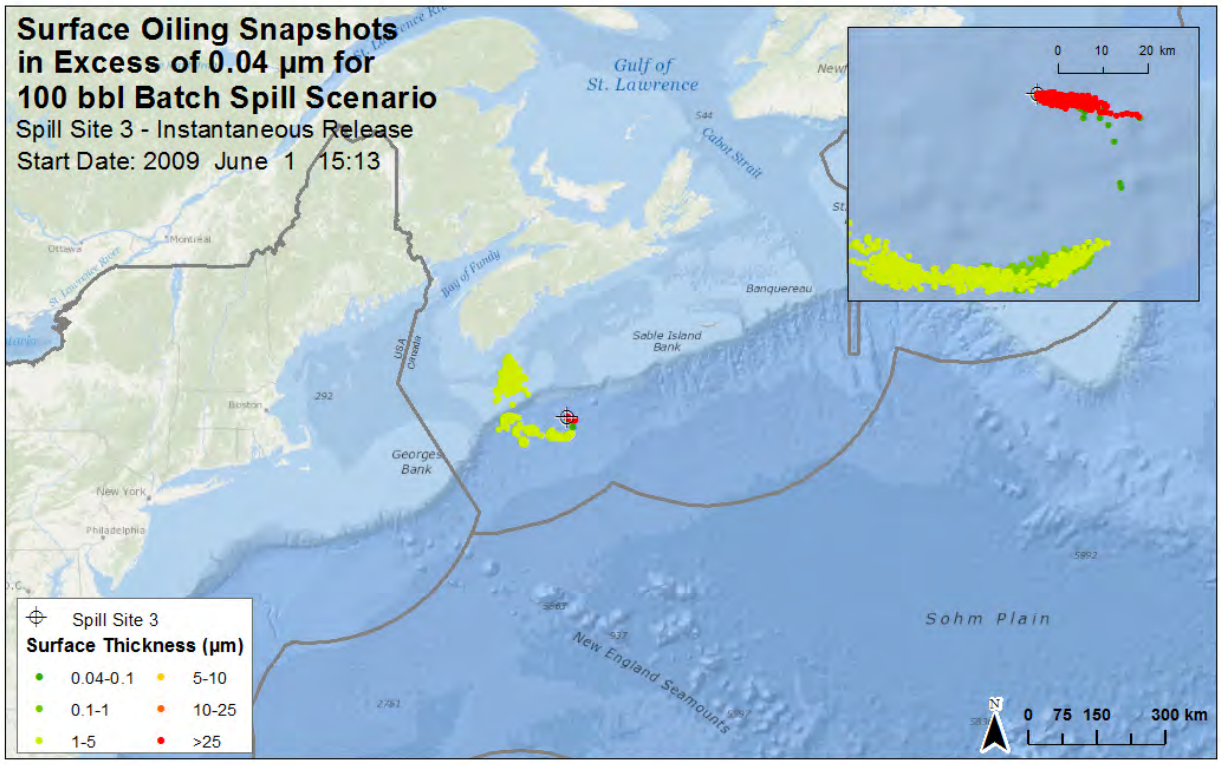
Surface Oiling Snapshots
in Excess of 0.04 µm for
100 bbl Batch Spill Scenario
Spill Site 3 - Instantaneous Release
Start Date: 2009 June 1 15:13
Gulf of St. Lawrence
Cabot Strait
Bay of Fundy
Banquereau
Sable Island Bank
Georges Bank
Sohm Plain
New England Seamounts
Montreal
Ottawa
Boston
New York
Philadelphia
USA
Canada
0 10 20 km
Spill Site 3
Surface Thickness (µm)
0.04-0.1
0.1-1
1-5
5-10
10-25
>25
0 75 150 300 km

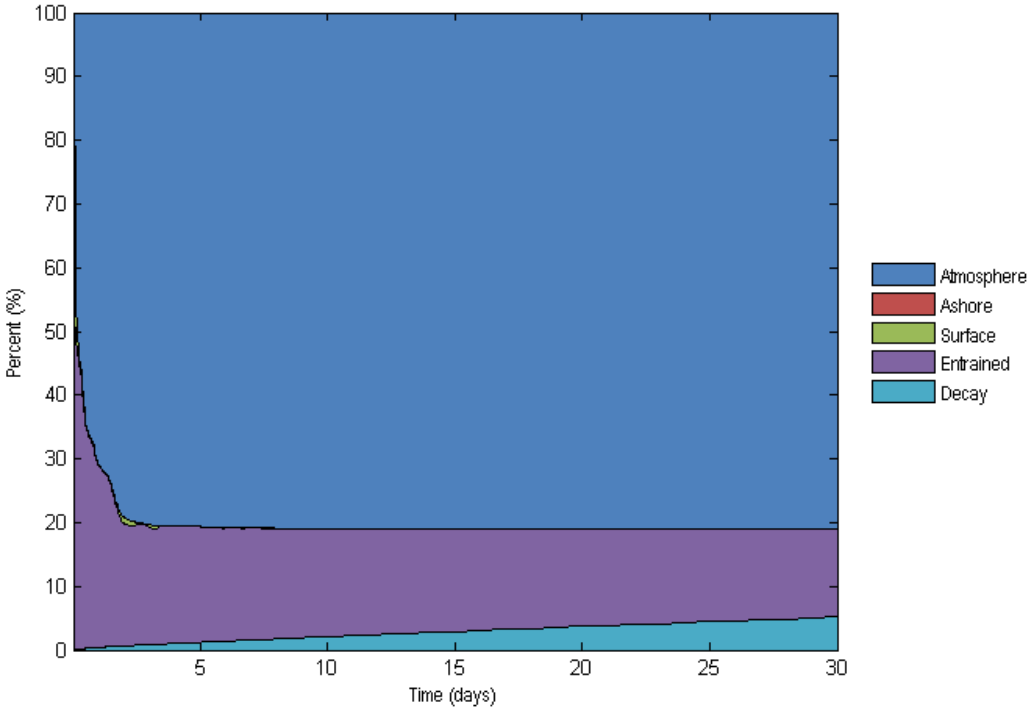

Figure 37. The total dissolved aromatic concentration in excess of 1ppb is depicted for the 100 bbl batch diesel spill at Site 3 (top of previous page), along with the associated surface thickness that is expected over the modelled 30 day period (bottom of previous page). The associated mass balance graph is included (above).

5 CONCLUSIONS

In general, Federated Crude oil, a relatively light oil, has a strong propensity to evaporate and dissolve within the water column. 30,000-200,000 km^2 of US and Canadian waters, combined, may be exposed to greater than the lowest investigated thresholds based upon the specific scenario and investigated threshold (Table 11). The larger volume of oil released at Site 2 results in larger surface oiling and water column dissolved aromatic exposure areas above thresholds for potential effects. However, the low thresholds do not consider the duration of exposure, and so are highly conservative (tending to overestimate potential area of effects) relative to where exposures would result in more likely, measurable effects.

The highest concentrations of water column dissolved aromatic compounds occur very close to the wellhead and at the surface (Figure 25). The large oil droplets released at depth, rise quickly and surface before the majority of the soluble and volatile fractions have entered the water column. Therefore, threshold exceedances are localized to the surface mixed layer in nearly the entire highlighted region of the water column dissolved aromatic maps. The surface mixed layer is a region roughly 40-100 m deep. In reality, the majority of threshold exceedances modelled

and likely observed would be in the wave mixed zone, a region only 10's of metres thick (Figure 26 through Figure 35).

Winter and summer type conditions yield seasonal trends. These include a higher likelihood of persistent oil on the surface during summer conditions, and a higher likelihood that a larger fraction of oil will be entrained within the water column during more turbulent wintertime conditions.

The amount of evaporation and decay is relatively consistent between model runs, and the majority of variability is found in the amount of oil either on the surface or within the water column (Figure 21 through Figure 35). The main cause of this is variable wind speed, whereby higher winds result in larger waves, which entrain surface oil into the water column. The maximum surface oiling cases resulted in approximately 10-20% of the total mass of released oil on the surface and 30-40% entrained, while the maximum water column dissolved aromatic cases had nearly no surface oiling and closer to 50% entrained.

The probability of shoreline oiling was <2% for modelled scenarios. Shoreline oiling was only observed during May-July, with shoreline contamination occurring 20-30 days after the initiation of the release. As such, it is expected that the small portion of oil that would strand would be in a highly weathered state. Site 1 is closer to shore, relative to Site 2, and shoreline oiling would occur along the southern coast of Nova Scotia. Site 2 is further offshore, with a flow rate nearly double that of Site 1. Shoreline oiling from Site 2 would occur along the Sable Island National Park.

The associated threshold exceedance maps in Sections 4.4.1, 4.4.2, and 4.4.3 represent the total area that each specific threshold may have been exceeded over the course of the entire 30-day model run. There may be effects within this area; however toxicity is the result of not only the concentration or thickness of oil, but also the duration of exposure. Thus, the areas indicated as potentially affected by oil exposure are conservatively large. Exposure modelling and effects were not conducted for this study.

Marine diesel is a low viscosity and a high aromatic-content product. Around 80% of the simulated diesel spills evaporated within 2-3 days, with only 2 km^2 and 20 km^2 experiencing in water concentrations of dissolved aromatics in excess of 1 ppb for the 10 bbl and 100 bbl spill, respectively. A small portion of weathered diesel may continue to be transported at the surface for some distance, however the volume of oil is quite small (Figure 36 and Figure 37).

6 REFERENCES

Bleck, R. 2002. An oceanic general circulation model framed in hybrid isopycnic-cartesian coordinates. Ocean Modeling, 4, 55-88.

Conkright, M.E, J.I. Antonov, O. Baranova, T. P. Boyer, H.E. Garcia, R. Gelfeld, D. Johnson, R.A. Locarnini, P.P. Murphy, T.D. O'Brien, I. Smolyar, C. Stephens, 2002: World Ocean Database 2001, Volume 1: Introduction. Ed: Sydney Levitus, NOAA Atlas NESDIS 42, U.S. Government Printing Office, Washington, D.C., 167 pp.

Daling, P.S. A.Lewis, S. Ramstad. 1999. The use of colour as a guide to oil film thickness – Main report. SINTEF Report STF66 F99082. 48p., SINTEF, Trondheim, Norway.

Egbert, G.D. and S.Y. Erofeeva. 2014 The OSU TOPEX/Poseidon Global Inverse Solution TPXO. http://volkov.oce.orst.edu/tides/global.html, February 20, 2014.

Environmental Science and Technology Center: Spill Technology Database, Oil Technology Database (ESTC). 2013. http://www.etc-cte.ec.gc.ca/databases/OilProperties/oil_prop_e.html

Fanneløp, T.K. and K. Sjoen , 1980a. Hydrodynamics of underwater blowouts, AIAA 8th Aerospace Sciences Meeting, January 14-16, Pasadena, California, AIAA paper, pp. 80-0219.

Fanneløp, T. K. and K. Sjoen, 1980b. Hydrodynamics of underwater blowouts, Norwegian Maritime Research, No. 4, pp. 17-33.

French, D., M. Reed, K. Jayko, S. Feng, H. Rines, S. Pavignano, T. Isaji, S. Puckett, A. Keller, F. W. French III, D. Gifford, J. McCue, G. Brown, E. MacDonald, J. Quirk, S. Natzke, R. Bishop, M. Welsh, M. Phillips and B.S. Ingram, 1996a. The CERCLA type A natural resource damage assessment model for coastal and marine environments (NRDAM/CME), Technical Documentation, Vol. I - Model Description. Final Report, submitted to the Office of Environmental Policy and Compliance, U.S. Dept. of the Interior, Washington, DC, April, 1996, Contract No. 14-0001-91-C-11.

French, D., M. Reed, S. Feng and S. Pavignano, 1996b. The CERCLA type A natural resource damage assessment model for coastal and marine environments (NRDAM/CME), Technical Documentation, Vol. III - Chemical and Environmental Databases. Final Report, Submitted to the Office of Environmental Policy and Compliance, U.S. Dept. of the Interior, Washington, DC, April, 1996, Contract No. 14-01-0001-91-C-11.

French, D., S. Pavignano, H. Rines, A. Keller, F.W. French III and D. Gifford, 1996c. The

CERCLA type A natural resource damage assessment model for coastal and marine environments (NRDAM/CME), Technical Documentation, Vol.IV - Biological Databases. Final Report, Submitted to the Office of Environmental Policy and Compliance, U.S. Dept. of the Interior, Washington, DC, April, 1996, Contract No. 14-01-0001-91-C-11.

French, D.P. and H. Rines, 1997. Validation and use of spill impact modeling for impact assessment. Proceedings, 1997 International Oil Spill Conference, Fort Lauderdale, Florida, American Petroleum Institute Publication No. 4651, Washington, DC, pp-829-834.

French, D.P., H. Rines and P. Masciangioli, 1997. Validation of an Orimulsion spill fates model using observations from field test spills. Proceedings, Twentieth Arctic and Marine Oil Spill Program Technical Seminar, Vancouver, Canada, June 10-13, 1997.

French McCay, D. and J.R. Payne, 2001. Model of Oil Fate and Water concentrations with and without application of dispersants. In Proceedings of the 24th Arctic and Marine Oil Spill Program (AMOP) Technical Seminar, Emergencies Science Division, Environment Canada, Ottawa, ON, Canada, pp. 601-653.

French McCay, D.P., 2002. Development and Application of an Oil Toxicity and Exposure Model, OilToxEx. Environmental Toxicology and Chemistry 21(10): 2080-2094.

French McCay, D.P., 2003. Development and Application of Damage Assessment Modeling: Example Assessment for the North Cape Oil Spill. Marine Pollution Bulletin, Volume 47, Issues 9-12, September-December 2003, pp. 341-359.

French McCay, D.P., 2004. Oil spill impact modeling: Development and validation. Environmental Toxicology and Chemistry 23(10): 2441-2456.

French McCay, D.P., and J.J. Rowe, 2004. Evaluation of Bird Impacts in Historical Oil Spill Cases Using the SIMAP Oil Spill Model. In Proceedings of the 27th Arctic and Marine Oil Spill Program (AMOP) Technical Seminar, Emergencies Science Division, Environment Canada, Ottawa, ON, Canada, pp. 421-452.

French McCay, D.P, 2009. State-of-the-Art and Research Needs for Oil Spill Impact Assessment Modeling. In Proceedings of the 32nd AMOP Technical Seminar on Environmental Contamination and Response, Emergencies Science Division, Environment Canada, Ottawa, ON, Canada, pp. 601-653.

French-McCay, D.P., 2011. Oil Spill Modeling for Ecological Risk and Natural Resource Damage Assessment. Paper 415, Proceedings of the 2011 International Oil Spill Conference, American Petroleum Institute, Washington, D.C., May 201

General Bathymetric Chart of the Oceans. 2013. http://www.gebco.net

Gundlach, E.R., 1987. Oil Holding Capacities and Removal Coefficients for Different Shoreline Types to Computer Simulate Spills in Coastal Waters. In Proceedings of the 1987 Oil Spill Conference, pp. 451-457.

Kolluru, V.S., 1993. Oil blowout model, Applied Science Associates, Inc., Narragansett, RI 02882.

Levitus S. 1982. Climatological Atlas of the World Ocean, NOAA Professional Paper 13. U. S. Government Printing Office: Washington, D. C.

Lunel, T., 1993a. Dispersion: Oil droplet size measurements at sea. In Proceedings of the 16th Arctic Marine Oilspill Program (AMOP) Technical Seminar, Environment Canada, Calgary, Alberta, June 7-9, 1993, pp. 1023-1056.

Lunel, T., 1993b. Dispersion: Oil droplet size measurements at sea. In Proceedings of the 1993 Oil Spill Conference, pp. 794-795.

Mackay, D., S. Paterson and K. Trudel, 1980. A mathematical model of oil spill behavior. Department of Chemical and Applied Chemistry, University of Toronto, Canada, 39p.

Mackay, D, W.Y. Shiu, K. Hossain, W. Stiver, D. McCurdy and S. Peterson, 1982. Development and calibration of an oil spill behavior model. Report No. CG-D-27-83, U.S. Coast Guard, Research and Development Center, Groton, Connecticut, 83p.

Maine Department of Environmental Protection: Environmental Vulnerability Index Maps. 2013. http://www.maine.gov/dep/spills/emergspillresp/evi/

McAuliffe, C.D., 1987. Organism exposure to volatile/soluble hydrocarbons from crude oil spills –a field and laboratory comparison. Proceedings of the 1987 Oil Spill Conference. Washington, D.C.: API. pp. 275-288.

McAuliffe, C.D., 1989. The Weathering of Volatile Hydrocarbons from Crude Oil Slicks on Water. In Proceedings of the 1989 Oil Spill Conference, San Antonio, Texas, American Petroleum Institute, Washington, D.C., pp. 357-364.

Milgram, J.H., 1983. Mean flow in round bubble plumes, Journal of Fluid Mechanics, Vol. 133, pp. 345-376.

National Imagery and Mapping Agency (NIMA), Chapter 31, Ocean Currents. The American Practical Navigator. Bethesda. 2013.

National Oceanic and Atmospheric Administration: Environmental Sensitivity Index (NOAA ESI). 2013. http://response.restoration.noaa.gov/esi

National Oceanic and Atmospheric Administration: National Data Buoy Center. 2013. http://www.ndbc.noaa.gov/station_page.php?station=44137

National Oceanic and Atmospheric Administration: National Geophysical Data Center (NOAA NGDC). 2013. http://www.ngdc.noaa.gov

National Research Council (NRC), 1985. Oil in the Sea: Inputs, Fates and Effects. National Academy Press, Washington, D.C. 601p.

Naval Research Laboratory: NOGAPS. 2013. http://www.nrlmry.navy.mil/metoc/nogaps/

New Brunswick Department of Natural Resources. 2013. http://www2.gnb.ca/content/gnb/en/departments/natural_resources.html

Nova Scotia Department of Natural Resources. 2013. http://novascotia.ca/natr/

Rye, H., 1994, Model for calculation of underwater blowout plume, Proceedings of the 17th Arctic and Marine Oilspill Program Technical Seminar, Canada, p. 849-865.

Rye, H. P. Brandvik, and M. Reed, 1996, Subsurface oil release field experiment- observations and modeling of subsurface plume behavior, Proceedings of the 19th Arctic Marine Oilspill Program, Technical Seminar, Calgary, Alberta, Canada, p 1417-1435.

SL Ross Environmental Research Ltd. 2011. Oil Spill Fate and Behaviour Modeling in Support of Corridor Resources Old Harry Prospect Drilling EA. Prepared for Corridor Resources Inc. 40 pp. + Appendix.

Spaulding, M.L., 1982. User's manual for a simple gas blowout plume model, Continental Shelf Institute, Trondheim, Norway.

Stiver, W. and D. Mackay, 1984. Evaporation rate of oil spills of hydrocarbons and petroleum mixtures. Environmental Science and Technology 18: 834-840.

Trudel, B.K., R.C. Belore, B.J. Jessiman and S.L. Ross. 1989. A Mico-computer Based Spill Impact Assessment System for Untreated and Chemically Dispersed Oil Spills in the U.S. Gulf of Mexico. 1989 International Oil Spill Conference.

UNESCO, 1981: The Practical Salinity Scale 1978 and the International Equation of State of Seawater 1980. UNESCO technical papers in marine science **36**, 25 pp.

VLIZ (2014). Maritime Boundaries Geodatabase, version 8. Available online at http://www.marineregions.org/. Consulted on 2014-04-14.

Youssef, M. and M.L. Spaulding, 1994. Drift Current Under the Combined Action of Wind and Waves in Shallow Water, in Proceedings of the 17th Arctic and Marine Oil Spill Program (AMOP) Technical Seminar, Vancouver, British Columbia, June 8-10, 1994, pp. 767-784.

Zheng, L. and P. Yapa, 1997, A numerical model for buoyant oil jets and smoke plumes, Proceedings of the 20 th Arctic Marine Oilspill Program, Technical Seminar, Vancouver, BC, Canada, p. 963-979.

Zheng, L. And Yapa, P.D., 1998. Simulation of oil spills from underwater accidents II: Model verification, Journal of Hydraulic Research, International Association of Hydraulic Research, The Netherlands, Vol 36, No. 1, p. 117-134.

Zheng, L. and P. D. Yapa, 1999. A deepwater jet/plume model and a parametric analysis, p. 285-299.

7 APPENDIX A: SIMAP MODEL DESCRIPTION

The analysis was performed using the model system developed by Applied Science Associates (ASA) called SIMAP™ (Spill Impact Model Analysis Package). SIMAP™ originated from the oil fates and biological effects submodels in the Natural Resource Damage Assessment Models for Coastal and Marine Environments (NRDAM/CME) and Great Lakes Environments (NRDAM/GLE), which ASA developed in the early 1990s for the U.S. Department of the Interior for use in "type A" Natural Resource Damage Assessment (NRDA) regulations under the Comprehensive Environmental Response, Compensation and Liability Act of 1980 (CERCLA). The most recent version of the type A models, the NRDAM/CME (Version 2.4, April 1996) was published as part of the CERCLA type A NRDA Final Rule (Federal Register, May 7, 1996, Vol. 61, No. 89, p. 20559-20614). The technical documentation for the NRDAM/CME is in French et al. (1996 a-c). This technical development involved several in-depth peer reviews, as described in the Final Rule.

While the NRDAM/CME and NRDAM/GLE were developed for simplified natural resource damage assessments of small spills in the United States, SIMAP™ is designed to evaluate fates and effects of both real and hypothetical spills in marine, estuarine and freshwater environments worldwide. Additions and modifications to prepare SIMAP™ were made to increase model resolution, allow modification and site-specificity of input data, allow incorporation of temporally varying current data, evaluate subsurface releases and movements of subsurface oil, track multiple chemical components of the oil, enable stochastic modelling, and facilitate analysis of results.

Below are brief descriptions of the fates and effects models presented in SIMAP™. Detailed descriptions of the algorithms and assumptions in the model are in published papers (French McCay, 2002; 2003; 2004; 2009). The model has been validated with more than 20 case histories, including the *Exxon Valdez* and other large spills (French and Rines, 1997; French McCay, 2003; 2004; French McCay and Rowe, 2004) as well as test spills designed to verify the model (French et al., 1997).

PHYSICAL FATES MODEL

The three-dimensional physical fates model estimates distribution (as mass and concentrations) of whole oil and oil components on the water surface, on shorelines, in the water column, and in sediments. Oil fate processes included are oil spreading (gravitational and by shearing), evaporation, transport, randomized dispersion, emulsification, entrainment (natural and facilitated by dispersant), dissolution, volatilization of dissolved hydrocarbons from the surface water, adherence of oil droplets to suspended sediments, adsorption of soluble and sparingly-soluble aromatics to suspended sediments, sedimentation, and degradation.

Oil is a mixture of hydrocarbons of varying physical, chemical, and toxicological characteristics. In the model, oil is represented by component categories, and the fate of each component is tracked separately. The “pseudo-component” approach (Payne et al., 1984; 1987; French et al., 1996a; Jones, 1997; Lehr et al., 2000) is used, where chemicals in the oil mixture are grouped by physical-chemical properties, and the resulting component category behaves as if it were a single chemical with characteristics typical of the chemical group.

The most toxic components of oil to aquatic organisms are low molecular weight aromatic compounds (monoaromatic and polycyclic aromatic hydrocarbons, MAHs and PAHs), which are both volatile and soluble in water. Their acute toxic effects are caused by non-polar narcosis, where toxicity is related to the octanol-water partition coefficient (K_{ow}), a measure of hydrophobicity. The more hydrophobic the compound, the more toxic it is likely to be. However, as K_{ow} increases, the compound also becomes less soluble in water, and so there is less exposure to aquatic organisms. The toxicity of compounds having log(K_{ow}) values greater than about 5.6 is limited by their very low solubility in water, and consequent low bioavailability to aquatic biota (French McCay, 2002, Di Toro et al., 2000). Thus, the potential for acute effects is the result of a balance between bioavailability (exposure), toxicity once exposed, and duration of exposure. French McCay (2002) contains a full description of the oil toxicity model in SIMAP™, and French McCay (2002) describes the implementation of the toxicity model in SIMAP™.

Because of these considerations, the SIMAP™ fates model focuses on tracking the lower molecular weight aromatic components divided into chemical groups based on volatility, solubility, and hydrophobicity. In the model, the oil is treated as comprising eight components (defined in Table 1). Six of the components (i.e., all but the two non-volatile residual components representing non-volatile aromatics and aliphatics) evaporate at rates specific to the pseudo-component. Solubility is strongly correlated with volatility, and the solubility of aromatics is higher than aliphatics of the same volatility. The MAHs are the most soluble, the 2-ring PAHs are less soluble, and the 3-ring PAHs slightly soluble (Mackay et al., 1992). Both the solubility and toxicity of the non-aromatic hydrocarbons are much less than for the aromatics, and dissolution (and water concentrations) of non-aromatics is safely ignored. Thus, dissolved concentrations are calculated only for each of the three soluble aromatic pseudo-components.

Table 1. Definition of four distillation cuts and the eight pseudo-components in the model (Monoaromatic Hydrocarbons, MAHs; Benzene + Toluene + Ethylbenzene + Xylene, BTEX; Polycyclic Aromatic Hydrocarbons, PAHs).

Characteristic	Volatile and Highly Soluble	Semi-volatile and Soluble	Low Volatility and Slightly Soluble	Residual (non-volatile and very low solubility)
Distillation cut	1	2	3	4
Boiling Point (^{o}C)	< 180	180 - 265	265 - 380	>380
Molecular Weight	50 - 125	125 - 168	152 - 215	> 215
Log(K_{ow})	2.1-3.7	3.7-4.4	3.9-5.6	>5.6
Aliphatic pseudo-components: Number of Carbons	volatile aliphatics: C4 – C10	semi-volatile aliphatics: C10 – C15	low-volatility aliphatics: C15 – C20	non-volatile aliphatics: > C20
Aromatic pseudo-component name: included compounds	MAHs: BTEX, MAHs to C3-benzenes	2 ring PAHs: C4-benzenes, naphthalene, C1-, C2-naphthalenes	3 ring PAHs: C3-, C4-naphthalenes, 3-4 ring PAHs with log(K_{ow}) < 5.6	$\geq$4 ring aromatics: PAHs with log(K_{ow}) > 5.6 (very low solubility)

This number of components provides sufficient accuracy for the evaporation and dissolution calculations, particularly given the time frame (minutes) over which dissolution occurs from small droplets and the rapid resurfacing of large droplets (see discussion above). The alternative of treating oil as a single compound with empirically-derived rates (e.g., Mackay et al., 1980; Stiver and Mackay, 1984) does not provide sufficient accuracy for environmental effects analyses because the effects to water column organisms are caused by MAHs and PAHs, which have specific properties that differ from the other volatile and soluble compounds. The model has been validated both in predicting dissolved concentrations and resulting toxic effects, supporting the adequacy of the use of this number of pseudo-components (French McCay, 2003).

The lower molecular weight aromatics dissolve from the whole oil and are partitioned in the water column and sediments according to equilibrium partitioning theory (French et al., 1996a; French McCay, 2004). The residual fractions in the model are composed of non-volatile and insoluble compounds that remain in the “whole oil” that spreads, is transported on the water surface, strands on shorelines, and disperses into the water column as oil droplets or remains on the surface as tar balls. This is the fraction that composes black oil, mousse, and sheen.

7.1 Oil Fate Model Processes

The schematic in Figure 1 depicts oil fates processes simulated in open water conditions, while the schematic in Figure 2 depicts oil fates processes that are simulated at and near the shoreline. Because oil contains many chemicals with varying physical-chemical properties, and

the environment is spatially and temporally variable, the oil rapidly separates into different phases or parts of the environment:

- Surface oil
- Emulsified oil (mousse) and tar balls
- Oil droplets suspended in the water column
- Oil adhering to suspended particulate matter in the water
- Dissolved lower molecular weight components (MAHs, PAHs, and other soluble components) in the water column
- Oil on and in the sediments
- Dissolved lower molecular weight components (MAHs, PAHs, and other soluble components) in the sediment pore water
- Oil on and in the shoreline sediments and surfaces

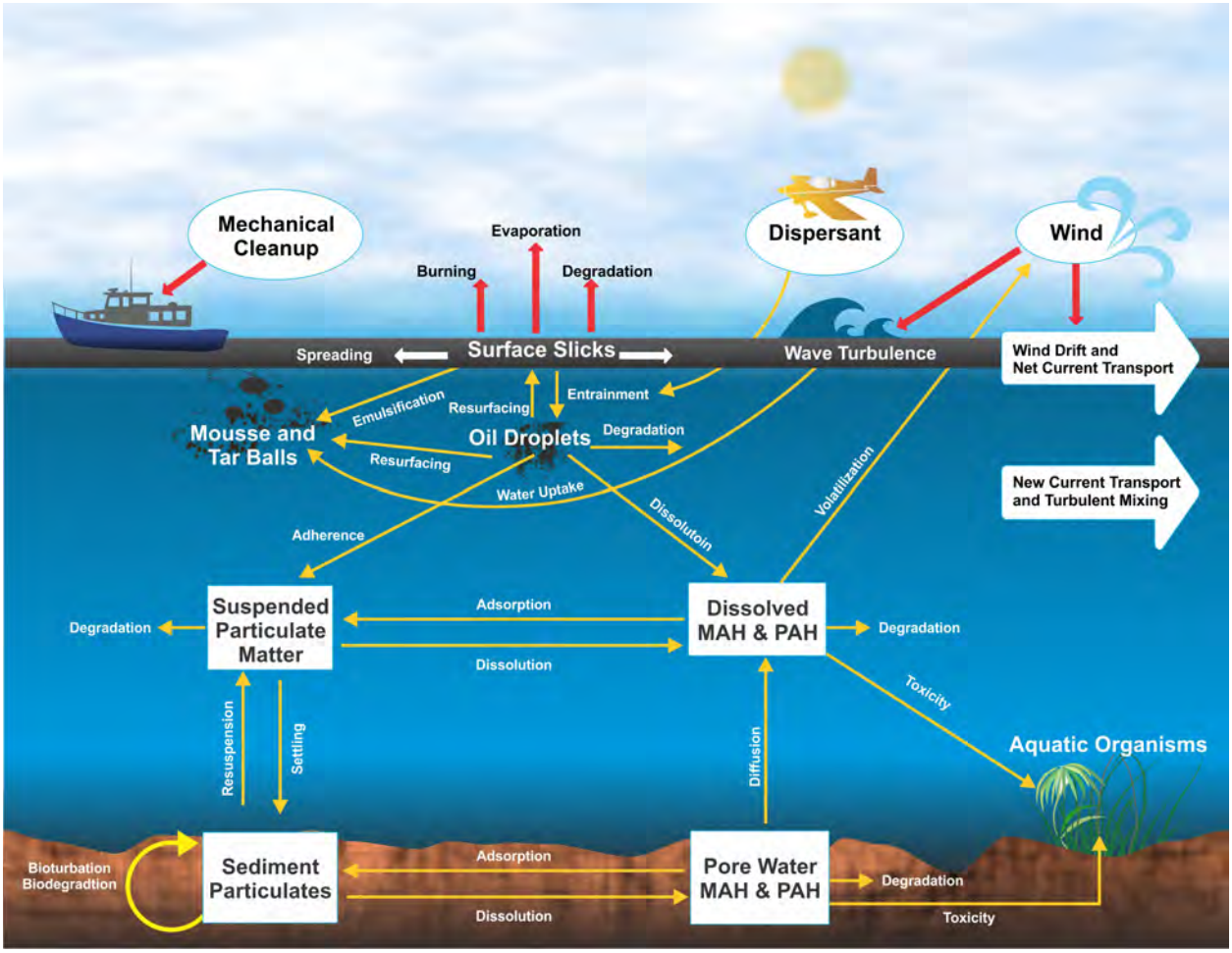

Figure 1. Simulated oil fates processes in open water.

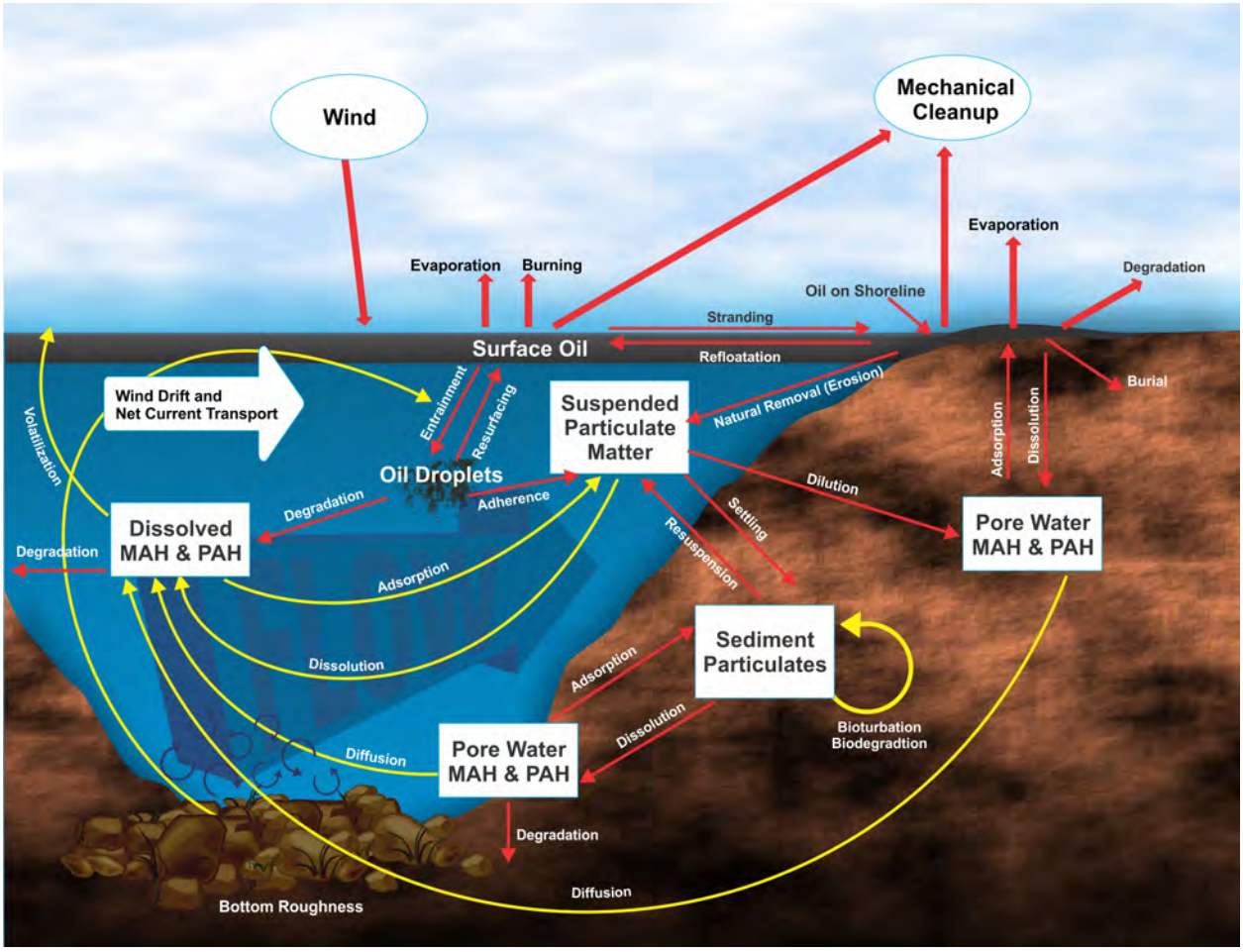

Figure 2. Simulated oil fates processes at the shoreline.

The schematics in Figure 1 and Figure 2 represent oil fates processes that are simulated in the model:

- Spreading is the thinning and broadening of surface slicks caused by gravitational forces and surface tension. This occurs rapidly after oil is spilled on the water surface. The rate of spreading is faster if oil viscosity is lower. Viscosity decreases as temperature increases. Viscosity increases as oil emulsifies.
- Transport is the process where oil is carried by currents.
- Turbulent dispersion: Typically there are also “sub-scale” currents (not included in the current data), better known as turbulence that move oil and mix it both in three dimensions. The process by which turbulence mixes and spreads oil components on the water surface and in the water is called turbulent dispersion.
- Evaporation is the process where volatile components of the oil diffuse from the oil and enter the gaseous phase (atmosphere). Evaporation from surface and shoreline oil increases as the oil surface area, temperature, and wind speed increase. As lighter components evaporate off, the remaining “weathered” oil becomes more viscous.

- Emulsification is the process where water is mixed into the oil, such that the oil makes a matrix with embedded water droplets. The resulting mixture is commonly called mousse. It is technically referred to as a water-in-oil emulsion. The rate of emulsification increases with increasing wind speed and turbulence on the surface of the water. Viscosity increases as oil emulsifies.
- Entrainment is the process where waves break over surface oil and carry it as droplets into the water column. At higher wind speeds, or where currents and bottom roughness induce turbulence, wave heights may reach a threshold where they break. In open waters, waves break beginning at about 12 knots of wind speed and wave breaking increases as wind speed becomes higher. Thus, entrainment becomes increasingly important (higher rate of mass transfer to the water) the higher the wind speed. As turbulence from whatever source increases, the oil droplet sizes become smaller. Application of chemical dispersant increases the entrainment rate of oil and decreases droplet size at a given level of turbulence. Entrainment rate is slower, and droplet size is larger, as oil viscosity increases (by emulsification and evaporation loss of lighter volatile components). The droplet size determines how fast and whether the oil resurfaces.
- Resurfacing of entrained oil rapidly occurs for larger oil droplets. Smaller droplets resurface when the wave turbulence decreases. The smallest droplets do not resurface, as typical turbulence levels in the water keep them in suspension indefinitely. Local winds at the water surface can also prevent oil from surfacing. Resurfaced oil typically forms sheens. In open water where currents are relatively slow, surface slicks are usually blown down wind faster than the underlying water, resurfacing droplets come up behind the leading edge of the oil, effectively spreading the slicks in the down-wind direction.
- Dissolution is the process where water-soluble components diffuse out of the oil into the water. Dissolution rate increases the higher the surface area of the oil relative to its volume. As the surface area to volume ratio is higher for smaller spherical droplets, the smaller the droplets the higher the dissolution rate. The higher the wave turbulence, the smaller the droplets of entrained oil. Dissolution from entrained small droplets is much faster than from surface slicks in the shape of flat plates. The soluble components are also volatile, and evaporation from surface slicks is faster than dissolution into the underlying water. Thus, the processes of evaporation and dissolution are competitive, with evaporation the dominant process for surface oil.
- Volatilization of dissolved components from the water to the atmosphere occurs as they are mixed and diffuse to the water surface boundary and enter the gas phase. Volatilization rate increase with increasing air and water temperature.
- Adsorption of dissolved components to particulate matter in the water occurs because the soluble components are only sparingly so. These compounds (MAHs and PAHs) preferentially adsorb to particulates when the latter are present. The higher the concentration of suspended particulates, the more adsorption. Also, the higher the molecular weight of the compound, the less soluble, and the more the compound adsorbs to particulate matter.

- Adherence is the process where oil droplets combine with particles in the water. If the particles are suspended sediments, the combined oil/suspended sediment agglomerate is heavier than the oil itself and than the water. If turbulence subsides sufficiently, the oil-sediment agglomerates will settle.
- Sedimentation (settling) is the process where oil-sediment agglomerates and particles with adsorbed sparingly-soluble components (MAHs and PAHs) settle to the bottom sediments. Adherence and sedimentation can be an important pathway of oil in near shore areas when waves are strong and subsequently subside. Generally, oil-sediment agglomerates transfer more PAH to the bottom than sediments with PAHs that were adsorbed from the dissolved phase in the water column.
- Resuspension of settled oil-sediment particles and particles with adsorbed sparingly-soluble components (MAHs and PAHs) may occur if current speeds and turbulence exceed threshold values where cohesive forces can be overcome.
- Diffusion is the process where dissolved compounds move from higher to lower concentration areas by random motion of molecules and micro-scale turbulence. Dissolved components in bottom and shoreline sediments can diffuse out to the water where concentrations are relatively low. Bioturbation, groundwater discharge and hyporheic flow of water through stream-bed sediments can greatly increase the rate of diffusion from sediments (see below).
- Dilution occurs when water of lower concentration is mixed into water with higher concentration by turbulence, currents, or shoreline groundwater.
- Bioturbation is the process where animals in the sediments mix the surface sediment layer while burrowing, feeding, or passing water over their gills. In open-water soft-bottom environments, bioturbation effectively mixes the surface sediment layer about 10 cm thick (in non-polluted areas).
- Degradation is the process where oil components are changed either chemically or biologically (biodegradation) to another compound. It includes breakdown to simpler organic carbon compounds by bacteria and other organisms, photo-oxidation by solar energy, and other chemical reactions. Higher temperature and higher light intensity (particularly ultraviolet wavelengths) increase the rate of degradation.
- Floating oil may strand on shorelines and refloat as water levels rise, allowing the oil to move further down current (downstream).

For a spill on the water surface, the gravitational spreading occurs very rapidly (within hours) to a minimum thickness. Thus, the area exposed to evaporation is high relative to the oil volume. Evaporation proceeds faster than dissolution. Thus, most of the volatiles and semi-volatiles evaporate, with a smaller fraction dissolving into the water. Degradation (photo-oxidation and biodegradation) also occurs at a relatively slow rate compared to these processes.

Evaporation is more rapid as the wind speed increases. However, above about 12 knots (6 m/s) of wind speed and in open water, white caps begin to form and the breaking waves entrain oil as droplets into the water column. Higher wind speeds (and turbulence) increase entrainment and results in smaller droplet sizes. From Stoke's Law, larger droplets resurface faster and form

surface slicks. Thus, a dynamic balance evolves between entrainment and resurfacing. As high-wind events occur, the entrainment rate increases. When the winds subside to less than 12 knots, the larger oil droplets resurface and remain floating. Similar dynamics occur in turbulent streams.

The smallest oil droplets remain entrained in the water column for an indefinite period. Larger oil droplets rise to the surface at varying rates. While the droplets are under water, dissolution of the light and soluble components occurs. Dissolution rate is a function of the surface area available. Thus, most dissolution occurs from droplets, as opposed to from surface slicks, since droplets have a higher surface area to volume ratio, and they are not in contact with the atmosphere (and so the soluble components do not preferentially evaporate as they do from surface oil).

If oil is released or driven underwater, it forms droplets of varying sizes. More turbulent conditions result in smaller droplet sizes. From Stoke's Law, larger droplets rise faster, and surface if the water is shallow. Resurfaced oil behaves as surface oil after gravitational spreading has occurred. The surface oil may be re-entrained. The smallest droplets in most cases remain in the water permanently. As a result of the higher surface area per volume of small droplets, the dissolution rate is much higher from subsurface oil than from floating oil on the water surface.

Because of these interactions, the majority of dissolved constituents (which are of concern because of potential effects on aquatic organisms) are from droplets entrained in the water. For a given spill volume and oil type/composition, with increasing turbulence either at the water surface and/or at the stream bed: there is an increasing amount of oil entrained; the oil is increasingly broken up into smaller droplets; there is more likelihood of the oil remaining entrained rather than resurfacing; and the dissolved concentrations will be higher. Entrainment and dissolved concentrations increase with (1) higher wind speed, (2) increased turbulence from other sources of turbulence (waves on a beach, rapids, and waterfalls in rivers, etc.), (3) subsurface releases (especially under higher pressure and turbulence), and (4) application of chemical dispersants. Chemical dispersants both increase the amount of oil entrained and decrease the oil droplet size. Thus, chemical dispersants increase the dissolution rate of soluble components.

These processes that increase the rate of supply of dissolved constituents are balanced by loss terms in the model: (1) transport (dilution), (2) volatilization from the dissolved phase to the atmosphere, (3) adsorption to suspended particulate material (SPM) and sedimentation, and (4) degradation (photo-oxidation or biologically mediated). Also, other processes slow the entrainment rate: (1) emulsification increases viscosity and slows or eliminates entrainment; (2) adsorption of oil droplets to SPM and settling removes oil from the water; (3) stranding on shorelines removes oil from the water; and (4) mechanical cleanup and burning removes mass from the water surface and shorelines. Thus, the model-predicted concentrations are the

resulting balance of all these processes and the best estimates based on our quantitative understanding of the individual processes.

The algorithms used to model these processes are described in French McCay (2004). Lagrangian elements (spillets) are used to simulate the movements of oil components in three dimensions over time. Surface floating oil, subsurface droplets, and dissolved components are tracked in separate spillets. Transport is the sum of advective velocities by currents input to the model, surface wind drift, vertical movement according to buoyancy, and randomized turbulent diffusive velocities in three dimensions. The vertical diffusion coefficient is computed as a function of wind speed in the surface wave-mixed layer. The horizontal and deeper water vertical diffusion coefficients are model inputs.

The oil (whole and as pseudo-components) separates into different phases or parts of the environment, i.e., surface slicks; emulsified oil (mousse) and tar balls; oil droplets suspended in the water column; dissolved lower molecular weight components (MAHs and PAHs) in the water column; oil droplets adhered and hydrocarbons adsorbed to suspended particulate matter in the water; hydrocarbons on and in the sediments; dissolved MAHs and PAHs in the sediment pore water; and hydrocarbons on and in the shoreline sediments and surfaces.

7.2 Oil Fates Algorithms

7.2.1 Transport

Lagrangian particles (spillets) are moved in three dimensions over time. For each model time step, the new vector position of the spillet centre is calculated from the old plus the vector sum of east-west, north-south, and vertical components of advective and diffusive velocities:

$$X_t = X_{t-1} + \Delta t \, (U_t + D_t + R_t + W_t)$$

where X_t is the vector position at time t, X_{t-1} is the vector position the previous time step, Δt is the time step, U_t is the sum of all the advective (current) velocity components in three dimensions at time t, D_t is the sum of the randomized diffusive velocities in three dimensions at time t, R_t is the rise or sinking velocity of whole oil droplets in the water column, and W_t is the surface wind transport ("wind drift"). The magnitudes of the components of D_t are scaled by horizontal and vertical diffusion coefficients (Okubo and Ozmidov, 1970; Okubo, 1971). The vertical diffusion coefficient is computed as a function of wind speed in the surface wave-mixed layer (which ranges from centimetre scales in rivers and near lee shorelines to potentially metres in large water bodies away from shore when wind speeds are high), based on Thorpe (1984). R_t is computed by Stokes law, where velocity is related to the difference in density between the particle and the water, and to the particle diameter. The algorithm developed by Youssef and Spaulding (1993) is used for wind transport in the surface wave-mixed layer (W_t, described below).

7.2.2 Shoreline Stranding

The fate of spilled oil that reaches the shoreline depends on characteristics of the oil, the type of shoreline, and the energy environment. The stranding algorithm is based on work by CSE/ASA/BAT (1986), Gundlach (1987), and Reed and Gundlach (1989) in developing the COZOIL model for the U.S. Minerals Management Service. In SIMAP™, deposition occurs when an oil spillet intersects shore surface. Deposition ceases when the volume holding capacity for the shore surface is reached. Subsequent oil coming ashore is not allowed to remain on the shore surface. It is refloated by rising water, and carried away by currents and wind drift. The remaining shoreline oil is then removed exponentially with time. Data for holding capacity and removal rate are taken from CSE/ABA/BAT (1986) and Gundlach (1987), and are a function of oil viscosity and shore type. The algorithm and data are in French et al. (1996a).

7.2.3 Spreading

Spreading determines the areal extent of the surface oil, which in turn influences its rates of evaporation, dissolution, dispersion (entrainment) and photo-oxidation, all of which are functions of surface area. Spreading results from the balance among the forces of gravity, inertia, viscosity, and surface tension (which increases the diameter of each spillet); turbulent diffusion (which spreads the spillets apart); and entrainment followed by resurfacing, which can spatially separate the leading edge of the oil from resurfaced oil transported in a different direction by subsurface currents.

For many years Fay's (1971) three-regime spreading theory was widely used in oil spill models (ASCE, 1996). Mackay et al. (1980; 1982) modified Fay's approach and described the oil as thin and thick slicks. Their approach used an empirical formulation based on Fay's (1971) terminal spreading behaviour. They assumed the thick slick feeds the thin slick and that 80-90% of the total slick area is represented by the thin slick. In SIMAP™, oil spillets on the water surface increase in diameter according to the spreading algorithm empirically-derived by Mackay et al. (1980; 1982). Sensitivity analyses of this algorithm led to the discovery that the solution was affected by the number of spillets used. Thus, a formulation was derived to normalize the solution under differing numbers of surface spillets (Kolluru et al., 1994). Spreading is stopped when an oil-specific terminal thickness is reached.

7.2.4 Evaporation

The rate of evaporation depends on surface area, thickness, vapour pressure and mass transport coefficient, which in turn are functions of the composition of the oil, wind speed and temperature (Fingas, 1996; 1997; 1998; 1999; Jones, 1997). As oil evaporates its composition changes, affecting its density and viscosity as well as subsequent evaporation. The most volatile hydrocarbons evaporate most rapidly, typically in less than a day and sometimes in under an hour (McAuliffe, 1989). As the oil continues to weather, and particularly if it forms a water-in-oil emulsion, evaporation will be significantly decreased.

The evaporation algorithm in SIMAP™ is based on accepted evaporation theory, which follows Raoult's Law that each component will evaporate with a rate proportional to the saturation vapour pressure and mole fraction present for that component. The pseudo-component approach (Payne et al., 1984; French et al., 1996a; Jones, 1997; Lehr et al., 2000) is used, such that each component evaporates according to its mean vapour pressure, solubility, and molecular weight (Table 2-3). The mass transfer coefficient is calculated using the methodology of Mackay and Matsugu (1973), as described in French et al. (1996a).

7.2.5 ENTRAINMENT

As oil on the water surface is exposed to wind and waves, or if oil moves into a turbulent area of a stream or river, it is entrained (or dispersed) into the water column. Entrainment is a physical process where globules of oil are transported from the water surface into the water column due to breaking waves or other turbulence. It has been observed that entrained oil is broken into droplets of varying sizes. Smaller droplets spread and diffuse in the water column, while larger ones rise back to the surface.

Entrainment by Breaking Surface Wave Action

In open waters, breaking waves created by the action of wind and waves on the water surface are the primary sources of energy for entrainment. Entrainment is strongly dependant on turbulence and is greater in areas of high wave energy (Delvigne and Sweeney, 1988).

Delvigne and Sweeney (1988), using laboratory and flume experimental observations, developed a relationship for entrainment rate and oil droplet size distribution as a function of turbulent energy level and oil viscosity. Entrained droplets in the water column rise according to Stokes law, where velocity is related to the difference in density between the particle and the water, and to the particle diameter. The data and relationships in Delvigne and Sweeney (1988) are used in SIMAP™ to calculate mass and particle size distribution of droplets entrained. Particle size decreases with higher turbulent energy level and lower oil viscosity. The natural dispersion particle sizes observed by Delvigne and Sweeney (1988) are confirmed by field observations by Lunel (1993a,b).

Use of chemical dispersants (not modelled in the scenarios examined here) decrease the median particle size, increasing the number of droplets in the <70 µm range (Daling et al., 1990; Lunel, 1993a,b). Particle size distributions for dispersed oil are available for several oils from these studies. When dispersant is applied, the model entrains surface oil, creating subsurface droplets in the appropriate size distribution for dispersant use. The median particle size for permanently dispersed droplets is set at 20 microns, the median size observed by Lunel (1993a,b). The fraction of oil permanently dispersed is set by the assumed dispersant efficiency. The IKU/SINTEF studies provide data on the viscosity range where oils may be dispersed

chemically. Typically, dispersants are effective up to about 10,000 cp (Aamo et al., 1993; Daling and Brandvik, 1988; 1991; Daling et al., 1997). In the model, oil is dispersed up to 10,000 cp.

Entrained oil is well mixed in (i.e., mixed uniformly throughout) the wave-mixed zone. Vertical mixing is simulated by random placement of particles within the wave-mixed layer each time step. Settling of particles does not occur in water depths where waves reach the bottom (taken as 1.5 times wave height). Wave height is calculated from wind speed, duration and fetch (distance upwind to land), using the algorithms in CERC (1984). Wave height is on the scale of centimetres in small rivers and streams, and near lee shorelines; whereas it may increase to metres in open waters under windy conditions.

7.2.6 EMULSIFICATION (MOUSSE FORMATION)

The formation of water-in-oil emulsions, or mousse, depends on oil composition and turbulence level. Emulsified oil can contain as much as 80% water in the form of micrometre-sized droplets dispersed within a continuous phase of oil (Daling and Brandvik, 1988; Fingas et al., 1997). Viscosities are typically much higher than that of the parent oil. The incorporation of water also dramatically increases the oil/water mixture volume.

The Mackay and Zagorski (1982) emulsification scheme is implemented in SIMAP™ for floating oil. Water content increases exponentially, with the rate related to the square of wind speed and previous water incorporation. Viscosity is a function of water content. The change in viscosity feeds back in the model to the entrainment rate.

7.2.7 DISSOLUTION

Dissolution is the process by which soluble hydrocarbons enter the water from a surface slick or from entrained oil droplets. The lower molecular weight hydrocarbons tend to be both more volatile and more soluble than those of higher molecular weight. For surface slicks, since the partial pressures tend to exceed the solubilities of these lower molecular weight compounds, evaporation accounts for a larger portion of the mass than dissolution (McAuliffe, 1989), except perhaps under ice. Dissolution and evaporation are competitive processes. The dissolved component concentration of hydrocarbons in water under a surface slick shows an initial increase followed by a rapid decrease after some hours due to the evaporative loss of components. Most soluble components are also volatile and direct evaporation (volatilization) from the water column depletes their concentrations in the water. Dissolution is particularly important where evaporation is low (dispersed oil droplets and ice-covered surfaces). Dissolution can be significant from entrained droplets because of the lack of atmospheric exposure and because of the higher surface area per unit of volume.

The model developed by Mackay and Leinonen (1977) is used in SIMAP™ for dissolution from a surface slick. The slick (spillet) is treated as a flat plate, with a mass flux (Hines and Maddox,

1985) related to solubility and temperature. It assumes a well-mixed layer with most of the resistance to mass transfer lying in a hypothetical stagnant region close to the oil. For subsurface oil, dissolution is treated as a mass flux across the surface area of a droplet (treated as a sphere) in a calculation analogous to the Mackay and Leinonen (1977) algorithm. The dissolution algorithm was developed in French et al. (1996a).

7.2.8 VOLATILIZATION FROM THE WATER COLUMN

The procedure outlined by Lyman et al. (1982), based on Henry's Law and mass flux (Hines and Maddox, 1985), is followed in the SIMAP^{TM} fates model. The volatilization depth for dissolved substances is limited to the maximum of one half the wave height. Wave height is computed from the wind speed and fetch (CERC, 1984). The volatilization algorithm was developed in French et al. (1996a).

7.2.9 ADSORPTION AND SEDIMENTATION

Aromatics dissolved in the water column are carried to the sediments primarily by adsorption to suspended particulates, and subsequent settling. The ratio of adsorbed (C_a) to dissolved (C_{dis}) concentrations is computed from standard equilibrium partitioning theory as

$$C_a / C_{dis} = K_{oc} C_{ss}$$

K_{oc} is a dimensionless partition coefficient and C_{ss} is the concentration of suspended particulate matter (SPM) in the water column expressed as mass of particulate per volume of water. As a default, the model uses a mean value of total suspended solids of 10 mg/l (Kullenberg, 1982); alternatively suspended sediment concentration is specified as model input.

Sedimentation of oil droplets occurs when the specific gravity of oil increases over that of the surrounding water. Several processes may act on entrained oil and surface slicks to increase density: weathering (evaporation, dissolution and emulsification), adhesion or sorption onto suspended particles or detrital material, and incorporation of sediment into oil during interaction with suspended particulates, bottom sediments, and shorelines. Rates of sedimentation depend on the concentration of suspended particulates and the rates of particulate flux into and out of an area. In areas with high suspended particulate concentrations, rapid dispersal and removal of oil is found due to sorption and adhesion (Payne and McNabb, 1984).

Kirstein et al. (1987) and Payne et al. (1987) used a reaction term to characterize the water column interactions of oil and suspended particulates. The reaction term represents the collision of oil droplets and suspended matter, and both oiled and unoiled particulates are accounted for. The model formulation developed by Kirstein et al. (1987) is used to calculate the volume of oil adhered to particles. In the case where the oil mass is larger than the adhered sediment (i.e., the sediment has been incorporated into the oil) the buoyancy of the oil droplet will control its

settling or rise rate. The Stoke's law formulation is used to adjust vertical position of these particles. If the mass of adhered droplets is small relative to the mass of the sediment it has adhered to, the sediment settling velocity will control the fate of the combined particulate.

7.2.10 DEGRADATION

Degradation may occur as the result of photolysis, which is a chemical process energized by ultraviolet light from the sun, and by biological (bacterial) breakdown, termed biodegradation. In the model, degradation occurs on the surface slick, deposited oil on the shore, the entrained oil and aromatics in the water column, and oil in the sediments. A first order decay algorithm is used, with a specified (total) degradation rate for each of surface oil, water column oil and sedimented oil (French et al., 1999).

7.3 HABITAT TYPE

Ecological habitat types (Table 2) are broadly categorized into two zones within SIMAP^{TM}: shoreline and submerged (or intertidal versus subtidal in estuarine and marine areas, where intertidal habitats are those above spring low water tide level, with subtidal being all water areas below that level). In modelled scenarios, the shoreline habitats may become oiled as surface oil makes contact with these cells. Submerged or subtidal cells are always underwater. Intertidal/shoreline areas may be extensive, such that they are wide enough to be represented by an entire grid cell at the resolution of the grid. These are typically either mud flats or wetlands, and are coded 20 (seaward mudflat), 21 (seaward wetland), 50 (landward mudflat), or 51 (landward wetland). All other intertidal/shoreline habitats are typically much narrower than the size of a grid cell. Thus, these fringing intertidal/shore types (indicated by F in Table 2) have typical (for the region, e.g., French et al., 1996a for estuarine and marine areas) widths associated with them in the model. Boundaries between land and water are fringing habitat types. On the waterside of fringing grid cells, there may be extensive intertidal/shoreline grid cells if the wetlands or mudflats are extensive. Otherwise, subtidal/submerged habitats border the fringing cells.

Table 2. Classification of habitats. seaward (Sw) and landward (Lw) system codes are listed. (fringing types indicated by (F) are only as wide as the intertidal zone or shoreline width where oiling might occur. Others (W = water) are a full grid cell wide and have a fringing type on the land side.)

Habitat Code (Sw,Lw)	Ecological Habitat	F or W
Intertidal / Shore		
1,31	Rocky Shore	F
2,32	Gravel Shore	F
3,33	Sand Beach or Shore	F
4,34	Fringing Mud Flat	F

Habitat Code (Sw,Lw)	Ecological Habitat	F or W
5,35	Fringing Wetland (Emergent or Forested)	F
6,36	Macroalgal Bed	F
7,37	Mollusk Reef	F
8,38	Coral Reef (marine only)	F
Subtidal / Submerged		
9,39	Rock Bottom	W
10,40	Gravel Bottom	W
11,41	Sand Bottom	W
12,42	Silt-mud Bottom	W
13,43	Wetland (submerged areas)	W
14,44	Macroalgal Bed	W
15,45	Mollusk Reef	W
16,46	Coral Reef (marine only)	W
17,47	Submerged Aquatic Vegetation Bed	W
Intertidal / Shore		
18,48	Man-made, Artificial	F
19,49	Ice Edge	F
20,50	Extensive Mud Flat	W
21,51	Extensive Wetland (Emergent or Forested)	W

7.4 REFERENCES

Aamo, O.M., M. Reed and P. Daling, 1993. A laboratory based weathering model: PC version for coupling to transport models. In Proceedings of the 16th Arctic and Marine Oil Spill Program (AMOP) Technical Seminar, Environmental Protection Service, Emergencies Science Division, Environment Canada, Ottawa, ON, Canada, pp. 617-626.

ASCE Task Committee on Modeling Oil Spills, 1996. State-of-the-art Review of Modeling Transport and Fate of Oil Spills, Water Resources Engineering Division, ASCE, Journal of Hydraulic Engineering 122(11): 594-609.

Coastal Engineering Research Center (CERC), 1984. Shore Protection Manual, Vol. I. Coastal Engineering Research Center, Department of the Army, Waterways Experiment Station, U.S. Army Corps of Engineers, Vicksburg, Mississippi, 1,105p. plus 134p. in appendices.

CSE/ASA/BAT, 1986. Development of a Coastal Oil Spill Smear Model. Phase 1: Analysis of Available and Proposed Models, Prepared for Minerals Management Service by Coastal Science & Engineering, Inc. (CSE) with Applied Science Associates, Inc. (ASA) and Battelle New England Research Laboratory (BAT), 121p.

Daling, P.S. and P.J. Brandvik, 1988. A Study of the Formation and Stability of Water-in-Oil Emulsions. In Proceedings of the 11th Arctic and Marine Oil Spill Program Technical Seminar. Emergencies Science Division, Environment Canada, Ottawa, ON, Canada, pp.153-170.

Daling, P.S., D. Mackay, N. Mackay, and P.J. Brandvik, 1990. Droplet size distributions in chemical dispersion of oil spills: Towards a mathematical model. Oil and Chemical Pollution 7: 173-198.

Daling, P.S. and P.J. Brandvik, 1991. Characterization and prediction of the weathering properties of oils at sea – A manual for the oils investigated in the DIWO project. IKU SINTEF Group report 91.037, DIWO report no. 16 02.0786.00/16/91, 29 May 1991, 140p.

Daling, P.S., O.M. Aamo, A. Lewis, and T. Strom-Kritiansen, 1997. SINTEF/IKU Oil-Weathering Model: Predicting Oil's Properties at Sea. In Proceedings 1997 Oil Spill Conference, Publication No. 4651, American Petroleum Institute, Washington, D.C., pp. 297-307.

Daling, P.S. A.Lewis, S. Ramstad. 1999. The use of colour as a guide to oil film thickness – Main report. SINTEF Report STF66 F99082. 48p., SINTEF, Trondheim, Norway.

Delvigne, G.A.L. and C.E. Sweeney, 1988. Natural Dispersion of Oil. Oil and Chemical Pollution 4: 281-310.

Di Toro, D.M., J.A. McGrath and D.J. Hansen, 2000. Technical basis for narcotic chemicals and polycyclic aromatic hydrocarbon criteria. I. Water and tissue. Environmental Toxicology and Chemistry 19(8): 1951-1970.

Fay, J.A., 1971. Physical processes in the spread of oil on a water surface. In Proceedings, Conference on Prevention and Control of Oil Spills, sponsored by API, EPA, and US Coast Guard, American Petroleum Institute, Washington, D.C., June 15-17, 1971, pp. 463-467.

Fingas, M., 1996. The Evaporation of Crude Oil and Petroleum Products. PhD Dissertation, McGill University, Montreal, Canada, 181p.

Fingas, M., B. Fieldhouse, and J.V. Mullin, 1997. Studies of Water-in-Oil Emulsions: Stability Studies. In Proceedings of 20th Arctic and Marine Oil Spill Program (AMOP) Technical Seminar, Emergencies Science Division, Environment Canada, Ottawa, ON, Canada, pp. 21-42.

Fingas, M., 1997. The Evaporation of Oil Spills: Prediction of Equations Using Distillation Data. In Proceedings of the 20th Arctic and Marine Oil Spill Program (AMOP) Technical Seminar, Emergencies Science Division, Environment Canada, Ottawa, ON, Canada, pp. 1-20.

Fingas, M.F., 1998. Studies on the Evaporation of Crude Oil and Petroleum Products: II. Boundary Layer Regulation. Journal of Hazardous Materials, Vol. 57, pp.41-58.

Fingas, M.F., 1999. The Evaporation of Oil Spills: Development and Implementation of New Prediction Methodology. In Proceedings of the 1999 International Oil Spill Conference, American Petroleum Institute, Washington, D.C., pp. 281-287.

Fingas, M., B. Fieldhouse, and J.V. Mullin, 1997. Studies of Water-in-Oil Emulsions: Stability Studies. In: Proceedings of 20th Arctic and Marine Oil Spill Program (AMOP) Technical Seminar, Emergencies Science Division, Environment Canada, Ottawa, ON, Canada, pp. 21-42.

French, D., M. Reed, K. Jayko, S. Feng, H. Rines, S. Pavignano, T. Isaji, S. Puckett, A. Keller, F. W. French III, D. Gifford, J. McCue, G. Brown, E. MacDonald, J. Quirk, S. Natzke, R. Bishop, M. Welsh, M. Phillips and B.S. Ingram, 1996a. The CERCLA type A natural resource damage assessment model for coastal and marine environments (NRDAM/CME), Technical Documentation, Vol. I - Model Description. Final Report, submitted to the Office of Environmental Policy and Compliance, U.S. Dept. of the Interior, Washington, DC, April, 1996, Contract No. 14-0001-91-C-11.

French, D., M. Reed, S. Feng and S. Pavignano, 1996b. The CERCLA type A natural resource damage assessment model for coastal and marine environments (NRDAM/CME), Technical Documentation, Vol. III - Chemical and Environmental Databases. Final Report, Submitted to the Office of Environmental Policy and Compliance, U.S. Dept. of the Interior, Washington, DC, April, 1996, Contract No. 14-01-0001-91-C-11.

French, D., S. Pavignano, H. Rines, A. Keller, F.W. French III and D. Gifford, 1996c. The CERCLA type A natural resource damage assessment model for coastal and marine environments (NRDAM/CME), Technical Documentation, Vol.IV - Biological Databases. Final Report, Submitted to the Office of Environmental Policy and Compliance, U.S. Dept. of the Interior, Washington, DC, April, 1996, Contract No. 14-01-0001-91-C-11.

French, D.P. and H. Rines, 1997. Validation and use of spill impact modeling for impact assessment. Proceedings, 1997 International Oil Spill Conference, Fort Lauderdale, Florida, American Petroleum Institute Publication No. 4651, Washington, DC, pp-829-834.

French, D.P., H. Rines and P. Masciangioli, 1997. Validation of an Orimulsion spill fates model using observations from field test spills. Proceedings, Twentieth Arctic and Marine Oil Spill Program Technical Seminar, Vancouver, Canada, June 10-13, 1997.

French, D., H. Schuttenberg, and T. Isaji, 1999. Probabilities of Oil Exceeding Thresholds of Concern: Examples from an Evaluation for Florida Power and Light. In Proceedings of the

22nd Arctic and Marine Oil Spill Program (AMOP) Technical Seminar, June 2-4, 1999, Calgary, Alberta, Environment Canada, pp.243-270.

French McCay, D. and J.R. Payne, 2001. Model of Oil Fate and Water concentrations with and without application of dispersants. In Proceedings of the 24th Arctic and Marine Oil Spill Program (AMOP) Technical Seminar, Emergencies Science Division, Environment Canada, Ottawa, ON, Canada, pp. 601-653.

French McCay, D.P., 2002. Development and Application of an Oil Toxicity and Exposure Model, OilToxEx. Environmental Toxicology and Chemistry 21(10): 2080-2094.

French McCay, D.P., 2003. Development and Application of Damage Assessment Modeling: Example Assessment for the North Cape Oil Spill. Marine Pollution Bulletin, Volume 47, Issues 9-12, September-December 2003, pp. 341-359.

French McCay, D.P., 2004. Oil spill impact modeling: Development and validation. Environmental Toxicology and Chemistry 23(10): 2441-2456.

French McCay, D.P., and J.J. Rowe, 2004. Evaluation of Bird Impacts in Historical Oil Spill Cases Using the SIMAP Oil Spill Model. In Proceedings of the 27th Arctic and Marine Oil Spill Program (AMOP) Technical Seminar, Emergencies Science Division, Environment Canada, Ottawa, ON, Canada, pp. 421-452.

Gundlach, E.R., 1987. Oil Holding Capacities and Removal Coefficients for Different Shoreline Types to Computer Simulate Spills in Coastal Waters. In Proceedings of the 1987 Oil Spill Conference, pp. 451-457.

Hines, A.L. and R.N. Maddox, 1985. Mass Transfer Fundamentals and Application. Prentice-Hall, Inc., Englewood Cliffs, New Jersey, 542p.

Jones, R.K., 1997. A Simplified Pseudo-Component of Oil Evaporation Model. In Proceedings of the 20th Arctic and Marine Oil Spill Program (AMOP) Technical Seminar, Environment Canada, pp. 43-61.

Kirstein, B.E., J.R. Clayton, C. Clary, J.R. Payne, D. McNabb, Jr., G. Fauna and R. Redding, 1987. Integration of Suspended Particulate Matter and Oil Transportation Study. Minerals Management Service, OCS Study MMS87-0083, Anchorage, Alaska, 216p.

Kolluru, V., M.L. Spaulding and E. Anderson, 1994. A three dimensional subsurface oil dispersion model using a particle based approach. In Proceedings of 17th Arctic and Marine Oil Spill Program (AMOP) Technical Seminar, Vancouver, British Columbia, June

8-10, 1994, Emergencies Science Division, Environment Canada, Ottawa, ON, Canada, pp. 867-893.

Kullenberg, G. (ed.), 1982. Pollutant transfer and transport in the sea. Volume I. CRC Press, Boca Raton, Florida. 227 p.

Lehr, W.J., D. Wesley, D. Simecek-Beatty, R. Jones, G. Kachook and J. Lankford, 2000. Algorithm and interface modifications of the NOAA oil spill behavior model. In Proceedings of the 23rd Arctic and Marine Oil Spill Program (AMOP) Technical Seminar, Vancouver, BC, Environmental Protection Service, Environment Canada, pp. 525-539.

Lunel, T., 1993a. Dispersion: Oil droplet size measurements at sea. In Proceedings of the 16th Arctic Marine Oilspill Program (AMOP) Technical Seminar, Environment Canada, Calgary, Alberta, June 7-9, 1993, pp. 1023-1056.

Lunel, T., 1993b. Dispersion: Oil droplet size measurements at sea. In Proceedings of the 1993 Oil Spill Conference, pp. 794-795.

Lyman, C.J., W.F. Reehl, and D.H. Rosenblatt, 1982. Handbook of Chemical Property Estimation Methods. McGraw-Hill Book Co., New York, 960p.

Mackay, D. and R.M. Matsugu, 1973. Evaporation rates of liquid hydrocarbon spills on land and water. Canadian Journal of Chemical Engineering 51: 434-439.

Mackay, D. and P.J. Leinonen, 1977. Mathematical model of the behavior of oil spills on water with natural and chemical dispersion. Prepared for Fisheries and Environment Canada. Economic and Technical Review Report EPS-3-EC-77-19, 39p.

Mackay, D., S. Paterson and K. Trudel, 1980. A mathematical model of oil spill behavior. Department of Chemical and Applied Chemistry, University of Toronto, Canada, 39p.

Mackay, D., and W. Zagorski, 1982. Water-In-Oil Emulsions. Environment Canada Manuscript Report EE-34, Ottawa, Ontario, Canada, 93p.

Mackay, D, W.Y. Shiu, K. Hossain, W. Stiver, D. McCurdy and S. Peterson, 1982. Development and calibration of an oil spill behavior model. Report No. CG-D-27-83, U.S. Coast Guard, Research and Development Center, Groton, Connecticut, 83p.

Mackay, D., W.Y. Shiu, and K.C. Ma, 1992. Illustrated Handbook of Physical-Chemical Properties and Environmental Fate for Organic Chemicals, Vol. I-IV. Lewis Publishers, Inc, Chelsea, Michigan.

McAuliffe, C.D., 1987. Organism exposure to volatile/soluble hydrocarbons from crude oil spills –a field and laboratory comparison. Proceedings of the 1987 Oil Spill Conference. Washington, D.C.: API. pp. 275-288.

McAuliffe, C.D., 1989. The Weathering of Volatile Hydrocarbons from Crude Oil Slicks on Water. In Proceedings of the 1989 Oil Spill Conference, San Antonio, Texas, American Petroleum Institute, Washington, D.C., pp. 357-364.

Okubo, A. and R.V. Ozmidov, 1970. Empirical dependence of the coefficient of horizontal turbulent diffusion in the ocean on the scale of the phenomenon in question. Atmospheric and Ocean Physics 6(5):534-536.

Okubo, A., 1971. Oceanic diffusion diagrams. Deep-Sea Research 8:789-802.

Payne, J.R. and G.D. McNabb Jr., 1984. Weathering of Petroleum in the Marine Environment. Marine Technology Society Journal 18(3):24-42.

Payne, J.R., B.E. Kirstein, G.D. McNabb, Jr., J.L. Lambach, R. Redding R.E. Jordan, W. Hom, C. deOliveria, G.S. Smith, D.M. Baxter, and R. Gaegel, 1984. Multivariate analysis of petroleum weathering in the marine environment – sub Arctic. Environmental Assessment of the Alaskan Continental Shelf, OCEAP, Final Report of Principal Investigators, Vol. 21 and 22, Feb. 1984, 690p.

Payne, J.R., B.E. Kirstein, J.R. Clayton, Jr., C. Clary, R. Redding, G.D. McNabb, Jr., and G. Farmer, 1987. Integration of suspended particulate matter and oil transportation study. Final Report. Minerals Management Service, Environmental Studies Branch, Anchorage, AK. Contract No. 14-12-0001-30146, 216 p.

Stiver, W. and D. Mackay, 1984. Evaporation rate of oil spills of hydrocarbons and petroleum mixtures. Environmental Science and Technology 18: 834-840.

Thorpe, S.A., 1984. On the Determination of K in the Near Surface Ocean from Acoustic Measurements of Bubbles. Journal of Physical Oceanography 14: 855-863.

Youssef, M. and M.L. Spaulding, 1993. Drift current under the action of wind waves, Proceedings of the 16th Arctic and Marine Oil Spill Program Technical Seminar, Calgary, Alberta, Canada, pp. 587-615.

7.5 REFERENCES – SIMAP EXAMPLE APPLICATIONS AND VALIDATIONS

Copies of theses papers can be provided by sending a request to asa@assascience.com and requesting one or more specific papers.

French, D.P., and H. Rines, 1997. Validation and use of spill impact modeling for impact assessment. In Proceedings, 1997 International Oil Spill Conference, Fort Lauderdale, Florida, American Petroleum Institute Publication No. 4651, Washington, DC, pp-829-834.

French, D. P., 1998a. Estimate of Injuries to Marine Communities Resulting from the North Cape Oil Spill Based on Modeling of Fates and Effects. Report to US Department of

14 Commerce, National Oceanic and Atmospheric Administration (NOAA), Damage Assessment Center, Silver Spring, MD, January 1998.

French, D. P., 1998b. Updated Estimate of Injuries to Marine Communities Resulting from the North Cape Oil Spill Based on Modeling of Fates and Effects. Report to US Department of Commerce, National Oceanic and Atmospheric Administration (NOAA), Damage Assessment Center, Silver Spring, MD, December 1998.

French, D.P., 1998c. Modeling the Impacts of the North Cape, p. 387-430.In Proceedings, 21st Arctic and Marine Oilspill Program (AMOP) Technical Seminar, June 10-12, 1998, West Edmonton Mall Hotel Edmonton, Alberta, Canada, Emergencies Science Division, Environment Canada, Ottawa, ON, Canada.

French McCay, D. and James R. Payne, 2001.Model of Oil Fate and Water concentrations with and with out application of dispersants. In Proceedings of the 2001 24th Arctic and Marine Oil spill Program (AMOP) Technical Seminar, June 12-14, 2001, Environment Canada, pp.611-645.

French, D. P., Jones, M. A., and Coakley, L., 2001. Use of Oil Spill Modeling for Contingency Planning and Impact Assessment: Application for Florida Power and Light. In Proceedings of the 2001 International Oil Spill Conference & Exposition, American Petroleum Institute, March 26-29, 2001, Tampa, Florida.

French, D.P. and H. Schuttenberg, 1999.Evaluation of net environmental benefit using fates and effects modeling. Paper ID #321. In Proceedings, 1999 International Oil Spill Conference, American Petroleum Institute.

French McCay, D. 2002. Modeling Evaluation of Water Concentrations and Impacts Resulting from Oil Spills With and Without the Application of Dispersants. International Marine Environmental Seminar 2001, Journal of Marine Systems, Special Issue 2002.

French McCay, D., N. Whittier, S. Sankaranarayanan, J. Jennings, and D. S. Etkin, 2002.Modeling Fates and Impacts for Bio-Economic Analysis of Hypothetical Oil Spill Scenarios in San Francisco Bay. In Proceedings of the Twenty Fifth Arctic and Marine Oil

Spill Program (AMOP) Technical Seminar, Environment Canada, Calgary, AB, Canada, 2002, p. 1051-1074.

French McCay, D., N. Whittier, T. Isaji, and W.Saunders, 2003. Assessment of the Potential Impacts of Oil Spills in the James River, Virginia. In Proceedings of the 26th Arctic and Marine Oil Spill Program (AMOP) Technical Seminar, Emergencies Science Division, Environment Canada, Ottawa, ON, Canada, p. 857-878.

French McCay, D., N. Whittier, S. Sankaranarayanan, J. Jennings, and D. S. Etkin, 2003.Estimation of Potential Impacts and Natural Resource Damages of Oil. J. Hazardous Materials (in press).

French McCay, D. and N. Whittier, 2003.Modeling Assessment of Potential Fates and Exposure for Orimulsion and Heavy Fuel Oil Spills. In: Proceedings, International Oil Spill Conference, April 2003, Paper 157, American Petroleum Institute, Washington, DC.

French McCay, D.P., 2003. Development and Application of Damage Assessment Modeling: Example Assessment for the North Cape Oil Spill. Marine Pollution Bulletin, Volume 47, Issues 9-12, September-December 2003, pp. 341-359.

French McCay, D.P., and J.J. Rowe, 2004.Evaluation of Bird Impacts in Historical Oil Spill Cases Using the SIMAP Oil Spill Model. In Proceedings of the 27th Arctic and Marine Oil Spill Program (AMOP) Technical Seminar, Emergencies Science Division, Environment Canada, Ottawa, ON, Canada, pp. 421-452.

French-McCay, D.P., J.J. Rowe, N. Whittier, S. Sankaranarayanan, D. S. Etkin, and L. Pilkey-Jarvis, 2005. Evaluation of the Consequences of Various Response Options Using Modeling of Fate, Effects and NRDA Costs of Oil Spills into Washington Waters. In: Proceedings, International Oil Spill Conference, May 2005, Paper 395, American Petroleum Institute, Washington, DC.

French-McCay, D.P., N. Whittier, C. Dalton, J.J. Rowe, and S. Sankaranarayanan, 2005.Modeling fates and impacts of hypothetical oil spills in Delaware, Florida, Texas, California, and Alaska waters, varying response options including use of dispersants. In: Proceedings, International Oil Spill Conference, May 2005, Paper 399, American Petroleum Institute, Washington, DC.

French McCay, D., N. Whittier, J.J. Rowe, S. Sankaranarayanan and H.-S.Kim, 2005. Use of Probabilistic Trajectory and Impact Modeling to Assess Consequences of Oil Spills with Various Response Strategies. In Proceedings of the 28th Arctic and Marine Oil Spill Program (AMOP) Technical Seminar, Emergencies Science Division, Environment Canada, Ottawa, ON, Canada, pp. 253-271, 2005.

8 APPENDIX B: OILMAP DEEP MODEL DESCRIPTION

OILMAP Deep™ was used to characterize the near field blowout conditions for use in the SIMAP™ model, which characterized the far field effects. OILMAP Deep™ contains two sub-models, a plume model and a droplet size model. The plume model predicts the evolution of plume position, geometry, centerline velocity, and oil and gas concentrations until the plume either surfaces or reaches a terminal height at which point the plume is trapped. The droplet model predicts the size and volume (mass) distribution of the oil droplets. Provided below is an overview of blowout theory and modeling implementation.

8.1 BLOWOUT MODEL THEORY

RPS ASA's oil blowout model is based on the work of McDougall (gas plume model, 1978), Fanneløp and Sjøen (1980a, plume/free surface interaction), Spaulding (1982, oil concentration model), Kolluru, (1993, World Oil Spill Model implementation), Spaulding et.al. (2000, hydrate formation) and Zheng et.al. (2002, 2003, gas dissolution). A simplified integral jet theory is employed for the vertical as well as for the horizontal motions of the gas-oil plume. The necessary model parameters defining the rates of entrainment and spreading of the jet are obtained from laboratory studies (Fanneløp and Sjøen 1980a). The gas plume analysis is described in McDougall (1978), Spaulding (1982), and Fanneløp and Sjøen (1980a). The hydrate formation and dissociation is formulated based on a unique equilibrium kinetics model developed by R. Bishnoi and colleagues at the University of Calgary. A brief description of the governing equations used in RPS ASA's blowout model and the solution methodology are described in Spaulding et al., 2000. The core components of this model are conservation of water mass, conservation of oil mass, conservation of momentum, and conservation of buoyancy.

Oil droplet size distribution calculations are based on the methodology presented by Yapa and Zheng (2001a&b) and Chen and Yapa (2007), which uses a maximum diameter calculation and the associated volumetric droplet size distribution. The maximum diameter can is determined using Hinze (1955) and coefficients consistent with Chen and Yapa (2007). The droplet size distribution is defined using a Rosin-Rammler (1933) function.

8.2 BLOWOUT MODEL IMPLEMENTATION

The results of the near-field blowout model provide information to the far field fates model about the plume (the three dimensional extent of the mixture of gas/oil/water) and a characterization of the initial dispersion / mixing of the oil discharged during the blowout. Key factors in this analysis are the volume flux of oil and gas, gas to oil ratio (GOR), depth, exit flow velocity and environmental water column conditions (the profile of water temperature and density), which affect both the trap height and the potential for hydrate formation. Other factors such as duration

of the blowout and ambient currents are also included but are less important.

The OILMAP Deep™ blowout model implementation is done in two parts; the first is the plume model described in the previous section, based on the McDougall bubble plume model; the second is the oil droplet size distribution and volume fraction calculation. While they are based on the same scenario blowout specifications (e.g. oil type and flow rate, gas oil ratio and depth), the model predictions are treated separately and do not interact. The two parts of the model predictions only come together at the collapse of the near field plume, at the trap height, where the depth and droplet distribution predictions are used for initialization of the far field particle model simulation.

The blowout plume model solves equations for conservation of water mass, momentum, buoyancy, and gas mass as described in Section 2.1 of the OILMAP Deep™ Technical Documentation, using integral plume theory. An additional equation for the conservation of oil at the plume centerline is also solved.
The plume model prediction is defined externally by a small set of parameters including:

- Blowout release depth
- Oil discharge rate
- Oil density
- Gas : oil ratio (GOR) at the surface
- Atmospheric pressure
- Ambient seawater density profile
- Plume spreading coefficient (l)
- Entrainment parameter (α)
- Slip velocity of gas bubbles in the oil plume
- Ambient current velocity
- Water column profile of temperature and density

The blowout plume models the evolution of the plume within the water column, solving for the position, radius, velocity and oil and gas concentrations along the centerline. The blowout droplet model solves for the distribution of mass within droplet sizes associated with the turbulence of the release. Typically, the near-field model is on the timescale of seconds and length scale of hundreds of metres, where the far-field model is on the scales of hours/days and kilometres. The details of the near field modelling that are passed along to the far field model include the distribution of the release mass in different droplet sizes at the appropriate initial position in the water column.

8.3 REFERENCES

Chen, F.H. and P.D. Yapa. 2007. Estimating the Oil Droplet Size Distributions in Deepwater Oil Spills. Journal of Hydraulic Engineering, Vol. 133, No. 2, pp. 197-207.

Fanneløp, T.K. and K. Sjoen , 1980a. Hydrodynamics of underwater blowouts, AIAA 8th Aerospace Sciences Meeting, January 14-16, Pasadena, California, AIAA paper, pp. 80-0219.

Fanneløp, T. K. and K. Sjoen, 1980b. Hydrodynamics of underwater blowouts, Norwegian Maritime Research, No. 4, pp. 17-33.

Hinze, J. O. 1955 Fundamentals of the hydrodynamics mechanisms of splitting in dispersion process. AIChE J. 1, 289–295.

Kolluru, V., M.L. Spaulding and E. Anderson, 1994. A three dimensional subsurface oil dispersion model using a particle based approach. In Proceedings of 17th Arctic and Marine Oil Spill Program (AMOP) Technical Seminar, Vancouver, British Columbia, June 8-10, 1994, Emergencies Science Division, Environment Canada, Ottawa, ON, Canada, pp. 867-893.

McDougall, T.J., 1978. Bubble plumes in stratified environments, Journal of Fluid Mechanics, Vol. 85, Part 4, pp. 655-672.

Rosin, P. and E. Rammler, 1933. The Laws Governing the Fineness of Powdered Coal, Journal of the Institute of Fuel 7: 29–36Seo, I.W. and K.O. Baek, 2004. Estimation of the Longitudinal Dispersion Coefficient Using the Velocity Profile in Natural Streams. Journal of Hydraulic Engineering. March 2004.

Spaulding, M.L., 1982. User's manual for a simple gas blowout plume model, Continental Shelf Institute, Trondheim, Norway.

Spaulding, M.L., 1984. A vertically averaged circulation model using boundary-fitted coordinates. Journal of Physical Oceanography 14: 973-982.

Spaulding, M.L., P.R. Bishnoi, E. Anderson, and T. Isaji, 2000, An Integrated Model for Prediction of Oil Transport from a Deep Water Blowout.

Yapa, P. D., Zheng, L., and Chen, F. H. 2001a. A model for deepwater oil/gas blowouts. Mar. Pollution Bull., 43, 234–241.

Yapa, P. D., Zheng, L., and Chen, F. H. 2001b. Clarkson deepwater oil & gas ~CDOG model. Rep. No. 01–10, Dept. of Civil and Environmental Engineering, Clarkson Univ., Potsdam, N.Y.

Zheng, L. and Yapa, P.D., 2002. Modelling Gas Dissolution in Deepwater Oil/Gas Spills, Journal of Marine Systems, Elsevier, the Netherlands, March, 299-309

Zheng, L., Yapa, P.D. and Chen, F.H., 2003. A Model for Simulating Deepwater Oil and Gas Blowouts - Part I: Theory and Model Formulation, Journal of Hydraulic Research, IAHR, August, Vol. 41(4), 339-351

9 APPENDIX C: ENVIRONMENTAL DATA

A summary of various environmental data is provided to demonstrate the expected trends and variability that may be expected with the spatial and temporal domain of the model. This includes local hydrodynamics and wind, which are two important forcing parameters for subsurface and surface oil, respectively.

9.1 GENERAL DESCRIPTION OF LOCAL HYDRODYNAMICS

The Gulf Stream is a western boundary current that forms the western boundary of the North Atlantic subtropical gyre. It transports a significant amount of warm water poleward, with average speeds of about 1.7 m/s, and peak values greater than 2 m/s. The current slows to around 0.4 - 0.5 m/s as it widens to the north. The width of the Gulf Stream is about 100-200 km wide as at flows along the eastern coast of the United States (Johns et al., 1995). The Gulf Stream is a continuation of the Florida Current, which is fed by the Loop Current and Antilles Current. The position of the Gulf Stream varies seasonally, with a more northern position in the fall and shifting south during winter and early spring (Figure 1). The range of meridional variation is relatively small (30-40 km), however, recent studies have suggested that this range may be closer to 100 km (Mariano et al.,, 2002). The Gulf Stream transport varies in phase with the seasonal north-south fluctuations. The maximum amount of water transported north occurs in the fall, with peak-to-peak amplitude in sea surface height of 10-15 cm (Gyory et al.,, 2013). These fluctuations are mostly confined to the upper 200-300 m of the water. The meandering and transport of the Gulf Stream intensifies downstream of Cape Hatteras and reaches a maximum near 65°W (Hogg et al.,, 1995). Upon reaching the Grand Banks, the structure of the Gulf Stream changes from a single front, to multiple branching fronts. One branch flows northward along the continental slope, eventually turning east and becoming the North Atlantic Current, while the other branch flows southeastward known as the Azores Current. When the Gulf Stream encounters the cold water of the Labrador Current, principally in the vicinity of the Grand Banks, there is little mixing of the waters. Instead, the juncture is marked by a sharp contrast in temperature and is called the cold wall (NIMA, 2013) (Figure 2).

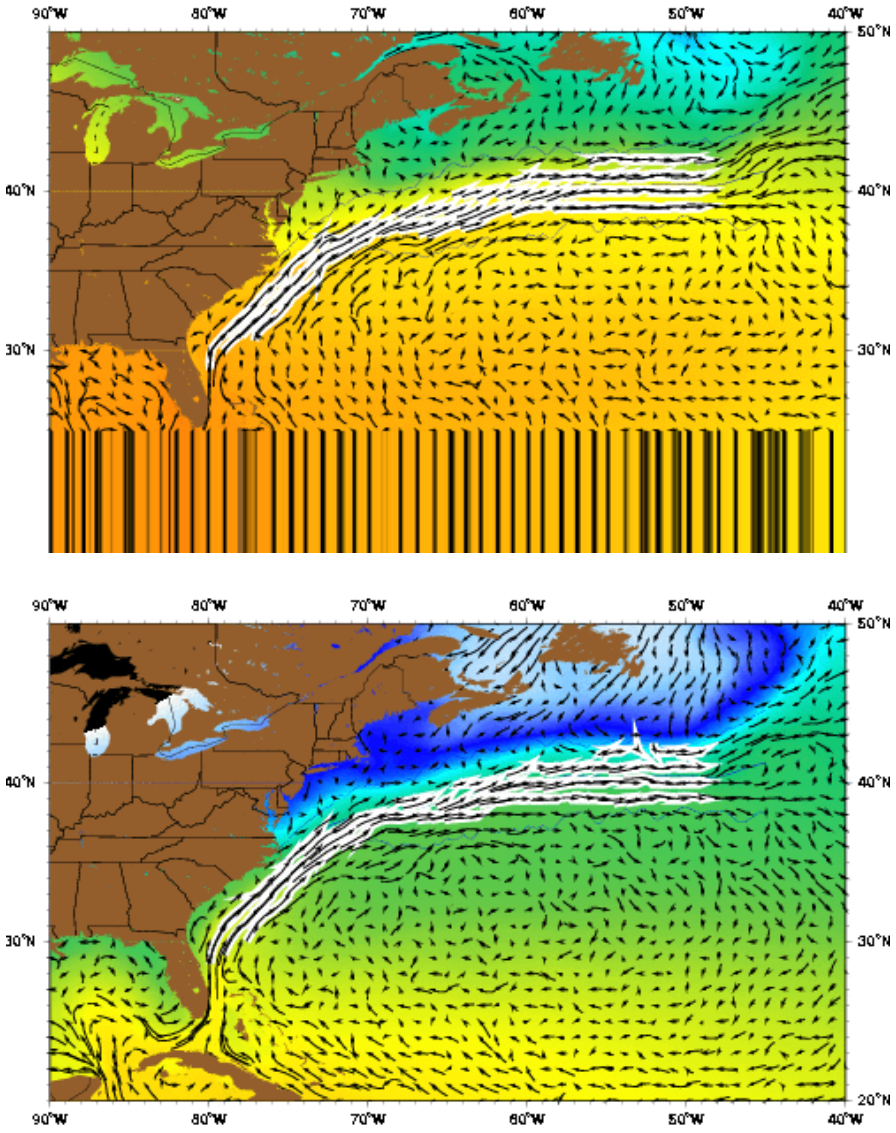

Figure 1. Gulf Stream seasonal circulation. Summer (top) and winter (bottom) (Source: Gyory et al., 2013).

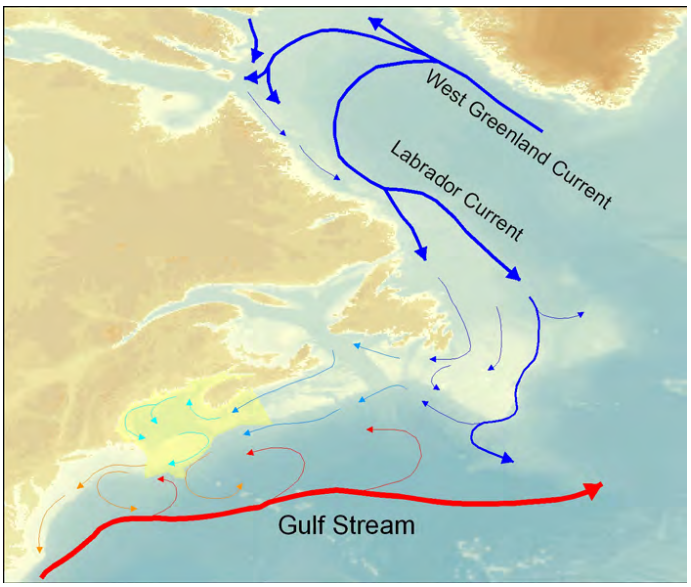

Figure 2. Schematic of major currents in Northeast Atlantic. Currents are colour coded for temperature, with red representing warmer currents and blue for colder currents. The Gulf of Maine is shaded in yellow (Source: GoMA census 2013).

The Labrador Current flows southeastward from Hudson Strait (60°N) along the continental slope to the Tail of the Grand Banks, around 43°N (Figure 3). The current is a continuation of the Baffin Island Current, which transports both the cold and relatively low salinity waters from Baffin Bay, and the warmer and more saline waters from a branch of the West Greenland Current (Lazier et al., 1993). The Labrador Current is the southward component of the North Atlantic subpolar gyre and transports cold water into the warmer Gulf Stream region. The Labrador Current has speeds of about 0.3 – 0.5 m/s along the shelf edge (Reynaud et al., 1995). The current exhibits some seasonal variation in speed in the upper 400 metres of the water column. The minima occur during March-April, while the maxima are typically in late fall. This is thought to be due to buoyancy forcing rather than wind forcing (Lazier and Wright, 1993). The large salinity variations induced by the additional freshwater transport from the north in spring and summer, which is largely confined to the waters over the shelf, contributes to the seasonality. Lazier and Wright (1993) revealed that there are two regimes in the Labrador Current. The first lies on the shelf and upper-slope, which is the main Labrador Current that was previously discussed. The second regime, referred to as the deep Labrador Current, is seaward of the shelf and lies over the lower continental slope around the 2500 m isobath. This is a more barotropic flow that exhibits a different annual cycle than the main current. The minimum speed appears in summer and the maximum in winter (Lazier and Wright, 1993).

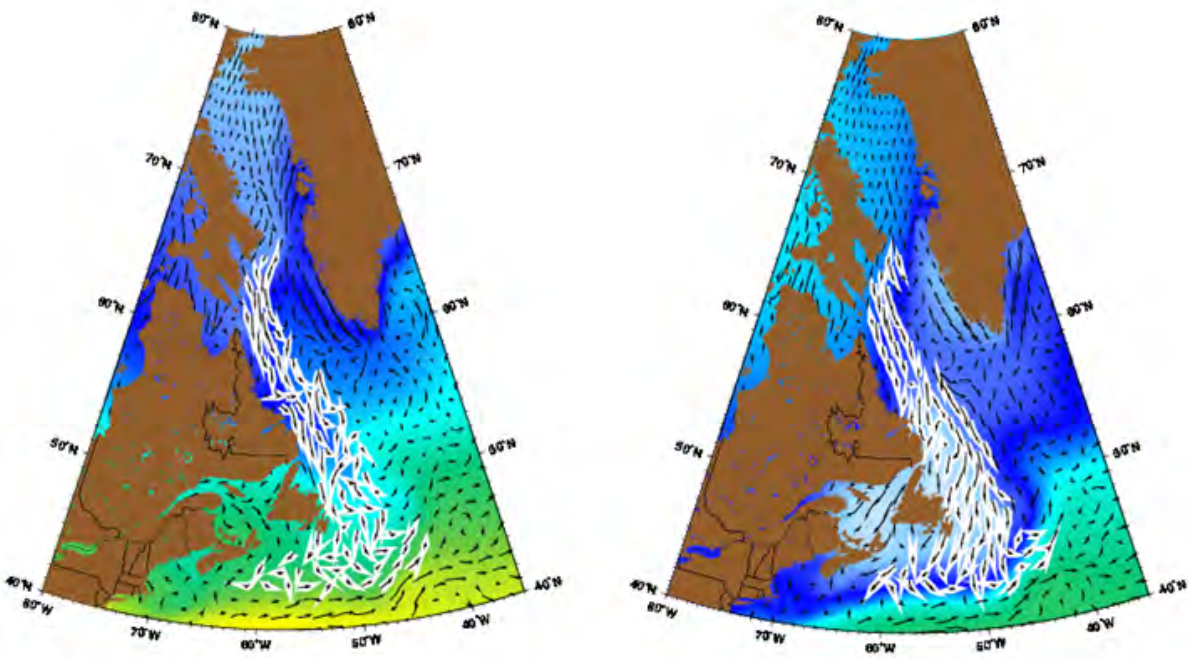

Figure 3. Labrador Current during summer (left) and winter (right) (Source: Gyory et al., 2013).

The surface flow into the Gulf of Maine is fed primarily by the cold, deep Labrador Current that enters along the Scotian Shelf and Northeast Channel to the south of Nova Scotia. This current helps drive the predominantly counterclockwise circulation of the Gulf of Maine. The circulation in the Gulf is characterized by several cyclonic gyres, with limbs that flow toward and around Georges Bank, although the intermediate and deep circulation generally is isolated the Bank (Figure 4) (Lynch et al., 1998). The Scotian Shelf's location is in a transition zone for several key forcings: it is downstream of the North Atlantic's subpolar western boundary current, has slope water intrusions that contribute to pronounced along-shelf variations in hydrographic properties, and is near the entrance to the tidal system of the Bay of Fundy and Gulf of Maine (Hannah et al., 2001). The southwestward flow along the Nova Scotia shelf edge and upper continental slope varies seasonally, with a stronger transport in winter and weaker transport in summer (Figure 5). Off the western Scotian Shelf, there are further fluctuations that involve a reduced westward extent of the slope water gyre in winter, spring, and summer (Hannah et al., 2001).

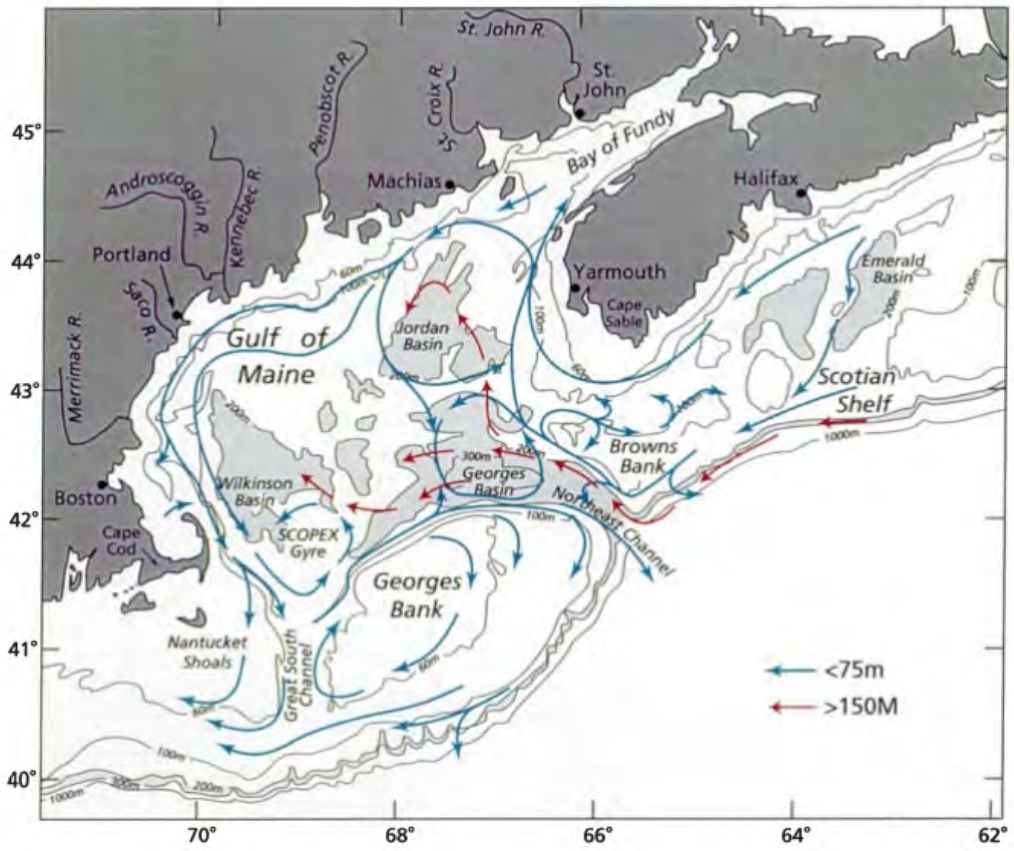

Figure 4. Typical water circulation in the spring along the Scotian Shelf and in the Gulf of Maine (Source: Miller et al., 1998).

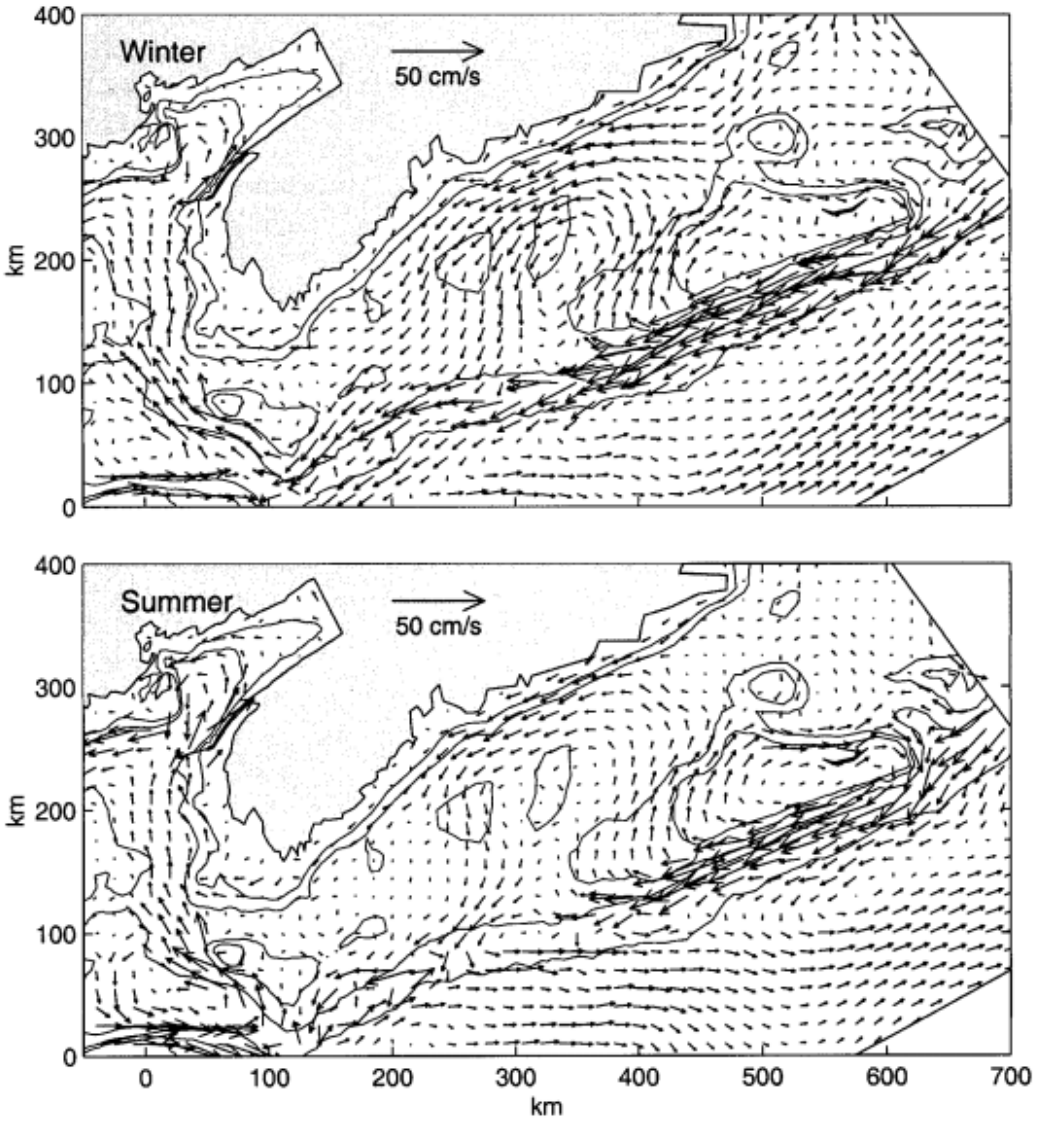

Figure 5. Seasonal-mean model velocities over the Scotian Shelf, averaged between 20-50 m below the surface for winter (top) and summer (bottom) (Source: Hannah et al., 2001).

The highest tides on earth occur in the Gulf of Maine, ranging as much as 16 m in the easternmost reaches of the Bay of Fundy. The currents created by these tides keep waters well mixed, thus increasing available nutrients and productivity. The currents in the Gulf of Maine are influenced by fluctuations in river outflow, which are often enhanced during spring runoff. The St. John River flows approximately 670 km, where it discharges at a rate of 990 m^3/s into the Bay of Fundy (GoMA, 2013).

9.2 MODELLED HYDRODYNAMICS

9.2.1.1 REGIONAL CIRCULATION - HYCOM GLOBAL SIMULATION

HYCOM is a primitive equation, general circulation model, produced by the United States Navy (HYCOM; Bleck, 2002). The vertical coordinates are isopycnal in the open, stratified ocean, but use the layered continuity equation to make a dynamically smooth transition to terrain-following coordinates in shallow coastal regions, and to z-level coordinates in the mixed layer and/or unstratified seas. The hybrid coordinate extends the geographic range of applicability of traditional isopycnic coordinate circulation models toward shallow coastal seas and unstratified parts of the world ocean. It maintains the significant advantages of an isopycnal model in stratified regions while allowing more vertical resolution near the surface and in shallow coastal areas, hence providing a better representation of the upper ocean physics. HYCOM is designed to provide a major advance over the existing operational global ocean prediction systems, since it overcomes design limitations of the present systems as well as limitations in vertical and horizontal resolution. The result should be a more streamlined system with improved performance and an extended range of applicability (e.g., the present systems are seriously limited in shallow water and in handling the transition from deep to shallow water).

Global HYCOM with 1/12° horizontal resolution at the equator (~7 km at mid-latitudes) is the ocean model component of an eddy-resolving operational nowcast/forecast system. There are 26-27 vertical layers within the selected modelled region. The model provides nowcasts and forecasts of the three-dimensional global ocean environment. HYCOM is initially delivered with a thermodynamic “energy loan” ice model, but later will be coupled to the Polar Ice Prediction System 3.0 via the Earth System Modelling Framework (ESMF). Coupling between the ocean and ice models will more properly account for the momentum, heat and salt fluxes at the ocean/ice interface. The final component of the nowcast/forecast system is the Navy Coupled Ocean Data Assimilation (NCODA) which is a multivariate optimal interpolation scheme that will be used to assimilate surface observations from satellites, including altimeter and Multi-Channel Sea Surface Temperature (MCSST) data, sea ice concentration and profile data such as XBTs (expendable bathythermographs), CTDs (conductivity temperature depth) and ARGO floats (Cummings, 2005). By combining these observations via data assimilation and using the dynamical interpolation skill of the model, the three-dimensional ocean state can be more accurately nowcast and forecast.

9.2.1.2 TIDES CURRENTS – TOPEX/POSEIDON GLOBAL INVERSE SOLUTION (TPXO)

Depth averaged tidal currents for the dispersion simulations were derived using the Oregon State University TOPEX/Poseidon Global Inverse Solution TPXO, a global model of ocean tides (Egbert and Erofeeva, 2014). The latest version (TPXO8.0) utilizes a least-squares best-fit of the Laplace Tidal Equations, as well as along track averaged data from TOPEX/Poseidon and Jason (on TOPEX/POSEIDON tracks since 2002) obtained with OSU Tidal Inversion Software (OTIS). A full description of the methods used to compute the model are described in details by

Egbert, Bennett, and Foreman, 1994 and Egbert and Erofeeva, 2002. Each successive version of the TPXO model improves upon the last, based upon utilization of longer satellite time series, more data sites to integrate, improved bathymetry, and improved grid resolution of global and local grids. The tides are provided as complex amplitudes of earth-relative sea-surface elevation for eight primary (M2, S2, N2, K2, K1, O1, P1, Q1), two long period (Mf, Mm), and 3 non-linear (M4, MS4, MN4) harmonic constituents. The TPXO solution is provided on a 1440x721, ¼ degree by ¼ degree resolution full global grid. Tidal forcing is stored as a harmonic constant.

9.2.1.3 Hydrodynamics Summary for Representative Spill Sites

At each of the modelled sites, daily HYCOM currents were obtained by interpolating the values from the nearest model grid points. At the model cell closest to Site 1, the water column is represented in 26 discrete vertical layers; at Sites 2 and 3, the HYCOM model contains 27 vertical layers. Summary statistics from the hydrodynamic inputs are discussed further below, although it is worth noting that the flow characteristics for each site are quite similar.

Vertical profiles derived from the nearest HYCOM grid points show the average magnitude of currents with depth at each location (Figure 6 through Figure 8). Surface currents in the region of moderate speed (20-30 cm/s) although currents greater than 60 cm/s do occur approximately 5% of the time. This range of flow speeds is comparable to measurements of the Labrador Current along the shelf edge (Reynaud, 1995). Current intensity decreases rapidly with depth in the water column and average HYCOM speeds drop to approximately 10 cm/s by 400 metres depth. Current roses showing the statistical distribution of modelled currents (by depth interval) indicate directionally variable currents at the surface, which become strongly oriented to the west and southwest at depth. At all three sites, currents near the seabed are extremely weak (average speeds between 4-5 cm/s).

When viewed as monthly averages, statistics from the HYCOM dataset also reflect seasonal variability in current speeds, particularly in the upper water column as noted above (Figure 9 through Figure 11). Surface velocities during the boreal fall (Oct—Dec) are approximately 15%-20% faster than those during spring months. The strongest surface currents (>30 cm/s, on average) occur between November and February and the slowest (~25 cm/s) between April and June. Monthly current roses (Figure 12 through Figure 14) also indicate stronger currents with more westerly distribution during the late fall and winter months. By contrast, subsurface currents below 400 m experience flow minima during the late summer (Figure 9 through Figure 11).

Figure 15 through Figure 17 present time series (stick plots) of current vectors for the complete HYCOM model period at Sites 1, 2, and 3 respectively. The highly variable currents at the surface, and interannual fluctuations in flow intensity represented in the model emphasize the complex spatial and temporal circulation patterns in the region, which are not fully captured in a regional flow schematic (e.g. Figure 2). The seasonal variability in currents are regular and repeatable features for all years in the time series and the dataset maintains these oscillations

for depths above 150 m. At both locations, current directions become more consistent with depth and net westerly/south-westerly flow in the model becomes apparent at depths below 500 m. Bottom currents at all sites are characterized by generally weak, westerly oriented currents that persists year-round.

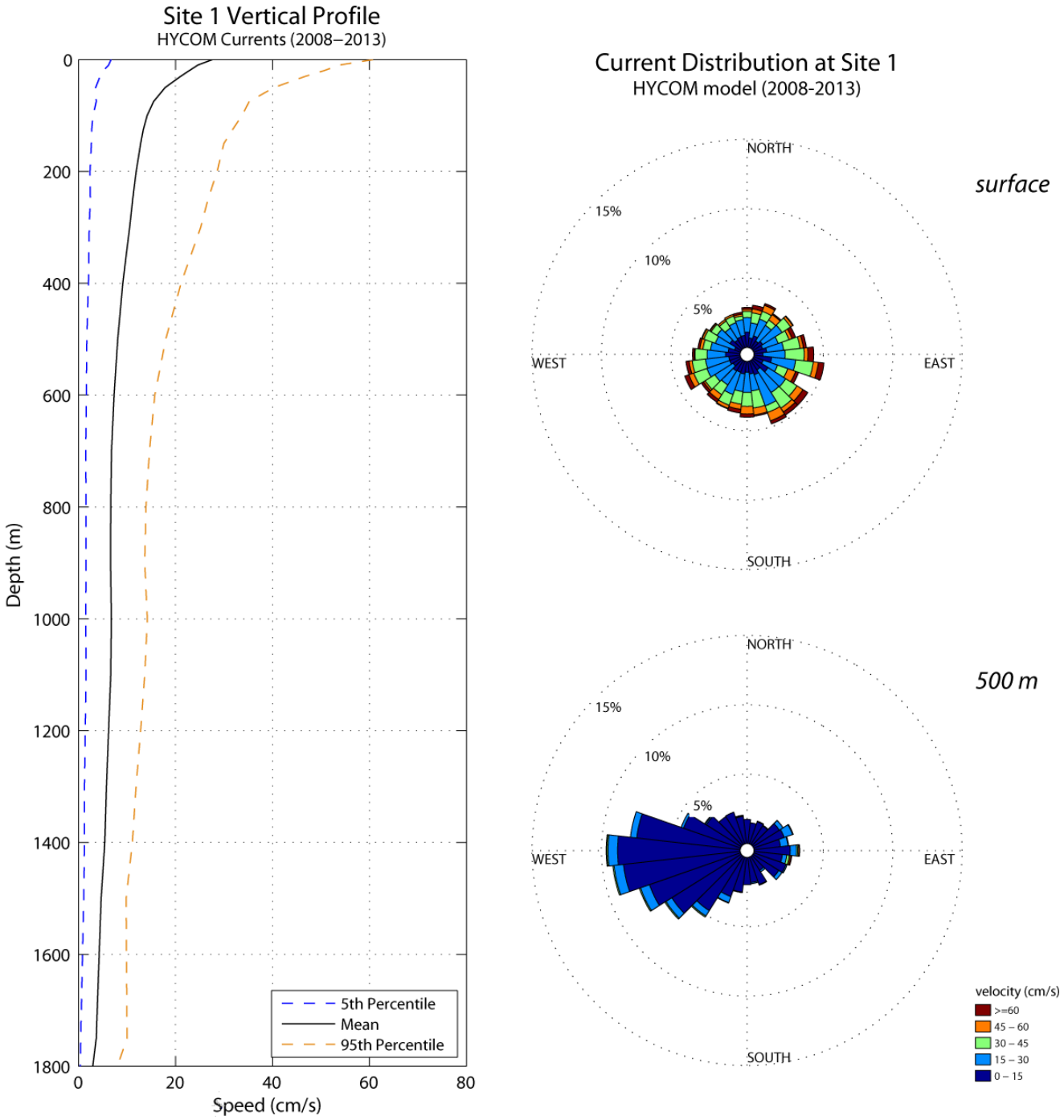

Figure 6. Vertical profile (left) and current roses showing the distribution of current speeds (right) for Site 1, derived from HYCOM model currents between 2008 and 2013.

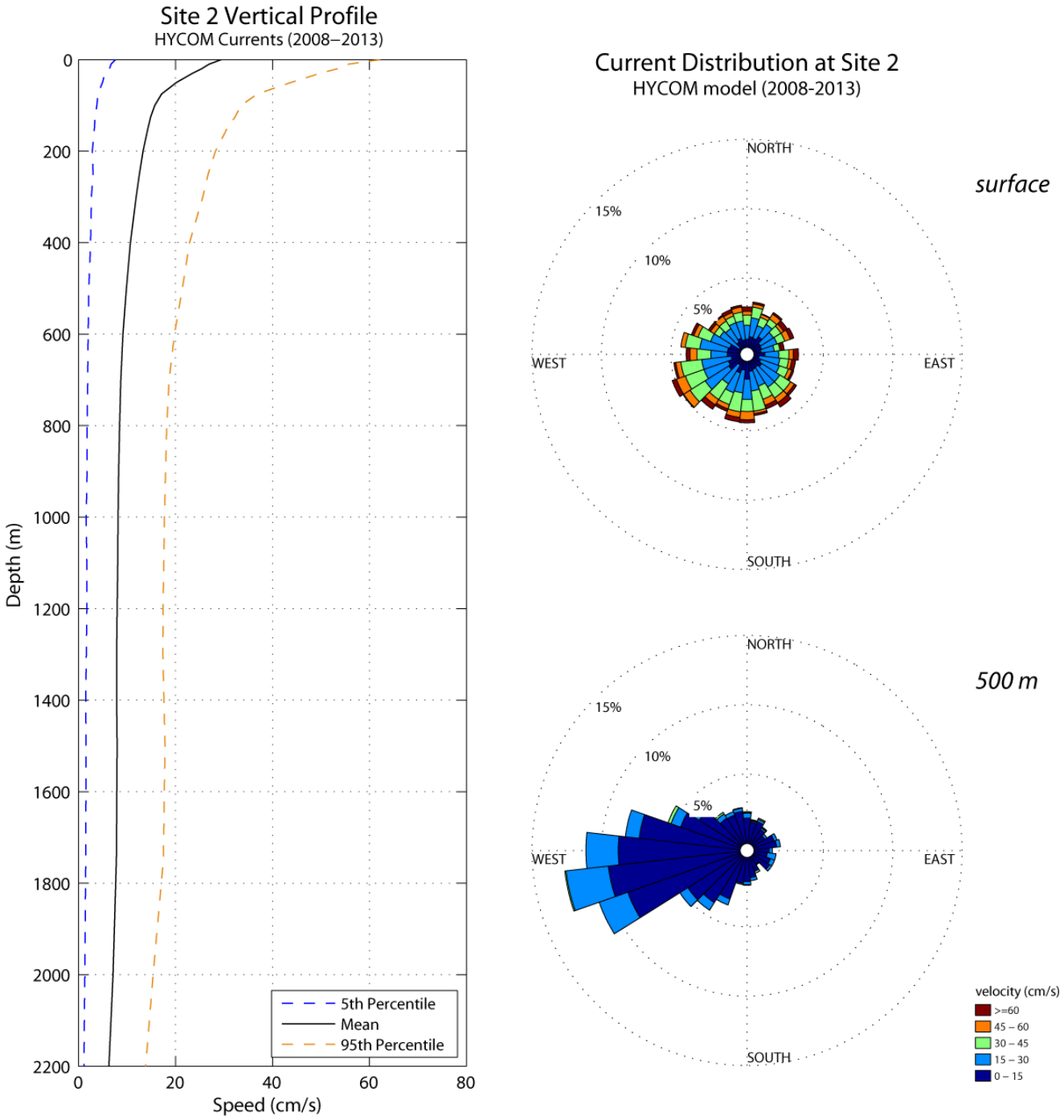

Figure 7. Vertical profile (left) and current roses showing the distribution of current speeds (right) for Site 2, derived from HYCOM model currents between 2008 and 2013.

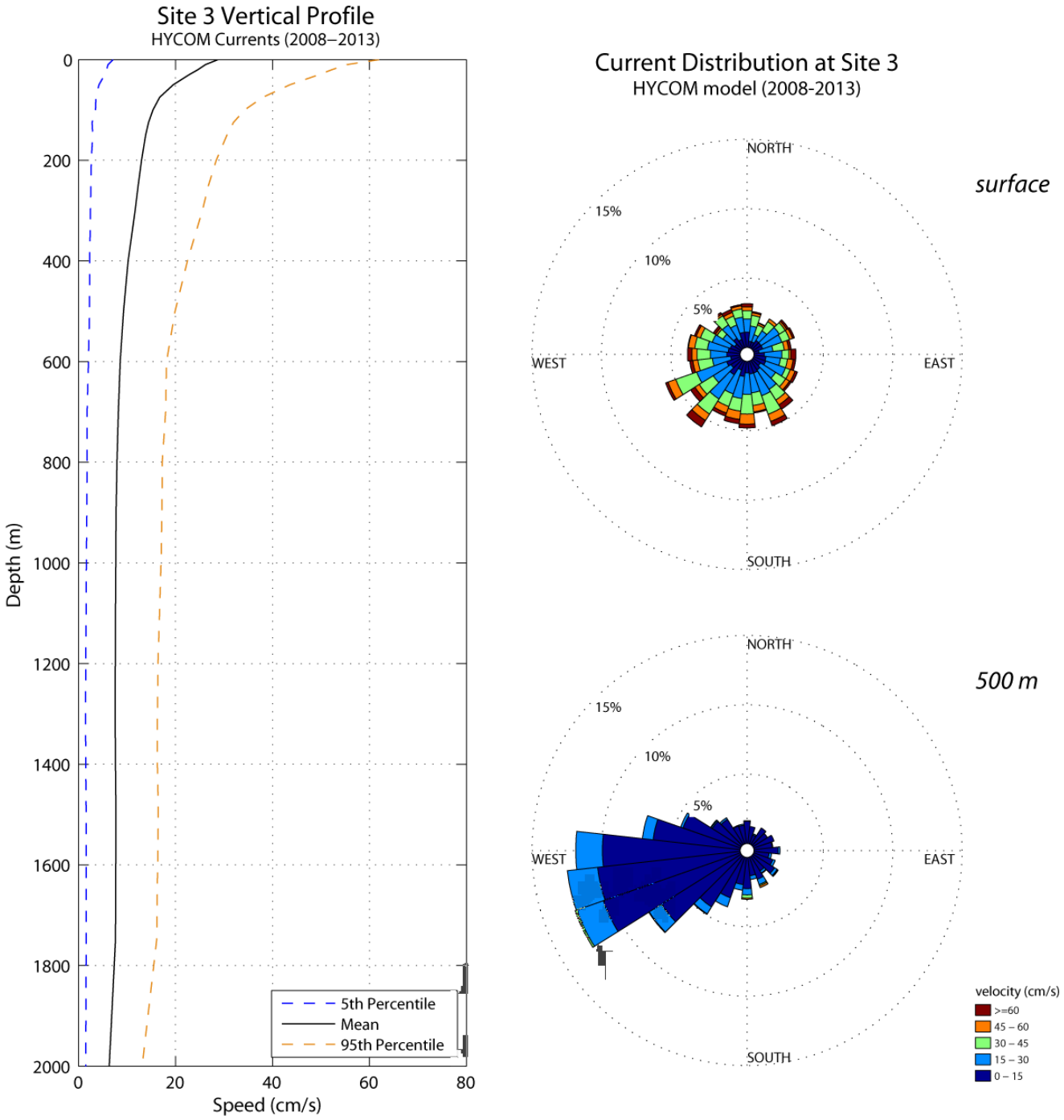

Figure 8. Vertical profile (left) and current roses showing the distribution of current speeds (right) for the Site 3, derived from HYCOM model currents between 2008 and 2013.

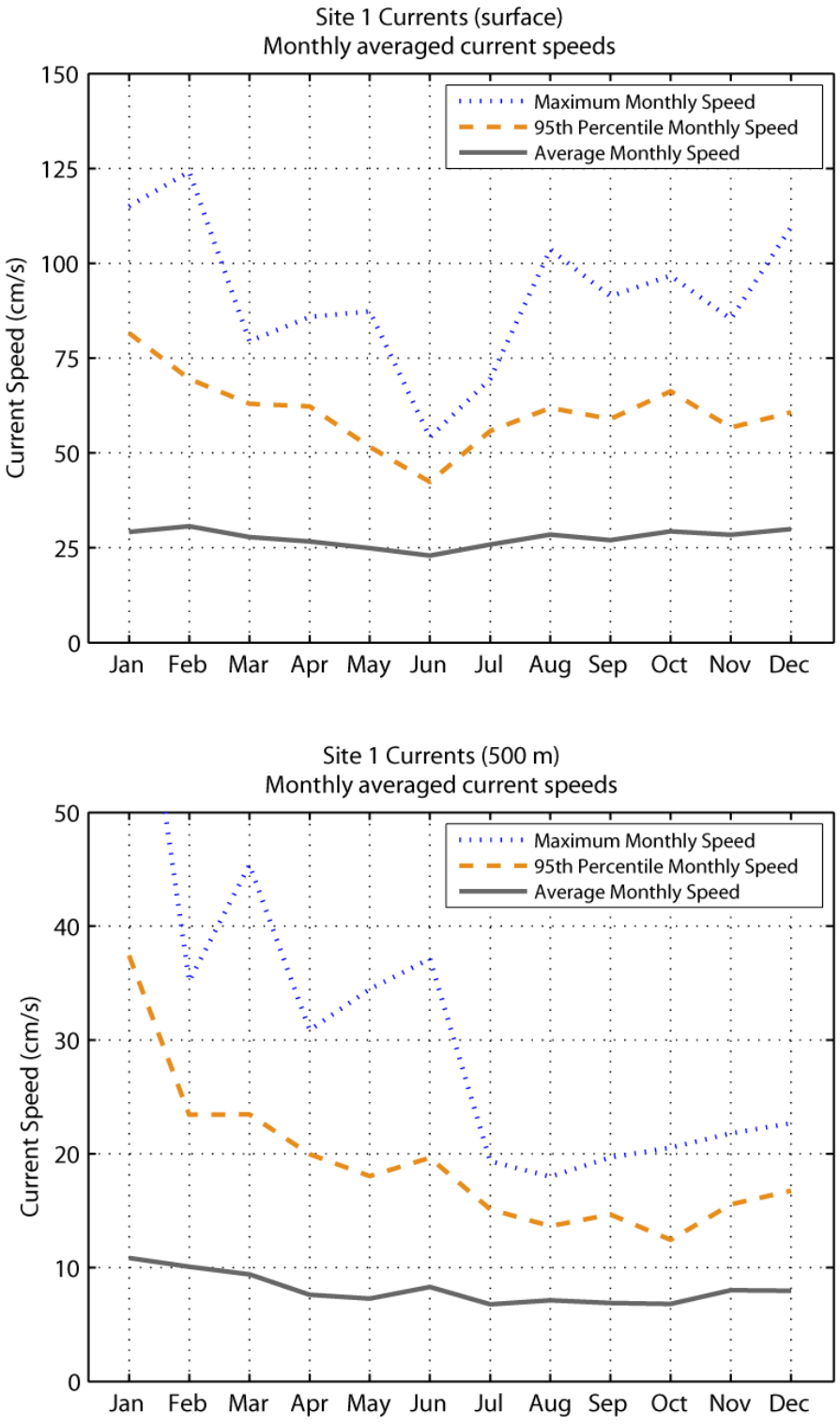

Figure 9. Monthly averaged current speeds at Site 1 derived from the HYCOM global dataset. Average current speeds are shown for the surface (top figure) and 500 m (bottom figure) water depths.

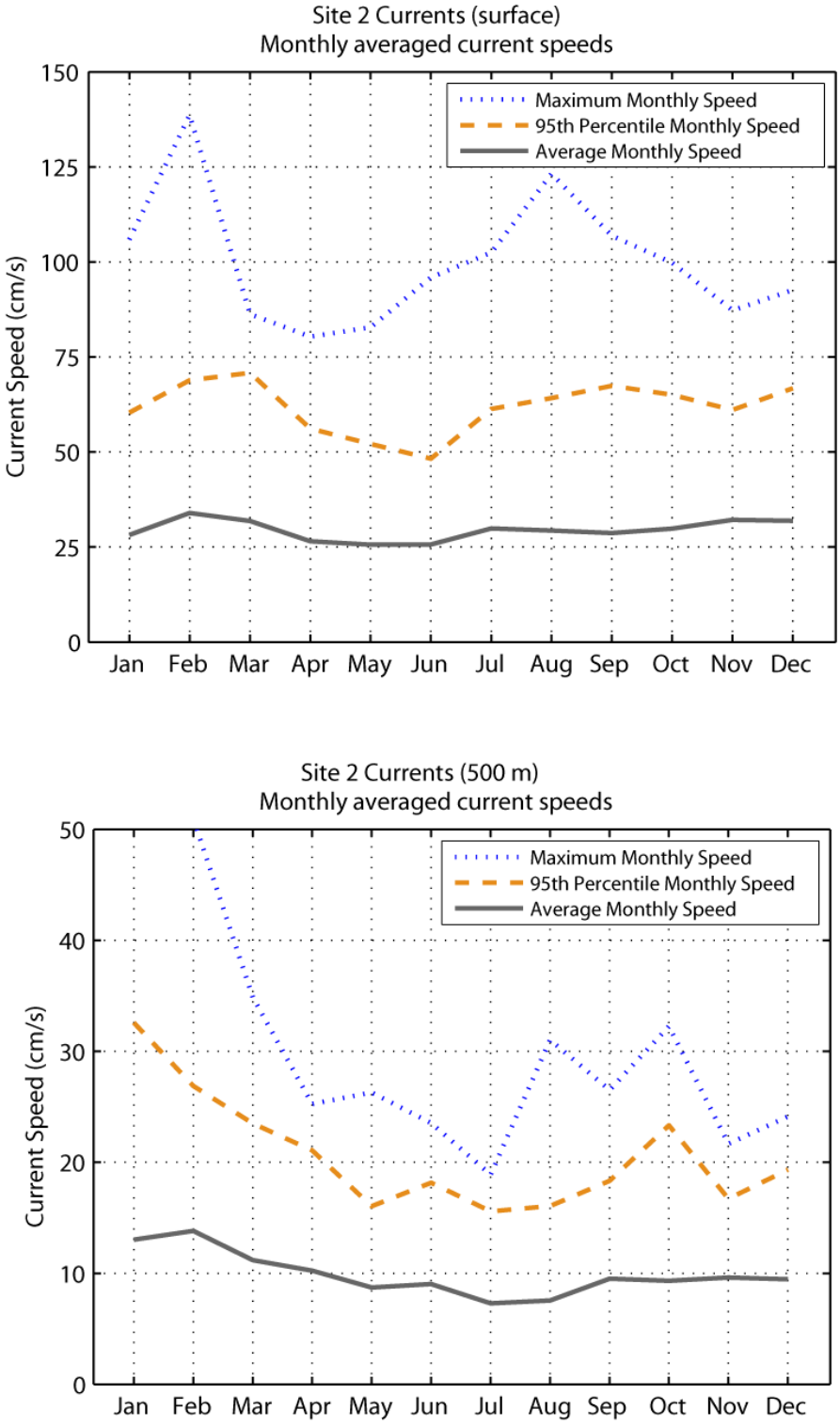

Figure 10. Monthly averaged current speeds at Site 2 derived from the HYCOM global dataset. Average current speeds are shown for the surface (top figure) and 500 m (bottom figure) water depths.

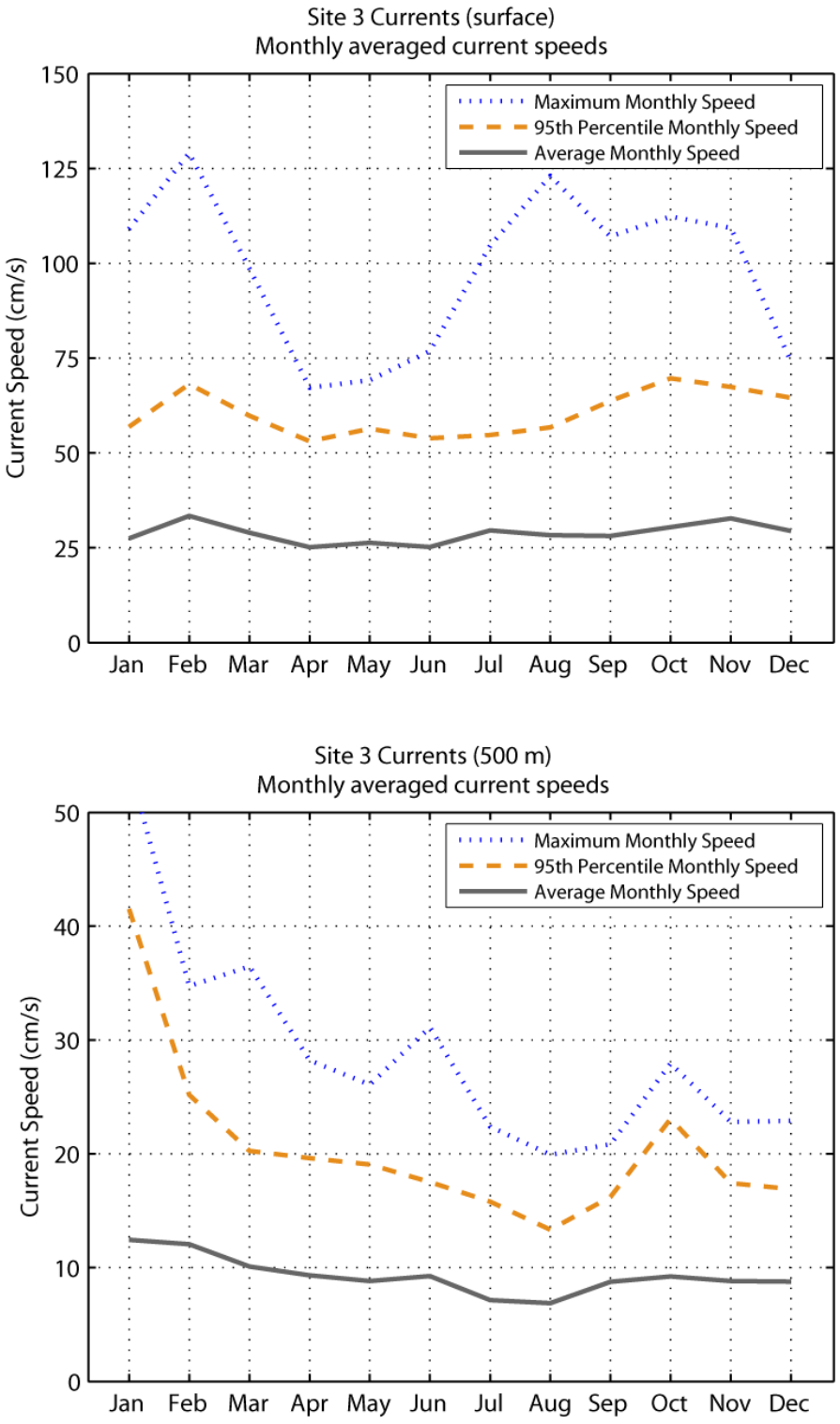

Figure 11. Monthly averaged current speeds at Site 3 derived from the HYCOM global dataset. Average current speeds are shown for the surface (top figure) and 500 m (bottom figure) water depths.

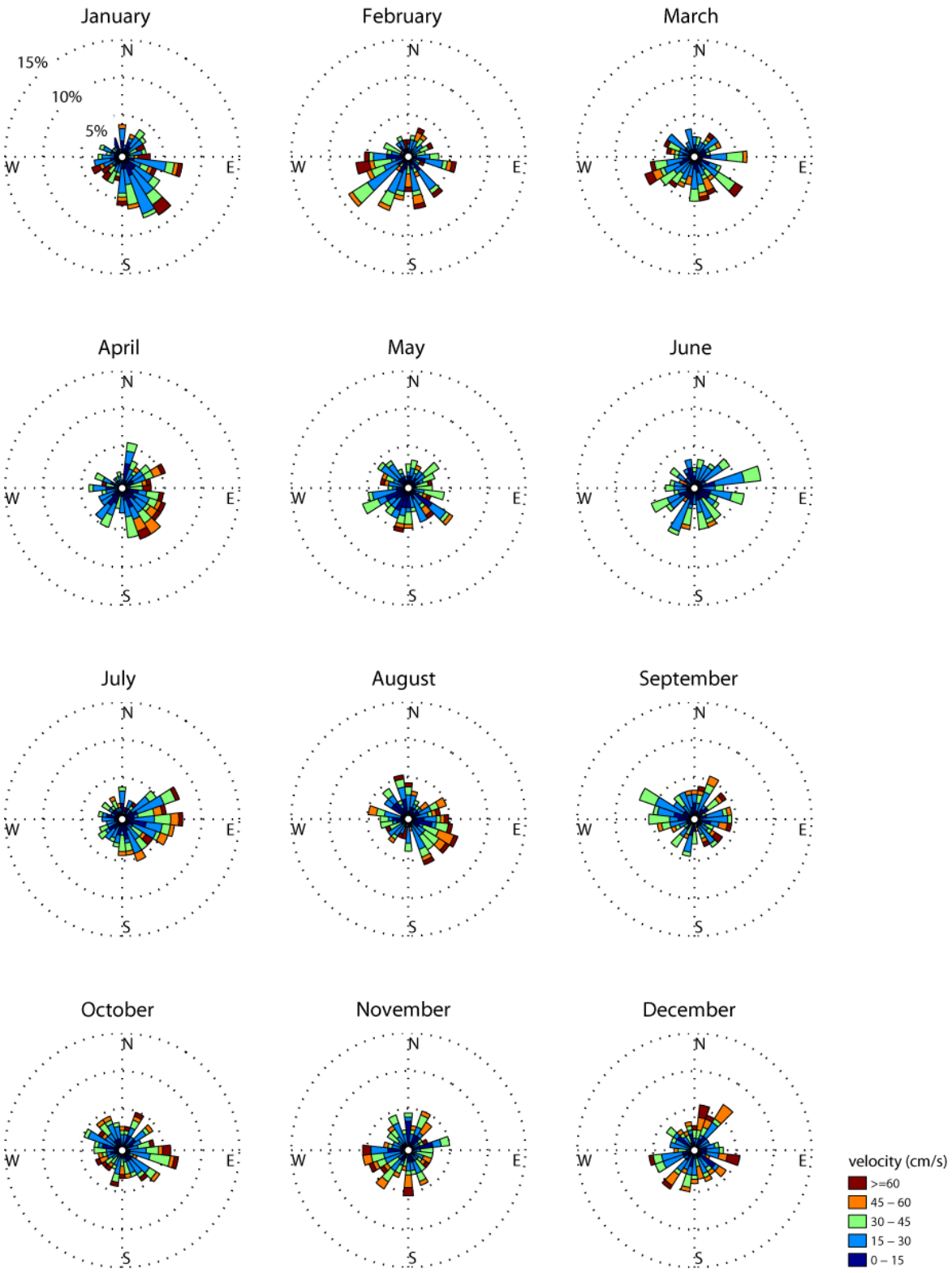

Figure 12. Current roses showing the distribution of surface currents (speed and direction) by month at Site 1, derived from HYCOM model currents between 2008 and 2013.

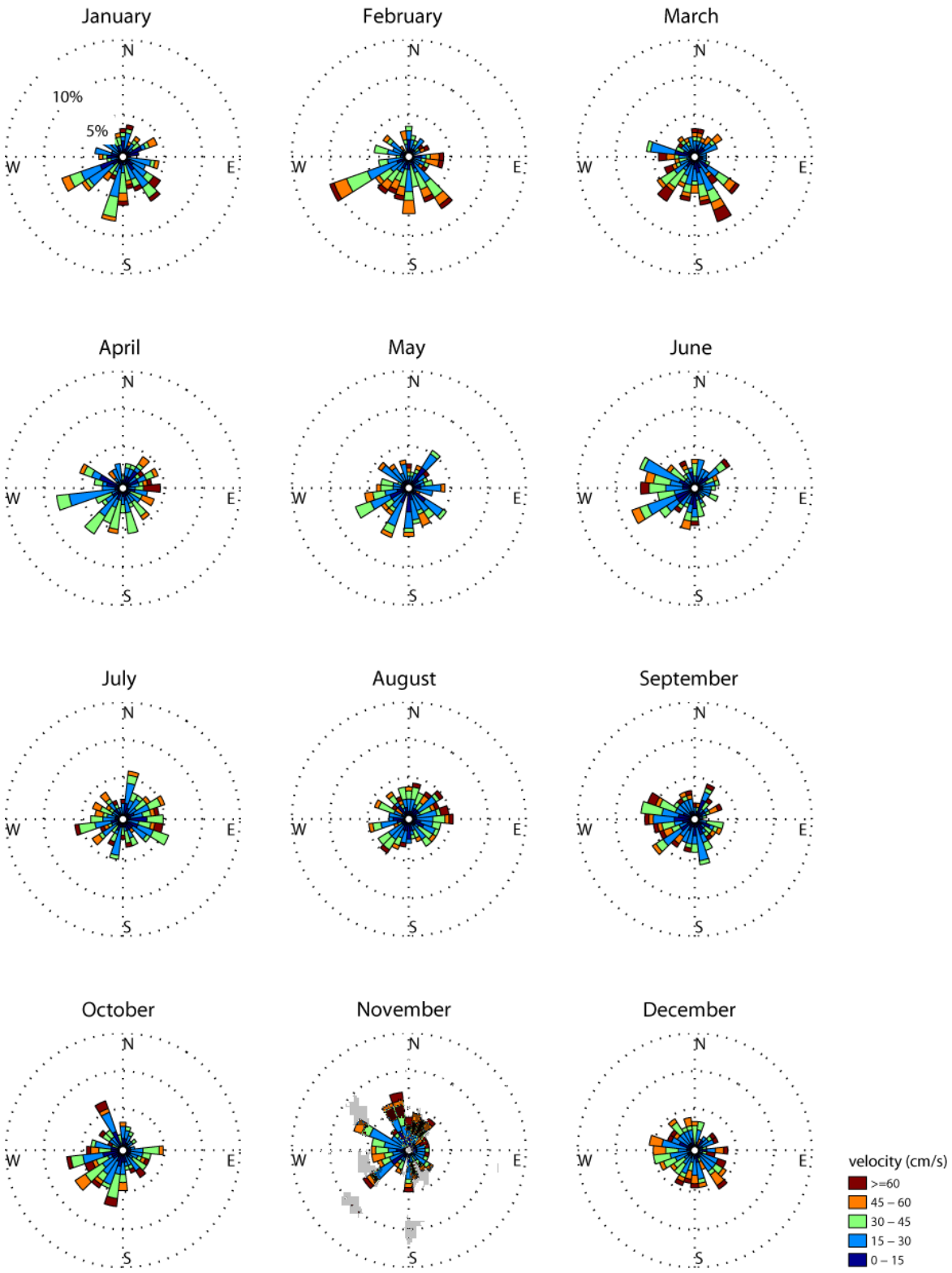

Figure 13. Current roses showing the distribution of surface currents (speed and direction) by month at the Site 2, derived from HYCOM model currents between 2008 and 2013.

Figure 14. Current roses showing the distribution of surface currents (speed and direction) by month at Site 3, derived from HYCOM model currents between 2008 and 2013.

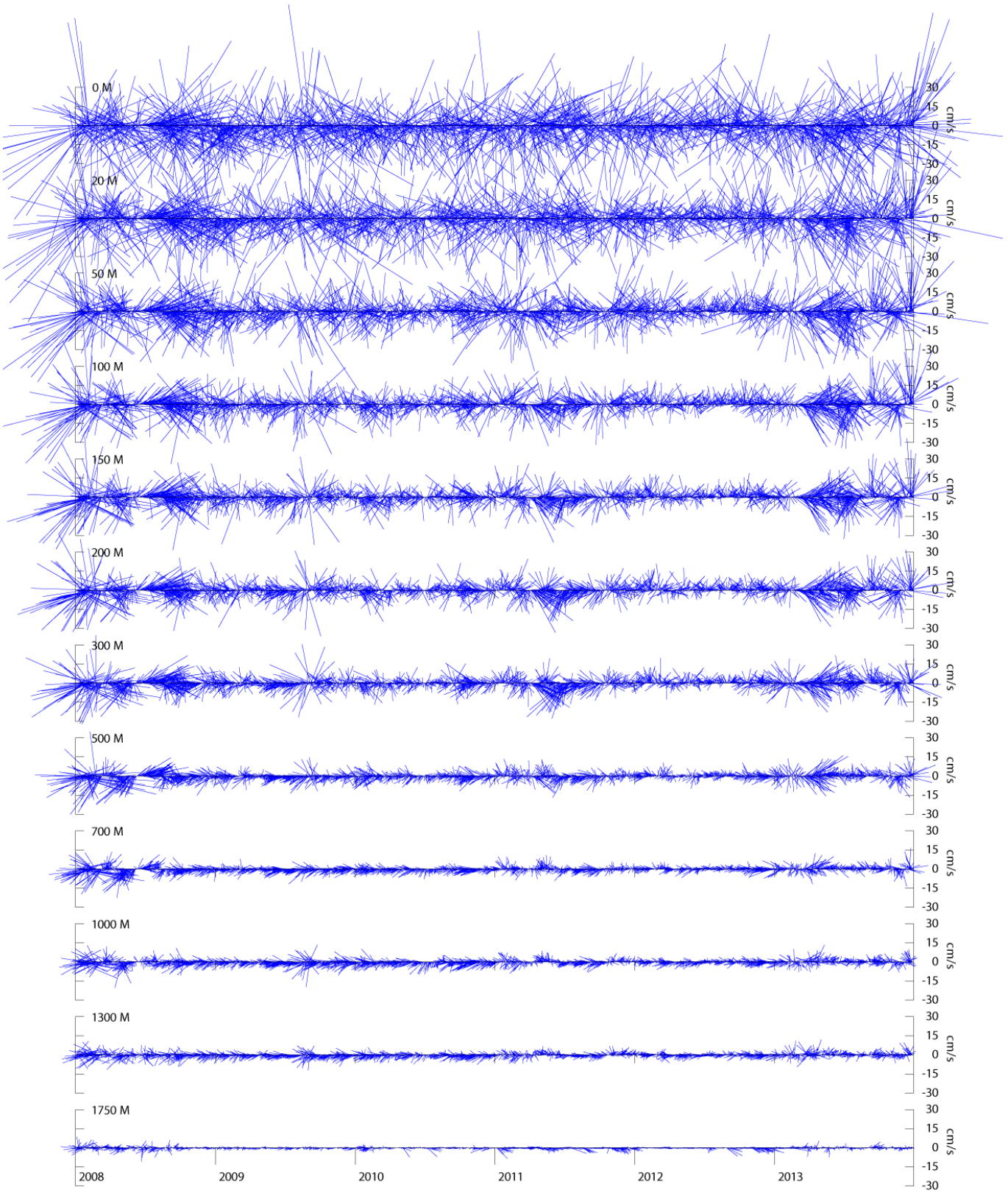

Figure 15. Time series of HYCOM model currents with depth at Site 1.

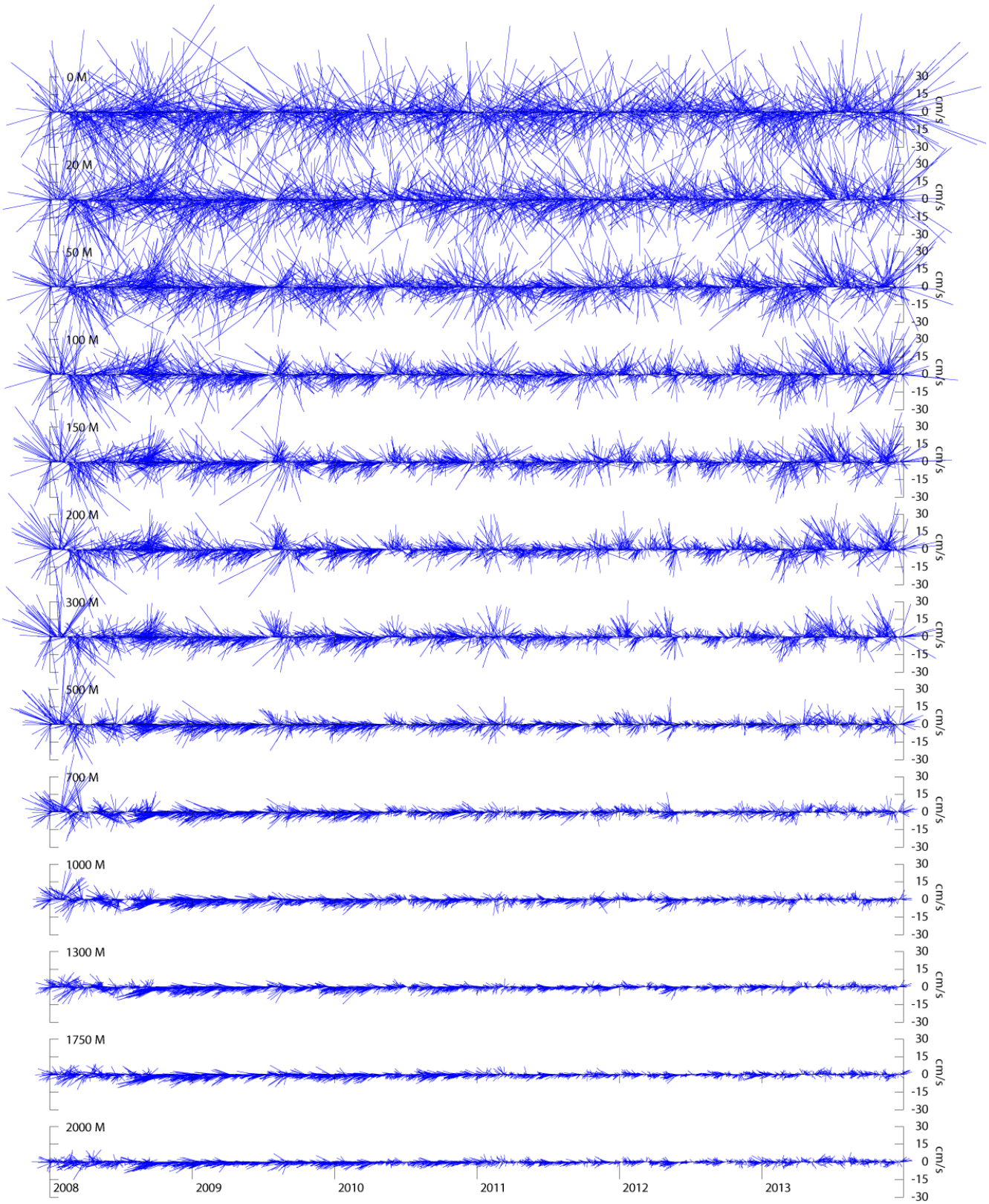

Figure 16. Time series of HYCOM model currents with depth at Site 2.

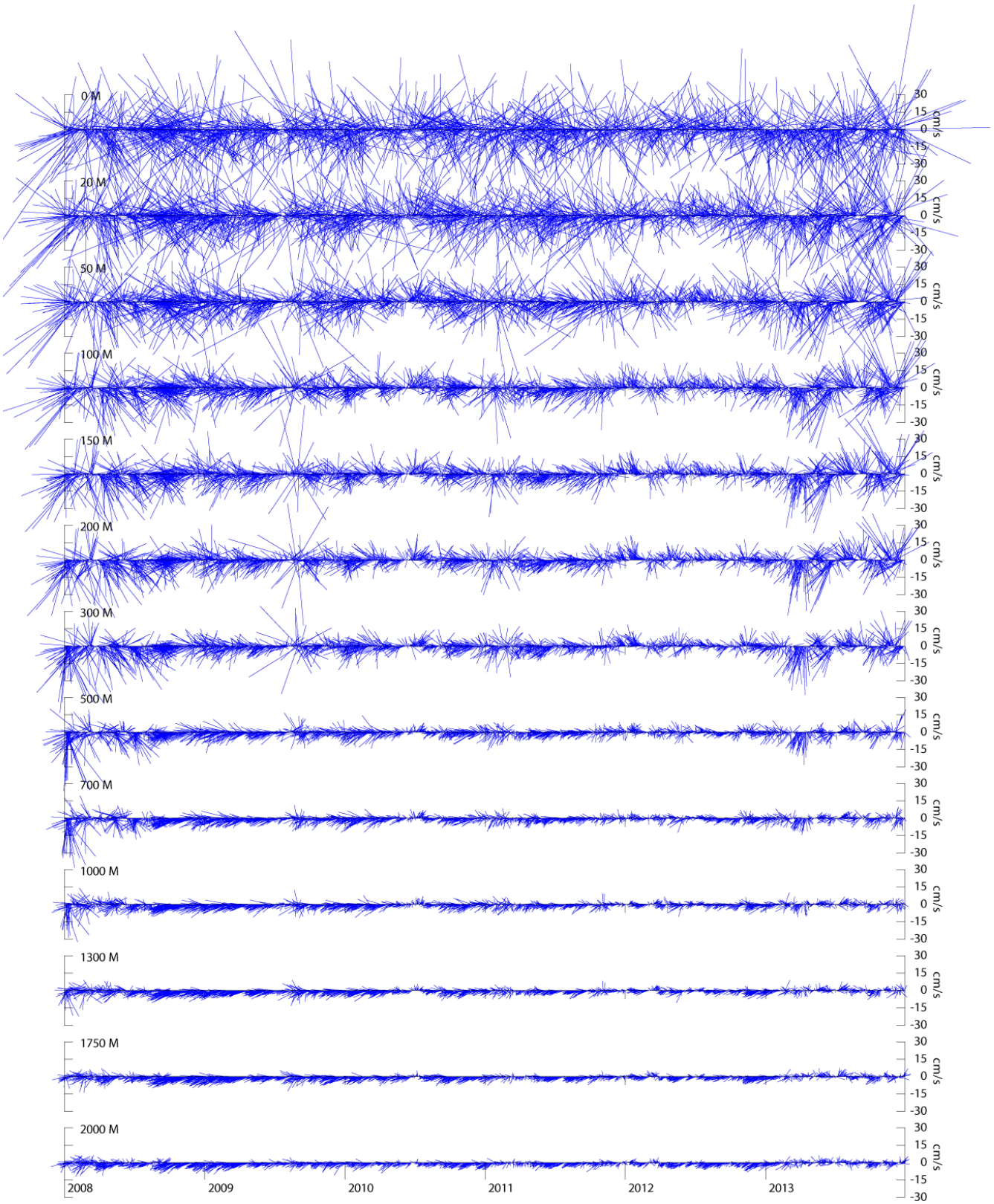

Figure 17**.** Time series of HYCOM model currents with depth at Site 3.

9.2.2 WIND

The model uses time-varying wind speeds and directions for the specific time and space of the spill and simulation. Wind data was gathered from the U.S. Navy Operational Global Atmospheric Prediction System (NOGAPS), a state-of-the-art meteorological model. The NOGAPS model has many features similar to other climate and numerical weather prediction (NWP) models and has been continuously developed over the past twenty years at the Naval Research Laboratory (NRL) in Monterey, CA (NRL, 2013). It is a robust global model that forms the backbone of the Navy's ensemble prediction system, providing forecasts of up to 10 days for a number of atmospheric parameters. It is additionally used as a research tool for understanding global atmospheric dynamics, air/sea interaction, tropical cyclone prediction, and meso-scale weather patterns, among a wide range of other applications.

NOGAPS predicts global atmospheric parameters for 18 vertical levels between the surface and 10 mb height, with a hybrid vertical coordinate system that is defined by the terrain at low levels and constant pressure surfaces at high levels (Bayler and Lewit, 1992). For this study, the winds from the 10 m vertical level were used.

NOGAPS uses a sophisticated data assimilation process to incorporate previous model run data and current observational data to provide an updated Nowcast/Analysis (or Tau 0) for the globe. The observations used for this assimilation include a combination of in-situ point observations, satellite-derived data, ship observations, and upper air observations. While the comprehensive assimilation process ensures that major features are captured in the model output, the NOAA National Oceanographic Data Center verification indicates that NOGAPS slightly under-analyzes and under-forecasts the 10 metre wind speeds stronger than 10 m/s, especially in coastal locations. For this reason, the particular NOGAPs 10 metre wind dataset used for this study was sourced from a version of the dataset compiled by the HYCOM Consortium, which takes the original NOGAPS output hosted by the U.S. Global Ocean Data Assimilation Experiment (GODAE) and applies a QuickSCAT correction to them. NASA's Quick Scatterometer (QuickSCAT) SeaWinds satellite uses microwave radar to measure near-surface wind speed and direction over the Earth's oceans. Thus, by assimilating the NOGAPS dataset with the QuickSCAT dataset, a more accurate representation of regional wind patterns is expected.

This QuickSCAT-corrected NOGAPS data is provided at 0.5 degree horizontal resolution with a 3-hour time step from 2003 to the present. This corresponds to the same wind dataset used to force the HYCOM global hydrodynamic model. For more information, Hogan and Rosmond (1991) provide detailed documentation of the complete NOGAPS model.

The U.S. Navy Operational Global Atmospheric Prediction System (NOGAPS) provides continuous wind data from 2003 to present. Winds from 2005 through 2013 were acquired and used in surface forcing of oil for this modelling. Additional wind information was obtained from a nearby Canadian NOMAD buoy, Station 44137 – East Scotia Slope (42.234°N, 62.018°W)

(NOAA NDBC, 2013). This buoy is owned and maintained by Environment Canada's Department of Fishers and Oceans. Comparisons between the QuickSCAT-corrected NOGAPS wind dataset and the buoy data were made for the period between 2005-2010 below.

NOGAPS output at the grid point nearest to each spill site (Figure 18) was used to characterize local winds at each spill location. To assess the appropriateness and accuracy of the NOGAPS model, empirical data from buoy Station 44137 was compared to the nearest NOGAPS grid point in the study area. Only the buoy data closest to the spill sites of interest was selected for this comparison (Figure 18). Although the locations of the selected NOGAPS grid points, sites of interest, and buoy data are not the same, they are close enough to each other to allow for meaningful comparisons and characterization of the study area. All comparisons were made using data from 2005-2010.

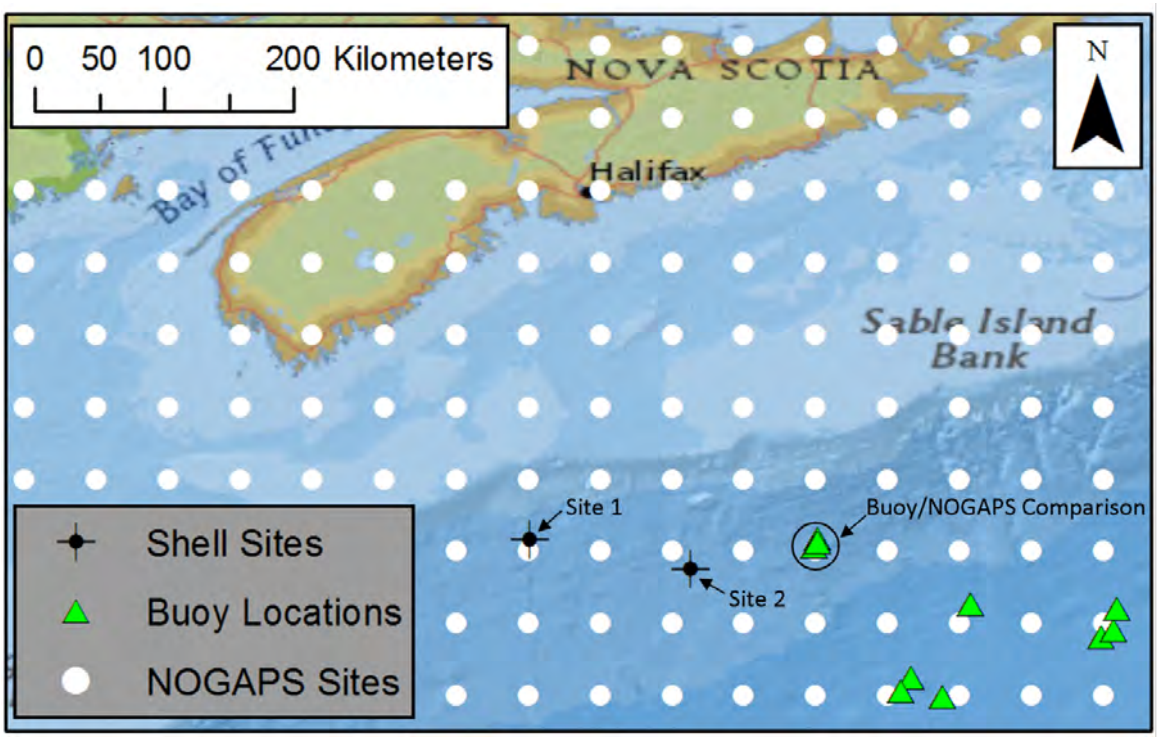

Figure 18. NOGAPS wind gridding, spill sites, and buoy data for empirical comparisons.

According to the NOGAPS model, winds near Sites 1 and 2 average between about 12-21 knots throughout the year (Figure 19), although maximum speed can be much higher. Average wind speeds are strongest in winter, weakest in summer, and intermediate during the spring and fall. Agreement between NOGAPS and empirical wind speed data from buoy c44137 (Figure 20) is very good, with a similar pattern of stronger winter speeds and weaker summer speeds observed in both datasets. The NOGAPS wind speeds are slightly stronger than the buoy recorded wind speeds by about 2-3 knots on average.

Comparisons between winter (October through March) and summer (April through September) months were made to demonstrate seasonality in wind speed and direction. Wind roses depict very similar in wind directions at sites 1 and 2 with stronger winds during the winter, when compared to the summer (Figure 21). In winter, winds are predominantly from the northwest in excess of 20 kts. During the summer, winds are predominantly from the southwest in the 10-20kt range. At the comparison site, buoy and NOGAPS data are very similar, exhibiting the same pattern of wind speed and direction by season (Figure 22). Annual average winds exhibit little spatial variability in the study area (Figure 23), although speeds tend to decline over land.

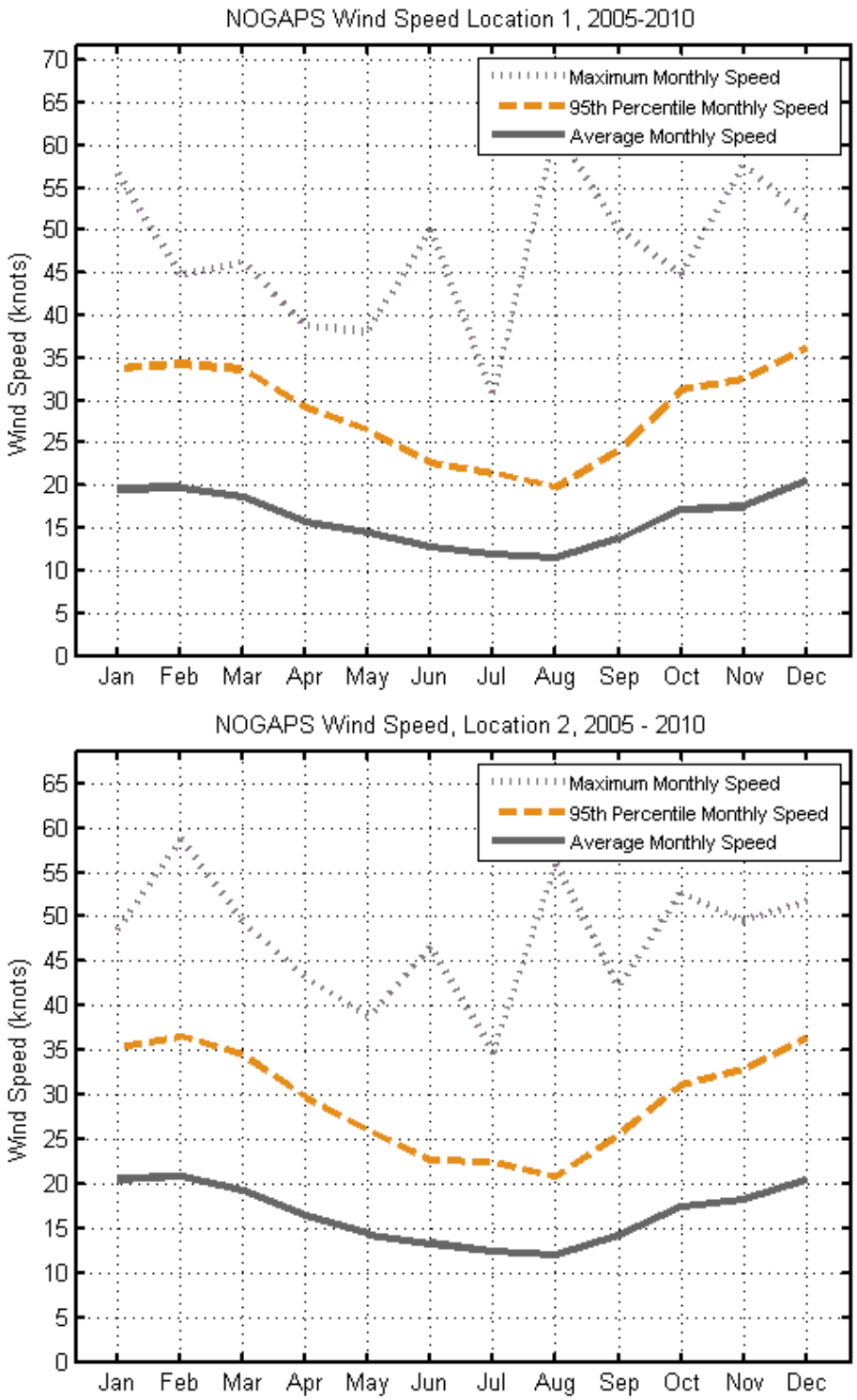

Figure 19. NOGAPS wind speed statistics: monthly average (grey solid), 95th Percentile (orange), and maximum (grey dashed) wind speed for Site 1 (top) and Site 2 (bottom).

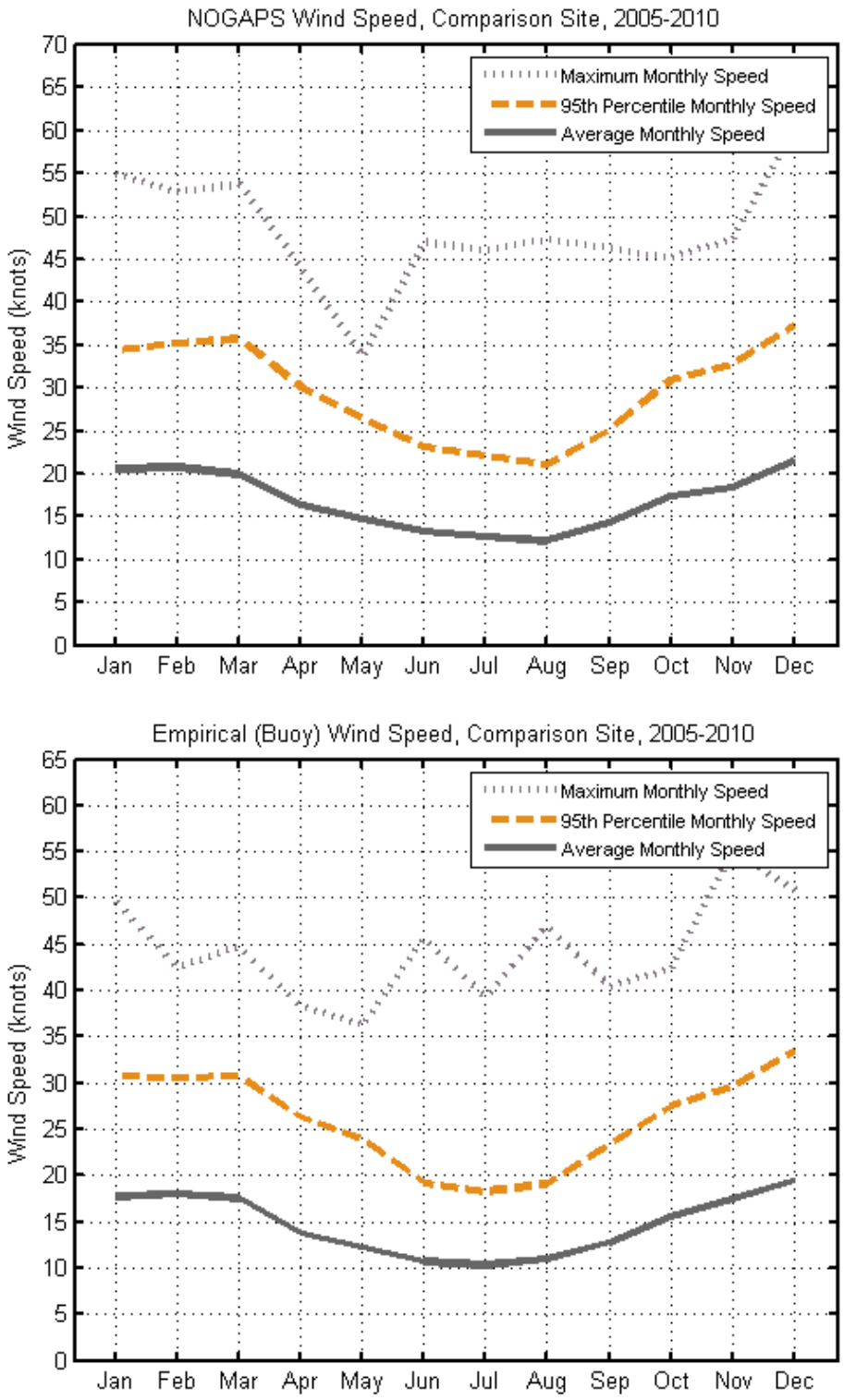

Figure 20. NOGAPS wind speed statistics: monthly average (grey solid), 95th Percentile (orange), and maximum (grey dashed) wind speed for the comparison site, NOGAPS data (top) and buoy data (bottom).

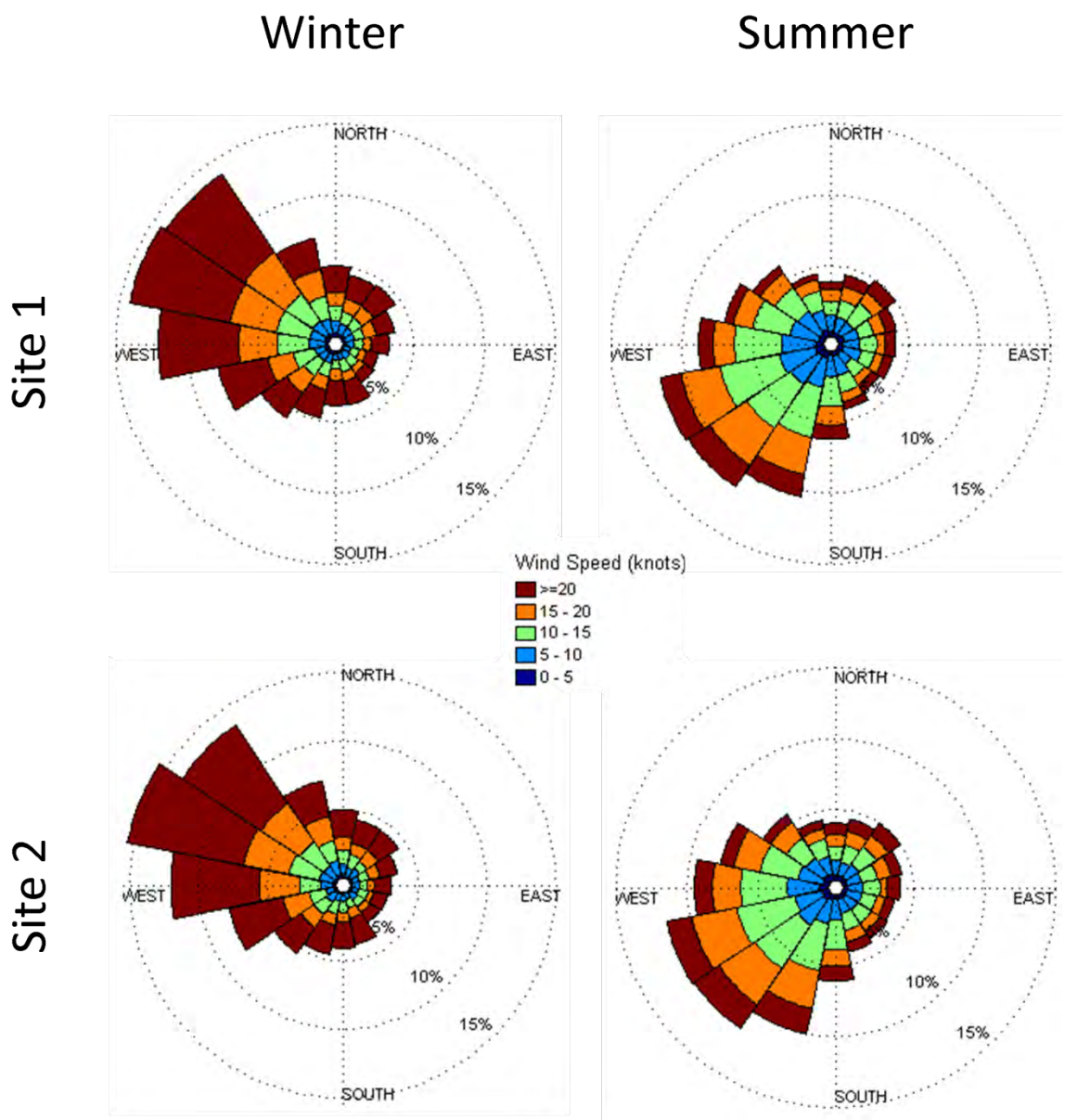

Figure 21. NOGAPS seasonal wind roses for Sites 1 and 2 using data from 2005-2010. Wind speeds in knots, using meteorological convention (direction wind is coming from).

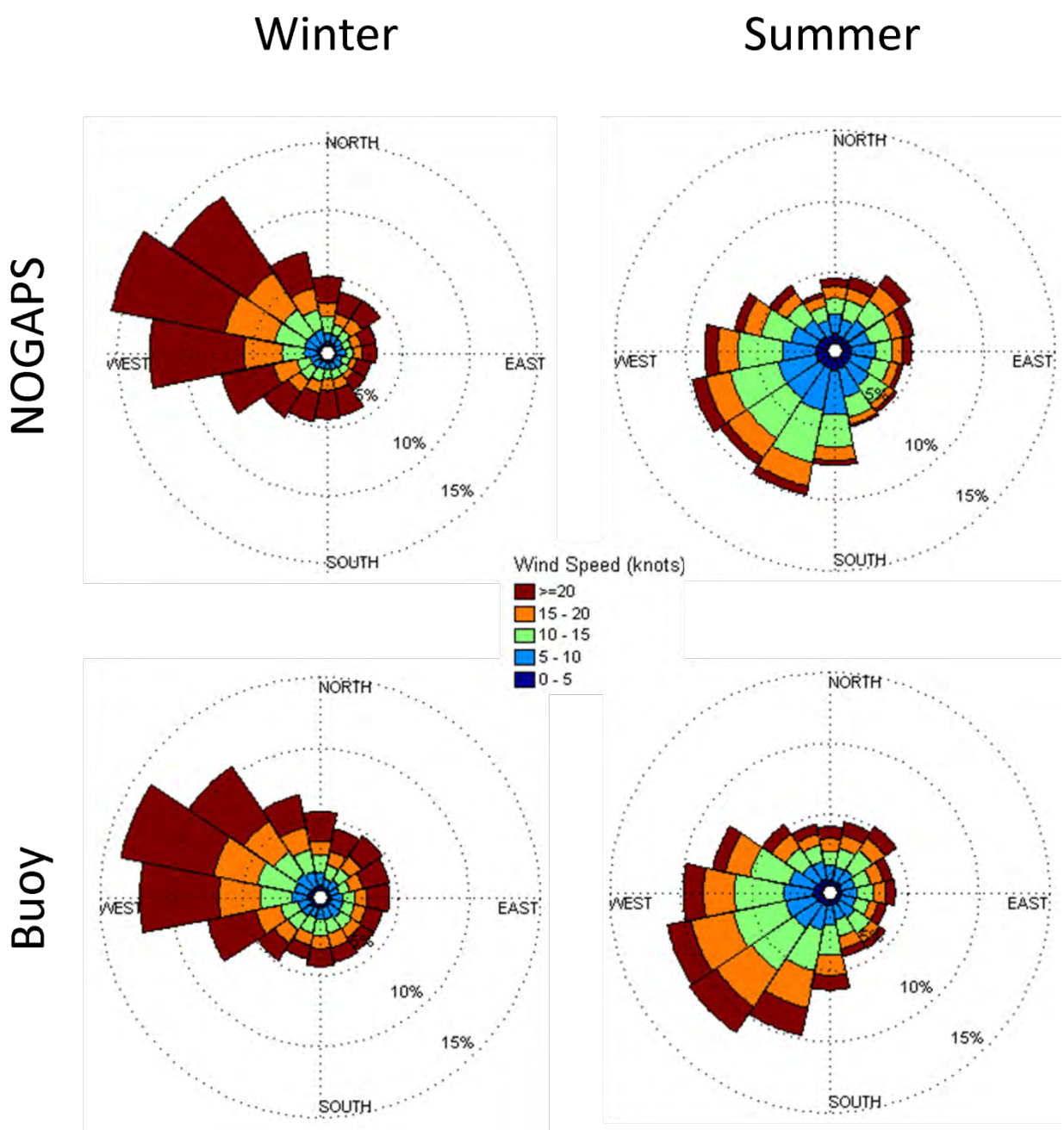

Figure 22. Seasonal wind roses for NOGAPS and buoy data from 2005-2010 at the comparison site. Wind speeds in knots, using meteorological convention (direction wind is coming from).

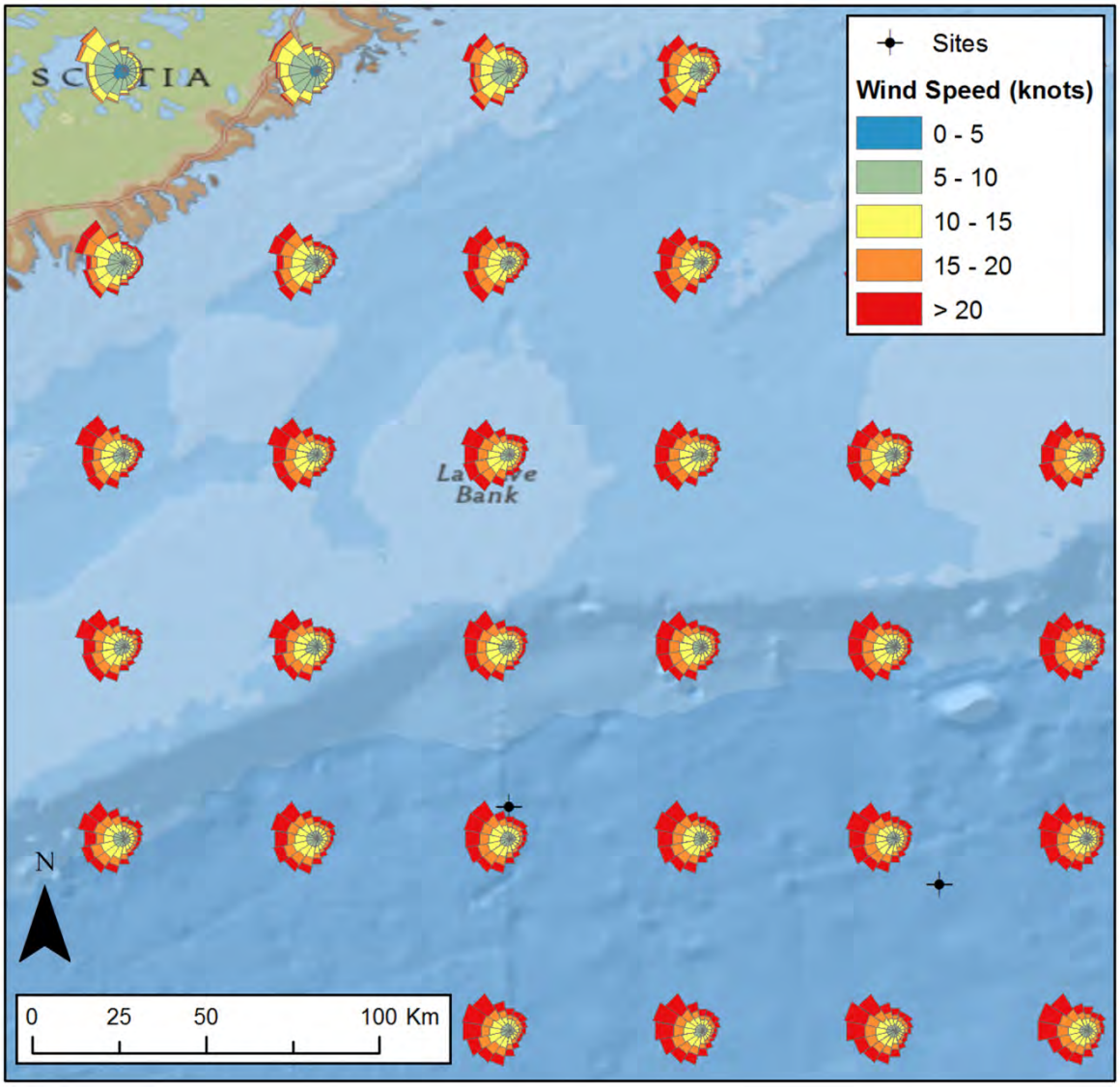

Figure 23. Spatial variability of yearly NOGAPS wind field near the sites of interest represented by rose diagrams; wind speeds in knots, using meteorological convention (i.e. direction wind is coming from).

9.3 REFERENCES

Bayler, G. and H. Lewit. 1992. The Navy Operational Global and Regional Atmospheric Prediction Systems and the Fleet Numerical Oceanography Center. Weather and Forecasting , Vol. 7, No. 2.

Bleck, R. 2002. An oceanic general circulation model framed in hybrid isopycnic-cartesian coordinates. Ocean Modeling, 4, 55-88.

Cummings, J.A. 2005. Operational multivariate ocean data assimilation. Quarterly Journal of the Royal Meteorological Society. Part C, 133(613), 3583-3604.

Egbert, G.D., A.F. Bennet, M.G.G. Foreman. 1994. TOPEX/POSEIDON tides estimated using a global inverse model. Journal of Geophysical Research: Oceans (1978-2012). Volume 99, Issue C12, pp. 24821-24852.

Egbert, G.D, S.Y. Erofeeva. 2002. Efficient Inverse Modeling of Barotropic Ocean Tides. American Meteorological Society. Volume 19, Issue 2, pp. 183-204.

Egbert, G.D. and S.Y. Erofeeva. 2014 The OSU TOPEX/Poseidon Global Inverse Solution TPXO. http://volkov.oce.orst.edu/tides/global.html, February 20, 2014.

Gulf of Maine Area Census of Marine Life (GoMA), "About the Gulf: Circulation." (2013). http://www.gulfofmaine-census.org.

Gyory J., Bischof, B., Marian, A.J., and Ryan, E.H., 2005. The Guinea Current. Ocean Surface Currents. http://oceancurrents.rsmas.miami.edu/atlantic/guinea.html.

Gyory, J., A. J. Mariano, and E. H. Ryan. "The Gulf Stream." Ocean Surface Currents. (2013). http://oceancurrents.rsmas.miami.edu/atlantic/gulf-stream.html.

Hannah, C. G., Shore, J. A., and Loder, J. W., (2001), Seasonal Circulation on the Western and Central Scotian Shelf. *Journal of Physical Oceanography,* **31**, 591-614.

Hogan, T.F., and T.E. Rosmond, 1991: The description of the Navy Operational Global Atmospheric System's spectral forecast model.

Hogg, N.G. and W.E. Johns, 1995: Western boundary currents. U.S. National Report to International Union of Geodesy and Geophysics 1991-1994, Supplement to Reviews of Geophysics*, 33,* 1311-1334.

Johns, W. E., Shay, T. J., Bane, J. M., and Watts, D. R., 1995. Gulf Stream structure, transport and recirculation near 68W, Journal of Geophysical Research. 100: C1, 817-838.

Lazier, J.R.N., and D.G. Wright, 1993: Annual Velocity variations in the Labrador Current, Journal of Physical Oceanography, 23, 659-678.

Lynch, D. R., Gentleman, W. C., McGillicuddy, D. J. Jr., and Davis, C. S., 1998, Biophysical simulations of *Calanus finmarchicus* population dynamics in the Gulf of Maine. Mar. Ecol. Prog. Ser. 169: 189-210.

Mariano, A.J., T.M. Chin and E.H. Ryan, R. Kovach and O.B. Brown, 2002: On Gulf Stream Path Variability. J. Physical Ocean. (submitted).

Miller, C. B., Lynch, D. R., Carlotti, F., Gentleman, W., and Lewis, C., 1998. Coupling of an individual-based population dynamic model of *Calanus finmarchicus* to a circulation model for the Georges Bank region. Fish. Oceanog. 7:3/4, 219-234.

Naval Research Laboratory: NOGAPS. 2013. http://www.nrlmry.navy.mil/metoc/nogaps/

Reynaud, T.H., A.J. Weaver, and R.J. Greatbatch, 1995: Summer mean circulation of the Northwestern Atlantic Ocean, Journal of Geophysical Research, 100, 779-816.